5-27-2020

Prediction of Gas-hydrate Equilibrium, Stability and Kinetic Nucleation in Porous Media

Yali Zhang
yz3208@rit.edu

R·I·T

Prediction of Gas-hydrate Equilibrium, Stability and Kinetic Nucleation in Porous Media

by

Yali Zhang

A dissertation submitted in partial fulfillment of the requirements
for the degree of Doctorate of Philosophy in Microsystems Engineering

Microsystems Engineering Program
Kate Gleason College of Engineering

Rochester Institute of Technology
Rochester, New York
May 27, 2020

Prediction of Gas-hydrate Equilibrium, Stability and Kinetic Nucleation in Porous Media
by
Yali Zhang

Committee Approval:

We, the undersigned committee members, certify that we have advised and/or supervised the candidate on the work described in this dissertation. We further certify that we have reviewed the dissertation manuscript and approve it in partial fulfillment of the requirements of the degree of Doctor of Philosophy in Microsystems Engineering.

_____

Dr. Patricia Taboada-Serrano Date
Associate Professor, Department of Chemical Engineering - KGCOE

_____

Dr. Michael Schrlau Date
Associate Professor, Department of Mechanical Engineering - KGCOE

_____

Dr. Nathaniel Barlow Date
Assistant Professor, School of Mathematical Sciences - COS

_____

Dr. Megan Elwood Madden Date
Professor, Robert & Doris Klabzuba Chair,
Stubbeman-Drace Presidential Professor of Geology and Geophysics, University of Oklahoma

_____

Committee member Date
Affiliation

Certified by:

_____

Dr. Bruce Smith Date
Director, Microsystems Engineering Program

ABSTRACT

Kate Gleason College of Engineering
Rochester Institute of Technology

Degree: Doctor of Philosophy **Program**: Microsystems Engineering

Author's Name: Yali Zhang

Advisor's Name: Dr. Patricia Taboada-Serrano

Dissertation Title: Prediction of Gas-hydrate Equilibrium, Stability and Kinetic Nucleation in Porous Media

Natural gas-hydrates are crystalline inclusion compounds with gas molecules (guest compounds) trapped within a host lattice formed by water molecules in an ice-like hydrogen-bonded framework. Natural gas-hydrates have the potential to become an important carbon-based resource addressing the increasing energy demand, and they pose a risk in terms of climate change. Accurate estimates of gas-hydrates global inventory, understanding of formation and dissociation processes of gas-hydrates, and evaluation of their environmental impact require models that accurately describe gas-hydrate stability in sediments and predict gas-hydrate kinetic nucleation processes. The hypothesis driving this work is that incorporation of selected sediment properties, i.e., surface energies and pore diameter, can lead to more accurate predictions of hydrate equilibrium, stability and nucleation in porous media.

In this work, a model for gas-hydrate equilibrium in porous media was developed from basic thermodynamic principles and tested against available experimental data published in the scientific literature. The proposed model predicts reported experimental data with high accuracy for the range of pore sizes (3.4 ~ 24.75 nm) of different materials reported in the literature. It was found that the wettability of the pore surface affects the shape of the hydrate phase inside the pore and consequently influences the equilibrium pressures of gas-hydrates formed in porous media.

A predictive macroscopic mathematical model describing the kinetic nucleation of gas-hydrates was developed based on Classical Nucleation Theory (CNT) in order to formulate correction factors for three types of interfaces mostly encountered in natural sediments (gas-liquid interface, liquid-solid interface and three-phase boundary lines). This approach, which incorporates the interfacial properties of sediments, can efficiently provide a fundamental understanding on the dependence of the formation mechanism of gas hydrates on a wide range of interfacial properties (wettability, substrate size, interfacial tension). The model predicts that hydrate nucleation is energetically favorable on confined surfaces with smaller contact-angle values, i.e., hydrophilic surfaces. Comparison between different types of interfaces leads to the conclusion that the nucleation of gas hydrates preferentially occurs in larger sediment pores. At the beginning of methane hydrate formation, for example, hydrate will preferentially nucleate at the gas-liquid interface. With the increase of hydrate volume or growth of the hydrate phase, the center of crystal growth moves towards the liquid-solid interface. In natural systems, gas hydrates form first on the concave liquid/solid interface and gas/liquid interface in sandstone sediments, gas/liquid interface and gas/liquid/solid triple boundary line in clay sediments and gas/liquid interface in pipeline with oil droplets.

The inclusion of sediment properties in the model for gas-hydrate equilibrium in sediments predict experimental data within a margin of %AAD lower than 2%, a significant improvement upon previous modeling attempts. Additionally, the inclusion of sediment properties in the models for kinetic nucleation of gas hydrates result in mathematical models that capture the qualitative information obtained from examination of gas-hydrate core samples. Therefore, the hypothesis of the present work was proven.

ACKNOWLEDGMENTS

I am heartily grateful to my advisor Dr. Taboada-Serrano, who provided me with the guidance and opportunity to work on this project and advised me to completion of this work. I would like to show my gratitude to my dissertation committee members, Dr. Elwood Madden, Dr. Schrlau, and Dr. Barlow, for their instructive suggestions and valuable comments on this thesis. I would also like to express my appreciation to the Microsystems Engineering program and the department of Chemical Engineering for their amazing support. Thanks go to Dr. Weinstein for his continuous support and insightful suggestions on my research. Thanks go also to Dr. Costas Tsouris from the Oak Ridge National Laboratory and Georgia Institute of Technology for stimulating our interest in this work, and to Dr. Peter Brewer and his team from Monterey Bay Aquarium Research Institute who provided the natural perspective for this work. I am also grateful to Julie Olney and Lisa Zimmerman for their continuous and reliable administrative support. I am deeply indebted to my parents, my husband Binghui Deng, my son William Deng, and friends for their help, support and understanding.

Lastly, I would like to acknowledge the financial support from the Kate Gleason Fund at the Rochester Institute of Technology.

Table of Contents

CHAPTER 1 INTRODUCTION

1.1 Overview

Natural gas hydrates (NGH), also known as burning ice, are believed to be an ideal source of natural gas for future exploitation. The extraction of gas containing especially methane from NGH accumulations is expected to play an increasing important role in global energy supply with a forecasted annual growth of 1.7% in the next two decades[1].

Traditionally, gas-hydrates have attracted wide attention due to their detrimental effects in the petroleum industry. Gas-hydrates can form in natural gas pipelines during natural gas production and transportation processes leading to clogging of the pipelines and disruption of operations. It was later discovered that gas-hydrates occur naturally in widespread environments around the globe. Recently, storing and transporting natural gas in the form of solid gas hydrates has gathered attention as a promising alternative method for gas storage and transportation due to the advantages of low cost, safety at relatively low pressures and high temperatures. Additionally, NGH present a high risk with respect to global climate as will be explained below. Over the past decades, significant effort has been conducted to study the behavior of NGH. In this chapter, background knowledge about NGH will be covered, including structure of NGH, applications of NGH and the state-of-the art on the research of NGH.

1.2 Gas Hydrates

Natural gas hydrates, gas-hydrates for short, are crystalline inclusion compounds with gas molecules (guest compounds) trapped within a host lattice formed by water molecules in an ice-like hydrogen-bonded framework as depicted. Van der Waals forces (physical bonding) between the guest molecule and water molecules stabilize the structure of gas-hydrates, preventing it from collapsing into the conventional ice structure[2,3]. Common guest-gas molecules include low-molecular weight hydrocarbons such as methane, ethane and other gases like H_2S, CO_2, H_2 and N_2.

Gas-hydrates are metastable compounds, whose formation and decomposition is determined by the environmental conditions in which they are formed, including temperature, pressure, composition of gas, salinity of water and the physical properties of their reservoirs. Gas-hydrates can be stable over a wide range of pressures and temperatures. For example, methane hydrates are stable from 70 to 350 K (-334 to 170 °F) at pressures from 20 nPa to 2 GPa (2.90075×10^{-12} to 2.90075×10^{5} psia)[4].

Gas-hydrates possess some unique properties, such as their large storage capacity for gas in stable conditions. For instance, 1 m^3 of water is capable of storing 216 m^3 of methane to form 1.26 m^3 of gas-hydrates at standard temperature/pressure conditions. This is equivalent to 1.09 m^3 of ice without gas trapped. Therefore, in a unit volume of solid gas-hydrates, 80% of the volume is occupied by water molecules and 20% by gas molecules[4,5].

1.3 Structure of Gas Hydrates

Most of the volume of gas-hydrates is occupied by water, thus many properties of gas-hydrates are similar to those of ice (e.g., density, physical appearance, and refractive index). The cavities of gas-hydrates are larger than the basic unit of ice crystal in order to allow guest molecules to be trapped inside[6]. Gas-hydrates exist mainly in three types of crystalline structures depending on the temperature and pressure conditions and the size of the guest molecules. These crystalline structures are known as structure I (sI), structure II (sII), and structure H (sH)[6]. X-ray diffraction, Raman spectroscopy and nuclear magnetic resonance (NMR) spectroscopy are the most effective experimental techniques to confirm and characterize the structures of gas-hydrates[6]. The structures sI and sII were confirmed by Von Stackelberg, Muller[2,3] and Claussen[7–9] via X-ray diffraction experiments. After 20 years, Ripmeester et al. discovered the structure H with NMR, X-ray and neutron powder diffraction measurements[10]. It was found that water molecules form different

patterns and cages through hydrogen bonds in each structure. Only one guest molecule can be trapped inside each cage.

Table.1. Summary of the structural details of three common unit crystals based on values reported by C.A. Koh, E.D. Sloan et al.[11]

Hydrate Structure	**I**		**II**		**H**		
Cavity	Small	Large	Small	Large	Small	Medium	Large
Description	5^{12}	$5^{12}6^2$	5^{12}	$5^{12}6^4$	5^{12}	$4^35^66^3$	$5^{12}6^8$
Number of cavities per unit cell	2	6	16	8	3	2	1
Average cavity radius (Å)	3.95	4.33	3.91	4.73	3.91†	4.06†	5.71†
Coordination number*	20	24	20	28	20	20	36
Number of water per unit cell	46		136		34		

*Number of oxygens at the periphery of each cavity. †Estimates of structure H cavities from geometric models.

The basic cage, the building blocker for all the three structures, is the 5^{12} cage (so called pentagonal dodecahedral cage or small cage), i.e., the cage contains 12 pentagonal faces. Structure I (sI) is most commonly encountered in nature because natural deposits generally generate methane gas (biogenic gas) without heavier hydrocarbon molecules. As shown in Table 1, the sI is composed of two small 5^{12} cages and six medium $5^{12}6^2$ cages (this cage contains 12 pentagonal and 2 hexagonal faces on the cage). Guest molecules such as CH_4, CO_2, H_2S, C_2H_6 normally form gas-hydrates with the structure I. The other two hydrate structures (sII and sH) as shown in Table 1 are less commonly found in natural environments but occur more commonly in artificially-synthesized hydrates with larger hydrocarbons. Gas-hydrates formed in oil and gas pipelines are mostly of structure II or structure H because natural-gas is composed of large amounts of heavier hydrocarbon molecules (e.g., propane, butane, pentane) and small amounts of methane molecules.

Structure II includes 16 small 5^{12} cages and 8 large hexacaidecahedral cage (cage of $5^{12}6^4$ contains 12 pentagonal and 4 hexagonal faces on the cage). Larger guest molecules (e.g., C_3H_8, O_2, N_2, Ar, Kr) can form structure II. Structure sH is made up of 3 small 5^{12} cages, 2 mid-sized $4^35^66^3$ cages (contains 3 square, 6 pentagons and 3 hexagons on the cage) and 1 large icosahedral $5^{12}6^8$ cage, which has 12 pentagonal and 8 hexagonal faces on the cage. Large molecules such as butane, methylcyclohexane and larger hydrocarbons usually form structure H. Surprisingly, hydrogen also forms hydrate of structure H[6,11].

Not all gas molecules are able to form gas-hydrates. There are two basic requirements for a gas molecule to form hydrates[12]. On one hand, the gas molecule should not be able to form or contain strong or moderately strong hydrogen bonds (e.g., H-F). On the other hand, the size of guest molecule should be located in the range between 3.5Å and 9Å. At normal pressures, guest molecules smaller than 3.5Å are too small to stabilize gas-hydrate cavities and molecules larger than 9Å are too large to fit into a gas-hydrate cavity without distorting the lattice. In addition, guest molecules between 3.5Å and 7.5Å can only form sI or sII[6,11]. Gas mixtures usually form mixed hydrate structures.

1.4 Development of Research on Gas Hydrates

In 1778, Priestley first observed clathrate hydrates by bubbling SO_2 into freezing water under laboratory conditions. In addition, he also discovered that gas-hydrates formed from other types of gas, including oxygen, hydrogen and others. However, Priestley didn't describe the crystals he synthesized as gas-hydrates. Thirty three years afterwards, Sir Humphrey Davy obtained aqueous chlorine clathrate (hydrate) in 1811 and named the crystal as a hydrate of gas. Therefore, Priestley is the first scientist who synthesized gas-hydrates in a laboratory and Davy is the first scientist to identify the materials as gas-hydrates. During the period from 1811 to 1934,

there was no significant research effort on the behavior of gas-hydrates. Research interests mainly focused on identifying the types of gas-hydrates and at which conditions (pressures and temperatures) gas-hydrates can form. Gas-hydrates were still a curiosity for scientists before 1934[4,11].

In 1934, Hammerschmidt was the first to find that solid gas-hydrates can plug natural-gas pipelines during gas transportation processes. From 1934 to 1965, the number of publications about gas-hydrates grew exponentially. Research on gas-hydrates during this period was principally motivated by flow assurance during gas production and transport. There are 144 publications that mainly investigate the formation conditions of gas-hydrates in bulk and provide effective methods to prevent gas-hydrates from clogging natural-gas pipelines. In addition, over this period of time, macroscopic models were developed to describe the phenomenon of pipeline plugging, and microscopic structures of gas-hydrates were also determined with microscopic tools[4,11].

In 1965, Makogon suggested that natural gas-hydrates can form in cooled sediments, which was later proved by laboratory experiments with real core samples. Starting in 1965, most of the research has focused on natural gas-hydrates in sediments, which are believed to be an unconventional source of energy in the coming future[4]. During the period from 1970 to 2005, natural gas-hydrates research programs were established in various countries worldwide[4]. Natural gas hydrates occur in geographically diverse settings, either in marine sediments or permafrost environments. After 2000, research interest on the accumulation of gas-hydrates was extended to moons and other planets such as Mars due to their low temperature and high pressure conditions, as well as the gases present around them[13–15].

Over the past decade, diverse topics related to gas-hydrates attracted researchers' attention, including: (1) potential of gas-hydrates as a promising future source of energy; (2) description, characterization and production performance of natural gas-hydrates deposits; (3) gas production from gas-hydrates; (4) thermodynamic stability of gas-hydrates; (5) kinetics of formation of hydrocarbon hydrates; (6) inhibition of gas-hydrates formation in pipelines and flowlines; (7) potential applications of gas-hydrates for gas storage, transportation, gas separation and carbon dioxide sequestration[16]; and (8) accumulations of gas-hydrates in planetary material (e.g., Martian subsurface)[14]. In addition, the risk posed by gas-hydrates (especially methane-hydrates) with respect to global climate has gained increasing attention[4,16]. According to the published research work, there are 82 countries conducting research work related to gas-hydrates. Among them, three counties (e.g., the United States, China and Japan) have produced 50% of the total number of publications as of 2016[1].

1.5 Relevance of Gas Hydrates

1.5.1 Gas Hydrates in Flow Assurance

Naturally, oil and gas wells always produce undesired water along with hydrocarbons. This mixture is suitable to form gas-hydrates. When the temperature decreases into the hydration range, gas-hydrates form and plug oil and gas pipelines, which can result in severe operational problems in the petroleum industry. Gas-hydrates deposit on pipe walls and further agglomerate to form large plugs during drilling, production, transportation and processing of oil and gas. Sometimes gas-hydrate formation causes pipeline blockages and other serious safety problems. For example, when the temperature is above the hydration range, gas-hydrates formed in pipelines will dissociate and detach first at the pipe wall. Then, any pressure gradient across the pipe will make the gas-hydrate plug move rapidly down the pipelines like a projectile. As a result, the downstream

gas will be compressed which will either cause pipeline blowouts or result in explosion of the plug through pipeline bends[11]. In other cases, when the pipeline is locally heated, the released gas from the hydrate plug sometimes can result in pipeline ruptures due to extremely high local pressures[11].

A proposed conceptual model is applied to describe gas-hydrates formation in a multiphase flow system containing water, oil, and gas[17]. In this model, four stages are involved in the mechanism of hydrate formation and deposition in hydrate plugging. First, water droplets are entrained in oil phase and gas bubbles are entrained in water phase. Second, gas hydrate formation occurs at the interfaces of water-oil and water-gas, followed by the third stage of aggregation of gas hydrates. Finally, hydrate particles agglomerate to larger aggregates that may cause a complete blockage[18]. The surface of gas-hydrates is inherently hydrophilic[19]. A thin layer of water film covers the hydrate surface, which results in a capillary bridge between gas-hydrates particles[20,21]. Gas-hydrates particles are bound together through capillary forces. As a result, agglomeration of hydrate particles always presents the high risk of blockage in oil and gas production and transportation lines.

Some methods have been developed to avoid gas hydrate plugs, including removing water prior to pipeline transportation, raising the temperature (e.g. insulation, bundles, electric or hot water heating), lowering the pressure, and shifting the equilibrium conditions for hydrate formation to lower temperatures and higher pressures by adding some thermodynamic inhibitors (TIs)[22]. These methods are very expensive and inconvenient, such as heated pipelines or the need for chemicals injection and regeneration facilities. In addition, TIs are not environmentally friendly due to their chemical toxicity[23]. In the last several decades, low dosage hydrate inhibitors (LDHIs), including kinetic hydrate inhibitors (KHIs) and anti-agglomerants (AAs), have become more attractive for subsea gas or oil production and transportation due to their effectiveness at low

dosage. Low dosage hydrate inhibitors do not change the thermodynamic conditions of the system, but they mainly work on the early stage of hydrate formation by altering the rheological properties of fluids in the system.

Kinetic hydrate inhibitors are usually water-soluble polymers, which can delay crystal nucleation or decrease hydrate formation rates in pipelines. Therefore, hydrocarbon fluids can be transported for a long time without hydrate agglomeration in lines. The lower the temperature below the equilibrium temperature in hydrate region, the shorter the hydrate induction time will be delayed and the less effective any inhibitor will become[24]. That is, the effectiveness of KHIs is limited when the subcooling (ΔT: driving force for hydrate formation) is larger than 12℃.[22]

Compared with KHIs, AAs are surface active chemicals which are effective at more extreme conditions (i.e. deeper field with higher sub-cooling) than KHIs. Anti-agglomerants do not hinder formation of hydrate crystal, but keep the hydrate particles small and away from other particles so that hydrate particles can be transported along with the fluids instead of forming plugs in pipelines. The schematic of a typical AA is show in Figure. 1.[25] Anti-agglomerants, as surfactants, contain hydrophilic heads which can attach to the hydrate crystal surface to modify the wetting properties of hydrate surface and hydrophobic (lipophilic) tails that make the crystal surface oil-wet and make hydrate particles easy to disperse in the liquid phase. Anti-agglomerants can decrease the capillary force between hydrate particles by lowering water-oil interfacial tension and increasing the contact angle of water molecules on the hydrate surface, thus preventing aggregation.

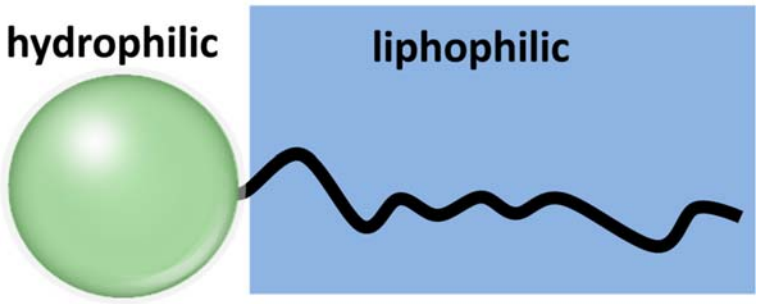

Fig.1. Schematic of an AA surfactant molecule, identifying hydrophilic and lipophilic based on the characterization by Zerpa et al.[25]

1.5.2 Gas Hydrates for Natural Gas Storage and Transport

Natural gas is expected to be the primary energy source for global economic development in the following decades. Therefore, it is necessary to develop effective technologies to store and transport natural gas safely and economically[1,26]. Many approaches have been studied worldwide for the storage and transport of natural gas. Natural gas can be stored and transported in the form of gas, liquid or solid.

Regarding to the available methods for the storage and transport of natural gas, one of the most common pathways for storing natural gas is underground inventory which includes depleted oil/gas reservoirs, aquifers and salt caverns. As for the transport of natural gas in gaseous form, gas pipeline is the most common method but sometimes it's not practical when one considers the distance, cost, feasibility and accessibility of the delivery location. Compressed natural gas (CNG) is a smaller-scale method for natural gas storage and transportation. However, this approach usually requires extremely high pressure (≥200 bars). With respect to safety concerns and storage capacity, CNG is not suitable for large-scale natural gas storage and long distance transport. Liquefied Natural Gas (LNG), natural gas stored and transported in form of liquid, has been considered as the most appropriate method for commercial application because of its tremendous volumetric storage capacity (600 v/v at STP conditions). However, this approach requires

extremely low temperature (-162 ℃) in order to keep natural gas stable and to overcome some other issues such as boil-off during the large-scale storage and long-distance transport processes. Therefore, the wide application of this method in natural gas storage and transport is discouraged. With respect to transport of natural gas in solid form, adsorbed natural gas (ANG) is one possible pathway to store natural gas by utilizing sorbent materials such as carbon nanotubes (CNTs), graphene, and some other metal organic frameworks. These sorbents are expected to provide higher storage capacity for natural gas due to their larger surface area and higher porosity compared to other methods discussed above[26]. However, the volumetric storage capacity reported in this method is lower which limits its practical application in the storage and transport of natural gas. Further studies are required to determine appropriate materials for the practical application of this approach.[27]

Solidified Natural Gas (SNG), which attempts to store and transport natural gas in the form of solid gas-hydrates, has been considered as a promising alternative for gas storage and transportation due to the advantages of low cost, safety at relatively low pressures and high temperatures (around water freezing point), and tremendous storage capacity (1 m^3 of methane hydrate is capable of storing 216 m^3 methane at standard temperature/pressure conditions)[5] when compared to other methods (Liquid Natural Gas (LNG) and Compressed Natural Gas (CNG))[28]. In addition, the method of SNG is environmentally friendly as it only utilizes water and very low concentration of promoters. Natural gas trapped in the gas-hydrates can be almost completely recovered by simple depressurization or thermal stimulation[26].

Currently, the process of applying the method of SNG to store and transport natural gas consists of four steps: formation of gas-hydrates; processing of the formed gas-hydrates; storage and transport of the processed gas-hydrates and dissociation of the gas-hydrates. Among them, the

formation of gas-hydrates is the most important part. Furthermore, formation rate and storage capacity of gas-hydrates are the essential technological challenges for the application of SNG. Therefore, enhancing the formation rate of gas-hydrates and improving the storage capacity of gas-hydrate are significant steps to be taken as they can effectively reduce capital-equipment and operation-cost requirements.[29]

1.5.3 Gas Hydrates as Energy Source

Global demand for energy is expected to increase from 524 quadrillion BTUs in 2010 to 820 quadrillion BTUs in 2040.[1] It has been predicted that more than 76% of global energy consumption will be provided by carbon based sources in 2040, in spite of the predicted growth of other renewable energy sources[1,30]. Natural gas is expected to play an increasing important role in global energy supply with a forecasted annual growth of 1.7% in the next two decades.[1] Therefore, untapped natural-gas sources will need to be developed to cover the increasing energy demand. In fact, natural gas is a kind of energy resource with 50% lower of CO_2 emissions than coal or oil.[26]

Natural gas-hydrates occur in geographically diverse settings, either in marine sediments or permafrost environments, which makes them an ideal source of natural gas for future exploitation. Natural gas-hydrates are considered to be distributed globally. Interest in gas hydrates as a natural gas source has become more prominent only in the last 50 years.[1] It is believed that the amount of energy stored as natural gas in naturally-occurring hydrates is larger than the worldwide conventional natural-gas reserves combined.[2,3,6] Many approaches have been attempted to estimate the total amount of natural gas-hydrates on earth. Previous estimates varied from $0.2 \times 10^{15} m^3$ methane (STP) to $3053 \times 10^{15} m^3$ methane (STP).[1] These large variations are due to limitations of information regarding gas-hydrate deposits (e.g., porosity, availability of methane and water, sedimentary conditions, etc.).[1] Most of these estimates of gas-hydrates reservoirs come

from indirect seismic evidence obtained with bottom simulating reflector (BSR) indications.[1–3,11] These measurements carry a high level of uncertainty.[11] Over the past four decades, estimates of energy content in gas-hydrates has decreased over time due to improved understanding and increased knowledge generated by field exploration of gas-hydrates reservoirs. Fugacity-based models to describe gas-hydrates stability regions were developed in parallel, which provide good predictions about the amount of energy when compared to field results.[1] These models have helped to round the estimates to a number of $44 \times 10^{15} m^3$ methane (STP) for continental gas-hydrates.[1] Current estimates are not equally accurate for all types of reservoirs. Permafrost gas-hydrates are usually concentrated in lenses or beads, facilitating exploration and modeling. Ocean gas-hydrates, on the other hand, can be highly dispersed thus increasing the uncertainty in measurements and models.

Experiments conducted on permafrost and ocean hydrates have verified that gas-hydrates reserved in sediments could be economically recovered at locations of high concentrations.[11] It has been estimated that the energy trapped in ocean hydrates should be several orders of magnitude larger than that in permafrost hydrates.[11] However, the estimates of the energy trapped in ocean hydrates exhibits larger error than that of the permafrost hydrated energy, making the identification of concentrated ocean gas-hydrates reservoirs more difficult.[11]

Currently, proposed methods to economically recover methane from gas-hydrates usually follow one of these three principles: (1) depressurization of gas-hydrates to destabilize and release methane; (2) thermalization to break up the water hydrogen bonds releasing methane; and (3) addition of strong hydrogen-bonding chemicals to disrupt gas-hydrate structures.[11] Theoretically, it is technically feasible to produce methane from gas-hydrates in the ocean or in the permafrost but it would require large investments. It is desirable to have means to predict more accurately true

volume, location and methane concentration of gas-hydrate reservoirs in order to progress towards exploitation.

1.5.4 Gas Hydrates Risk to Global Climate

Beyond production, one must consider that risk of gas-hydrates pose to global climate. The concept of "the clathrate gun hypothesis" has been proposed, which indicates that methane from gas-hydrates can make significant contributions to climate change.[31,32] This concept was developed based on the geological record that a gas-hydrates reservoir collapse around 14,000 years ago released enough methane to increase atmospheric methane concentration levels by as much as 4%,[11,33] and, that this increase may have triggered a period of global warming. In addition, according to the World Meteorological Organization (WMO), the atmospheric concentration of methane has continuously increased from 1984 to 2016 and reached a new high of about 1853 parts per billion (ppb) in 2016. This amount is about 257% of the pre-industrial level.[34] It has been reported that the global warming potential of methane is about 28 times more than that of carbon dioxide.[35] Possibly, the release of large volume of methane gas from methane-hydrates into the atmosphere is one of the reasons contributing to the observed methane increase.

Gas-hydrates can form and be stabilized in certain regions of marine and permafrost sediments with proper pressures (depth) and temperatures.[36] In marine sediments, gas-hydrates are only stable at depths below the seafloor.[11] When the conditions are outside the equilibrium region (temperature above and/or pressure below the equilibrium conditions), methane hydrates dissociate into liquid water and gaseous methane. A fraction of this gaseous methane, which has not been oxidized by microbes, can then enter into the atmosphere and act as a potent greenhouse gas (a given volume of methane causes about 28 times more greenhouse gas warming than carbon

dioxide)[37,38]. Therefore, the evolution of large quantities of methane from gas-hydrates is plausibly one explanation for environmental perturbations involving atmospheric warming.[11]

Dissociation of gas-hydrates deposited in seafloor can also result in the mass movement and further significantly reduce the slope stability. The unstable slope can be hazardous to foundations of equipment under the sea level, such as pipelines, platforms and manifolds.[11] Furthermore, collapse of ocean sediments can trigger destabilization of more gas-hydrates to spontaneously release the gaseous methane into the atmosphere, which may cause the rise of sea level and further global warming.

1.6 Summary

Gas-hydrates are crystalline inclusion compounds with gas molecules (e.g., methane, ethane, propane, carbon dioxide, nitrogen and hydrogen sulfide) trapped within a host lattice formed by water molecules in an ice-like, hydrogen-bonded framework at elevated pressures and reduced temperatures. Gas-hydrates have attracted increasing research interests over the past decades. The published research on gas-hydrates mainly focus on four fields of gas-hydrates, including pipeline flow assurance, gas storage and transportation, application as an energy resource and environmental effects. Great amount of effort has been carried out in order to understand the behavior of natural gas-hydrates, mechanism of gas-hydrates formation and dissociation, stability and environmental impact of gas-hydrates.

CHAPTER 2 RESEARCH DESIGN AND OBJECTIVES

2.1 Motivation

As stated earlier, natural gas-hydrates are significantly important as an energy resource and contributors to climate change. Being able to fully estimate the size and gas-content of natural gas-hydrate reservoirs is not just important in terms of future natural gas exploitation, but also from an environmental perspective, considering that methane gas is a potent greenhouse gas. Therefore, it's crucial to have the capability to predict the volume and stability zones of natural gas-hydrates in marine and permafrost sediments, which can guide the design of technologies for harvesting methane and natural gas from hydrate deposits, and, most importantly, predict destabilization of those deposits that may result in catastrophic gas release.[2,3] Accurate estimates of size and gas-content of gas-hydrate reservoirs has yet to be achieved, since estimates are highly dependent on thermodynamic models (assumptions) used in order to predict the zones of temperature and pressure where gas hydrates are thermodynamically stable.[1] It has been proposed that one of the main reasons for the uncertainties in model predictions of gas-hydrate stability zones is due to current models not fully including sediment properties in their formulations.[1]

In order to better control the process of gas-hydrates dissociation and the risk of natural gas-hydrates to global climate change, it is necessary to understand the formation process of gas-hydrates. Gas hydrate formation is a process which mainly consists of three stages before reaching equilibrium conditions: saturation, induction, and growth.[3] The first stage is the dissolution of gas molecules in the liquid until the liquid is completely saturated with gas. It takes a certain amount of equilibration time to reach the saturation point. The second stage, known as nucleation stage, is the induction stage in which small hydrate nuclei form or dissociate randomly until a cluster of critical radius is achieved. Once the time necessary to form nuclei of critical radius has been reached, the growth stage begins.[3] During the last stage gas hydrate grows rapidly and the gas

consumption increases linearly with time. Finally, the formation/dissociation of gas-hydrates achieves equilibrium under proper temperatures and pressures.

Most of experimental approaches conducted on the formation process of gas-hydrate focus on providing macroscopic rates of gas-hydrate growth. Few experimental studies focus on the nucleation process due to the temporal and spatial limitations of experimental monitors. However, studying nucleation process of gas-hydrates is an important part for understanding the formation process of gas-hydrates. Particularly, understanding how the sediment properties affect the nucleation process (heterogeneous nucleation) can help to understand the dissociation process of natural gas-hydrates in sediments. In addition, nucleation process of gas-hydrates plays an important role in other applications. For example, high nucleation rate can significantly enhance the formation rate of gas-hydrates for gas storage and transport. Lowering the nucleation rate of gas-hydrates can bring down the formation rate of gas-hydrates for avoiding gas-hydrates plugs in pipelines.

Based on the published literature, heterogeneous nucleation takes place more frequently than homogeneous nucleation because of the extremely slow nucleation rate of homogeneous nucleation[39]. In addition, a large volume of experimental work has provided evidence that foreign surfaces play an important role in the processes of kinetic formation and dissociation of gas-hydrates as well as the equilibrium of gas-hydrates.[40–43] Therefore, it is necessary to understand how the confinement surface properties modulate the nucleation process and equilibrium conditions of gas-hydrates in porous media in order to predict the behavior of gas-hydrates in natural marine and permafrost sediments.

2.2 Problem Statement

2.2.1 Equilibrium and Stability of Gas-hydrates

Gas hydrates naturally exist in mesoporous sediments with small mean pore radii[44–46], which are characteristic of fine-grained sediments. In bulk conditions (e.g., in pipelines and other equipment), gas hydrates are stable at temperatures around the freezing point of water and pressures above 3.15 MPa.[47] The equilibrium pressure required to stabilize hydrates in sediments shifts to higher pressure values than the one at bulk conditions for the same temperature. This fact was first confirmed by Handa and Stupin[47] who conducted experiments to investigate the equilibrium behavior of methane and propane hydrates in 70Å-radius porous media. These experiments showed that the equilibrium pressure of gas hydrates in porous media is 20-100% higher than those for hydrates in the bulk. Uchida et al.[48,49] measured the equilibrium conditions of methane, propane and carbon dioxide hydrates in pores of different sizes and observed that the equilibrium pressures of hydrates shifted significantly upward compared with that of the bulk hydrates at a given temperature. In light of these experiments, a selected number of models have been developed to adapt phase-equilibrium thermodynamic models that had been proposed for hydrates in bulk in order to describe gas-hydrate behavior in sediments.

It must be noted that the thermodynamic models for gas hydrates in porous media developed thus far make use of capillary effects within the chemical equilibrium condition as the means to adapt bulk-hydrate models to hydrates in sediments. However, these corrections do not include sediment properties, i.e., interactions of the sediments with all phases present in marine gas-hydrate reservoirs (free gas, liquid water and hydrate phases). It is believed that the omission of adequate sediment properties is one of the main causes for the large uncertainty of current models used to predict size and gas-content of gas-hydrate reservoirs.

2.2.2 Kinetic Nucleation Rate of Gas-hydrates

Once the thermodynamic conditions required for the existence of gas-hydrate have been established, gas-hydrate nucleation is a stochastic process which can produce a catastrophic appearance of the gas-hydrate phase. Understanding the nucleation process of gas-hydrates is the first step to understand and control the formation and dissociation processes of gas-hydrates.[50] Many experimental results have indicated that gas-hydrates formation process can be effectively promoted with the presence of foreign surfaces due to the large amounts of nucleation sites provided.[51–62] However, the mechanisms behind these experimental results and how the surface properties enhance the nucleation process are not well understood. In addition, with respect to energy exploitation from gas-hydrate accumulations, field results and numerical simulations of gas production have suggested that complex physical and chemical processes involving multiple phases and multiple components can cause an unexpected rate of gas production from gas-hydrates.[16,63,64] The arguments behind this suggestion include the following: (1) the effects between solid surface and fluid can hinder the depressurization-induced gas production from natural gas-hydrates reservoirs; (2) the morphology of rock surface can enhance the dissociation rate of gas-hydrates to some degree; and (3) the reduction of permeability and porosity can result in a significant reduction of gas production from natural gas-hydrates reservoirs.[63] Therefore, understanding how the foreign interface properties affect the nucleation process of gas-hydrates can provide insights into possible effects of solid surfaces in the dissociation process of gas-hydrates.

Studying the nucleation process of gas-hydrates experimentally is extremely challenging due to the difficulties in obtaining direct experimental measurements of the nucleation process.[42,65] Recently, some researchers studied the nucleation of gas-hydrates in the presence of solid surfaces

with Molecular Dynamics (MD) Simulations, which have been considered as an effective method to numerically understand the mechanisms of heterogeneous nucleation processes when the driving force in high enough.[66–69] MD simulations are limited to quantitatively analyze the nucleation rate of hydrates with various conditions (wide range of temperature value and interface properties) due to the limitations of timescale, length-scale and computation capacities of molecular approaches.[70] Therefore, more efficient and cheaper analysis aimed at quantitatively analyzing how the confinement surface properties modulate the nucleation process of gas-hydrates is still needed.

2.3 Hypothesis and Objectives

The ultimate goal of the study is to develop macroscopic mathematic models to predict how the properties of porous media (sediments) affect the thermodynamic equilibrium conditions and the nucleation rate of gas-hydrates in sediments. The hypothesis driving the work is that *the inclusion of appropriate sediment-properties, i.e., pore size, wettability, surface curvature and interfacial energies, can enable more accurate prediction of gas-hydrate stability and nucleation rate.*

The first objective is to develop a model to predict the equilibrium conditions of gas-hydrates in porous media. Thermodynamic equilibrium criteria will be applied to an ideal cylindrical pore, validated against published experimental porous media rather than correcting an existing model originally formulated for bulk conditions. The effects of confinement surface will be then naturally included in the mechanical equilibrium condition. The shape of the hydrate phase within the ideal cylindrical pore will be determined by the interfacial energies and the wetting angles of all the phases involved and the properties of the pore walls. Model parameters involved

will be obtained from independent sources published in the literature, including independent experimental measurements when available. This practice will ensure that the model is predictive.

The second objective of this work is to develop a mathematical model, incorporating the interface properties (wettability, surface curvature, substrate size and interfacial energies), to quantitatively describe the effects of various interfaces on the energy barrier and nucleation rate for hydrate nucleation. Incorporating this phenomenon into expressions for the rate of hydrate growth will enable eventual validation with experimental data for gas-hydrate growth. It is expected that such an approach will provide fundamental understanding on how the interface properties modulate the kinetic nucleation of gas-hydrates in a wide range of interfaces, and further understanding on how to effectively control the formation and dissociation of gas hydrates by modulating the properties of interfaces.

CHAPTER 3 MODEL FOR GAS-HYDRATE EQUILIBRIUM IN POROUS MEDIA THAT INCORPORATES PORE-WALL PROPERTIES

3.1 Motivation

Naturally-occurring gas hydrates (in permafrost and marine sediments) have the potential to contribute as a carbon-based source to the increasing energy demand. Accurate estimates of gas-hydrate global inventory, development of strategies for their exploitation, and the evaluation of their environmental impact require models that accurately present the physics of gas hydrates in marine sediments. Over the past decades, a number of thermodynamic models for gas hydrates in porous media were developed. Models thus far make use of capillary effects within the chemical equilibrium condition as the means to adapt bulk-hydrate models to hydrates in sediments.[71–74] Inclusion of capillary effects in chemical equilibrium conditions implies that chemical potentials are affected by interfacial energies, which is in fact a mechanical effect on the boundaries of the system. In addition, these corrections do not include sediment properties, i.e., interactions of the sediments with all phases present in marine gas-hydrate reservoirs (free gas, liquid water and hydrate phases).[75]

In this chapter, a new thermodynamic model for gas hydrates in pores predicting the equilibrium conditions of gas hydrates in porous media is presented. There are three assumptions leading the proposed model; (1) porous spaces are simplified as ideal cylindrical pores; (2) pores are not completely saturated with liquid phase: continuous free gas and dissolved gas are present in the pore; (3) the equilibrium pressure in the hydrate phase is different from that in liquid phase, but equal to that in gas phase and at the interfaces. This proposed model differs from previous models in the following aspects: (1) equilibrium criteria were applied directly to the cylindrical pore and its surroundings instead of incorporating capillary effects into bulk-equilibrium models; (2) the application of mechanical equilibrium criteria organically incorporates properties of the pore walls and interfaces into the equilibrium conditions; (3) the effects of confinement are then

naturally included in the mechanical equilibrium condition; (4) the interfacial energies and the wetting angles of all the phases involved and the properties of the pore walls determine the shape of the hydrate phase within the ideal cylindrical pore. Model parameters were obtained from independent sources published in the literature, including independent experimental measurements when available. The model predictions presented in this work depict high accuracy when compared to available experimental data in the literature.

3.2 Types of Sediments

Most of natural gas-hydrates in nature form in permafrost and ocean sediments. According to the well reservoir accumulations, natural gas-hydrates deposits can be characterized into four classes:[76,77] (1) reservoir accumulations are at the base of the gas-hydrates stability zone (GHSZ), and free gas exists in the hydrate-bearing layer; (2) gas-hydrates deposits are at the base of, or within the GHSZ, and a hydrate-saturated interval above a free water zone is involved; (3) gas-hydrates reservoirs are fully saturated with gas-hydrates phase without free water or free gas; (4) fine-grained accumulations present low intrinsic permeability and further low gas-hydrates saturations.

Most gas-hydrate reservoirs, especially marine reservoirs, are usually composed of unconsolidated sediments. Depending on the environment where gas-hydrates form, gas-hydrate deposits are classified into four types (type C, F, M, R).[77] Type C deposits comprise of poorly consolidated coarser-grained sediments. This type of deposit represents much of the permafrost settings but a smaller proportion of marine settings. With current technologies, type C deposits are the most promising reservoirs for potential energy recovery from gas-hydrates. In addition, type C contains two sub-types: C_{TB} (thinly bedded) and C_{MB} (massively-beded). Type F of gas-hydrate deposits are formed in sediments that are unconsolidated, fine-grained and low permeability. Type

F deposits are believed to be a potential energy resource. Type M deposits are massive hydrate mounds, which are related to cold seeps in very shallow sediments or outcrop on the sea floor. In the case type R deposits, gas-hydrates usually form in the porous media within rocks.

3.3 Background

Before 1999, most measurements and models focused on gas-hydrates formed in bulk conditions. Research work related to bulk gas-hydrates is crucial to understand the behavior of gas-hydrates in pipelines and flowlines. However, natural gas-hydrates mostly occur in porous media. The porous medium can significantly influence the equilibrium pressures of gas-hydrates. Handa and Stupin[47] first found that the porous media could significantly modulate the equilibrium pressures of methane and propane hydrates. In 1998, Uchida and his coworkers measured the equilibrium pressures for methane hydrates in pores of different sizes and found that pore size influences the equilibrium conditions of methane hydrates.[49]

In light of these experimental discoveries, Clarke et al. in 1999 proposed a model to predict the behavior of hydrate phase in submicron-sized pores (pore diameter of 140Å). The proposed model first incorporated the capillary effect by including Kelvin's equation into the condition for chemical equilibrium for gas hydrates. However, the interfacial tension considered in this model was only the one between liquid and gas phases. The pore size was assumed to be in uniform size in Clarke's work. When compared to experimental data, Clarke's model predicted the correct order of magnitude of the equilibrium pressure but was not quantitatively accurate. It predicted experimental data for gas-hydrate equilibrium in sediments with a deviation of 15% in the case of methane hydrate and a deviation of 29% for propane hydrate.[71] Also in 1999, Clennell et al. derived

an empirical model for hydrate stability from analysis of hydrate samples recovered from marine sediments,[78] which is particular to specific conditions.

Klauda and Sandler improved upon the previous models by applying the interfacial tension between hydrate and liquid water to correct the condition for chemical equilibrium in 2000.[72] Their model presented an absolute deviation from experimental data for hydrate equilibrium in sediments as low as 3.27% for low temperatures by adjusting the parameters of the Kihara cell potential used to model hydrate chemical potential.[72] In 2001, Klauda and Sandler extended their model to generic sediments via the incorporation of pore-size distributions and shape factors to account for the hydrate phase.[74]

Turner et al. incorporated the Kelvin-Clapeyron equation into the thermodynamic equilibrium model for hydrates in bulk in order to investigate the sensitivity of methane hydrate equilibrium to sediment pore size.[79]

Though models became increasingly more accurate, gains in accuracy were obtained at the expense of the use of one or more adjustable parameters. This work conducts fundamental thermodynamic analysis leading to straight forward incorporation of sediment properties to the proposed model.

3.4 Model Description

The model system, an ideal cylindrical pore, is assumed to be a closed system insulated with exception to the connections to two reservoirs. This system is connected through a thermal gate to a large, insulated reservoir of constant temperature (a thermostat) and through a piston to large, insulated reservoir of constant pressure (a barostat). At equilibrium, the total internal energy change for the global system (the closed system and the reservoirs) should be zero, leading to the following equation (as depicted in Figure.2):

$$dU{=}dU^{G} + dU^{L} + dU^{H} + dU^{\alpha} + dU^{\beta} + dU^{surr} {=}0 \quad (1)$$

The global system contains the following subsystems: free gas (G); liquid (L); hydrate (H); gas-hydrate interface (α); liquid-hydrate interface (Gβ) and reservoirs (surr). Note that the subscript j in the following equations represents the hydrate-forming gas (j = 1) and water (j = 2) in the system.

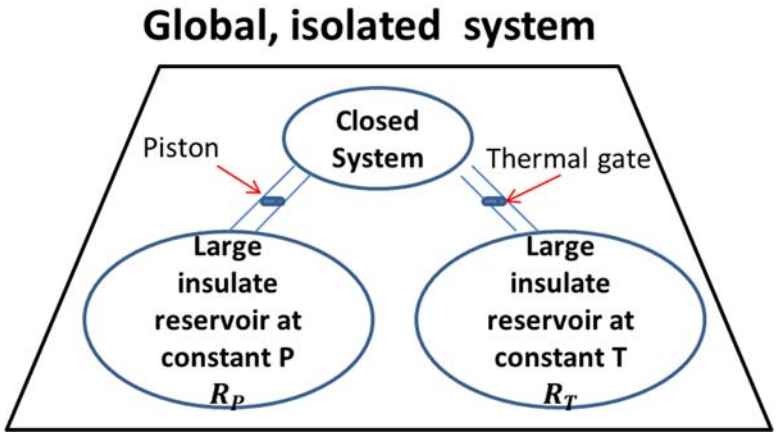

Fig.2. Schematic of the global system used in the model (based on Tester & Modell).

For the gas phase:

$$dU^{G}{=}T^{G}dS^{G} - P^{G}dV^{G} + \sum_{j=1}^{2} \mu_{\mathrm{j}}^{\mathrm{G}} d\mathrm{N}_{\mathrm{j}}^{\mathrm{G}} \quad (2)$$

For the liquid phase:

$$dU^{L}{=}T^{L}dS^{L} - P^{L}dV^{L} + \sum_{j=1}^{2} \mu_{\mathrm{j}}^{\mathrm{L}} d\mathrm{N}_{\mathrm{j}}^{\mathrm{L}} \quad (3)$$

For the hydrate phase:

$$dU^{H}{=}T^{H}dS^{H} - P^{H}dV^{H} + \sum_{j=1}^{2} \mu_{\mathrm{j}}^{\mathrm{H}} d\mathrm{N}_{\mathrm{j}}^{\mathrm{H}} \quad (4)$$

For the gas-hydrate interface (α):

$$dU^{\alpha}{=}T^{\alpha}dS^{\alpha} - P^{\alpha}dV^{\alpha} + \sigma_{\alpha}da_{\alpha} + \sum_{j=1}^{2} \mu_{\mathrm{j}}^{\alpha} d\mathrm{N}_{\mathrm{j}}^{\alpha} \quad (5)$$

For the liquid-hydrate interface (β):

$$dU^{\beta}=T^{\beta}dS^{\beta}-P^{\beta}dV^{\beta}+\sigma_{\beta}da_{\beta}+\sum_{j=1}^{2}\mu_{j}^{\beta}dN_{j}^{\beta} \quad (6)$$

For the surroundings (i.e., reservoirs):

$$dU^{surr}=T^{surr}dS^{surr}-P^{surr}dV^{surr} \quad (7)$$

Where U is the internal energy, S is entropy, V is volume, N is the number of components, T is temperature, P is pressure, and μ is chemical potential of component. Substituting eqs (2)—(7) into eq (1);

$$\begin{aligned}&T^{G}dS^{G}-P^{G}dV^{G}+\sum_{j=1}^{2}\mu_{j}^{G}dN_{j}^{G}+T^{L}dS^{L}-P^{L}dV^{L}+\sum_{j=1}^{2}\mu_{j}^{L}dN_{j}^{L}+T^{H}dS^{H}-P^{H}dV^{H}\\&+\sum_{j=1}^{2}\mu_{j}^{H}dN_{j}^{H}+T^{\alpha}dS^{\alpha}-P^{\alpha}dV^{\alpha}+\sigma_{\alpha}da_{\alpha}+\sum_{j=1}^{2}\mu_{j}^{\alpha}dN_{j}^{\alpha}+T^{\beta}dS^{\beta}-P^{\beta}dV^{\beta}\\&+\sigma_{\beta}da_{\beta}+\sum_{j=1}^{2}\mu_{j}^{\beta}dN_{j}^{\beta}+T^{surr}dS^{surr}-P^{surr}dV^{surr}=0\end{aligned} \quad (8)$$

The temperature and pressure of the liquid phase are assumed to be equal to the temperature and pressure of the large insulated reservoirs:

$$T^{L}=T^{surr}=T=constant$$

$$P^{L}=P^{surr}=P=constant \quad (9)$$

Additionally, since the system is closed, the following must be true:

$$dV^{L}=-dV^{G}-dV^{H}-dV^{\alpha}-dV^{\beta}-dV^{surr}$$

$$dS^{L}=-dS^{G}-dS^{H}-dS^{\alpha}-dS^{\beta}-dS^{surr}$$

$$dN_{j}^{L}=-dN_{j}^{G}-dN_{j}^{H}-dN_{j}^{\alpha}-dN_{j}^{\beta}\quad (j=1,2) \quad (10)$$

Then, substituting the set of eqs (9) and (10) into eq (8), the following condition for equilibrium is obtained:

$$(T^G - T)dS^G + (T^H - T)dS^H + (T^\alpha - T)dS^\alpha + (T^\beta - T)dS^\beta - (P^G - P)dV^G - (P^H - P)dV^H - (P^\alpha - P)dV^\alpha - (P^\beta - P)dV^\beta + \sum_{j=1}^{2}(\mu_j^G - \mu_j^L)d\mathrm{N}_j^G + \sum_{j=1}^{2}(\mu_j^H - \mu_j^L)d\mathrm{N}_j^H + \sum_{j=1}^{2}\left(\mu_j^\alpha - \mu_j^L\right)d\mathrm{N}_j^\alpha + \sum_{j=1}^{2}(\mu_j^\beta - \mu_j^L)d\mathrm{N}_j^\beta + \sigma_\alpha da_\alpha + \sigma_\beta da_\beta = 0 \quad (11)$$

In order for the equilibrium condition (eq 11) to be met, thermal equilibrium dictates that the temperature of all phases and interphases must be equal to that of the thermal reservoir or thermostat. Additionally, chemical equilibrium demands that the chemical potential of each component in all phases must be equal within the closed system.

$$T^G = T^H = T^\alpha = T^\beta = T$$

$$\mu_j^G = \mu_j^H = \mu_j^L = \mu_j^\alpha = \mu_j^\beta \quad (j=1, 2) \quad (12)$$

Finally, mechanical equilibrium is then given by eq (13).

$$-(P^G - P)dV^G - (P^H - P)dV^H - (P^\alpha - P)dV^\alpha - (P^\beta - P)dV^\beta + \sigma_\alpha da_\alpha + \sigma_\beta da_\beta = 0 \quad (13)$$

The gas-hydrate interface and the liquid-hydrate interface are assumed to pertain to the hydrate phase. Therefore, the two interfaces bear the pressure of the hydrate phase which is different from that in liquid water (i.e., the pressure of the reservoir RP).

$$P^H = P^\alpha = P^\beta$$

Then, eq (13) is simplified to:

$$-(P^G - P)dV^G - (P^H - P)dV^H + \sigma_\alpha da_\alpha + \sigma_\beta da_\beta = 0 \quad (14)$$

Additionally, it is assumed that the pressure in the hydrate phase is equal to that in the gas phase because gas phase is highly compressible and the interfacial tension (130 mJ/m^2) [80] of the hydrate phase is very large. Finally, eq (14) can be further simplified to the following mechanical equilibrium condition:

$$-(P^H - P)(dV^G + dV^H) + \sigma_\alpha da_\alpha + \sigma_\beta da_\beta = 0 \quad (15)$$

It must be noted that the constant pressure reservoir has a piston, so it accommodates changes in volume during phase change. Gas hydrates behave similarly to water ice in the sense that expansion takes place during phase change, which will be compensated by our constant-pressure reservoir Rp. It was determined that the loss in density during liquid water-hydrate phase transition is 9%,[3,81] which will be captured in our model as follows: $\mathrm{dV^H} = -1.09\mathrm{dV^L}$.

With these considerations, the final mechanical equilibrium condition for the system is given by the following expression:

$$P^H - P = \frac{\sigma_\alpha da_\alpha + \sigma_\beta da_\beta}{0.92 dV^H} \quad (16)$$

Therefore, at thermodynamic equilibrium conditions, eqs (12) and (16) must be met for gas hydrate to be stable at any given P, T and sediment properties.

The experimental study of Bahman Tohidi et al.[82] suggested that the amount of free-gas in some marine-sediment hydrate reservoirs is significant, as depicted in the schematic presented in Figure 3 based on this work. Free-gas bubbles coexist with dissolved-gas-saturated liquid in the sediments in most cases[82–84]. Additionally, the few experiments on gas-hydrate equilibrium in porous materials reported in the literature[79,81,85–87] were performed by wetting the porous media and then pressurizing with hydrate-forming gas. In light of these studies, which will be used for model validation, the proposed model assumed that the hydrate-crystallization process begins at

the gas-water interface to form a hydrate crust around the free-gas bubble. Additionally, the water phase was assumed to be saturated with dissolved methane gas, and to present characteristic surface-wetting behaviors depending on the surface properties of the porous medium.

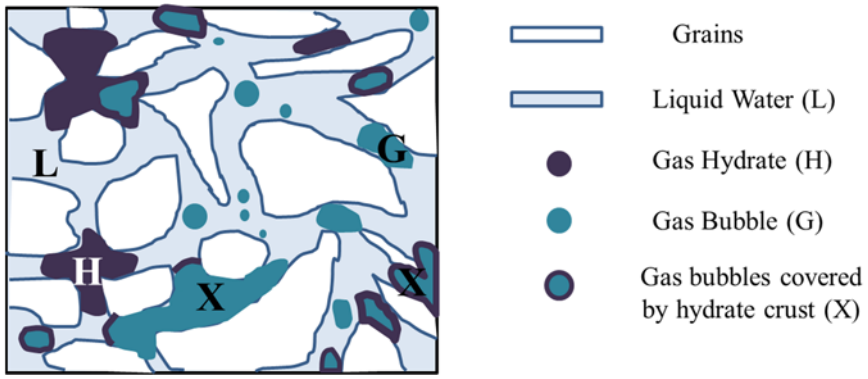

Fig.3. Schematic prepared based on the photograph of gas hydrates formation in porous media from experimental study of Tohidi *et al* [82].

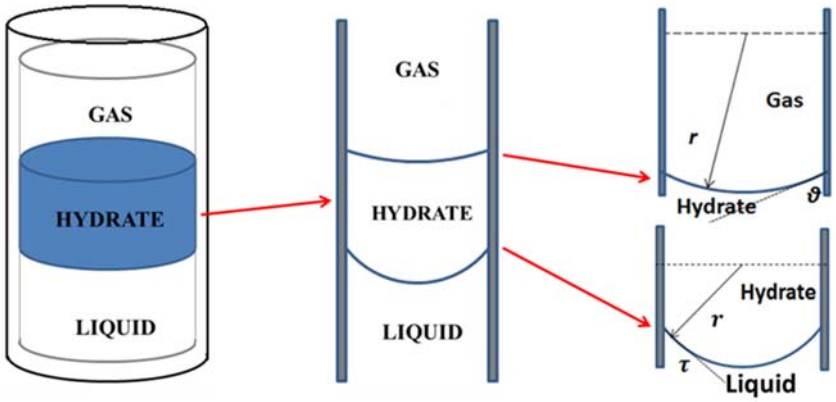

Fig.4. Schematic of the idealized cylindrical pore during gas-hydrate formation.

For simplicity, the porous materials were idealized as cylindrical pores according to the schematic presented in Figure 4. As stated earlier, there are three phases present in the cylindrical pore: gas phase (G), liquid phase (L) and solid hydrate phase (H). There are two interfaces in the pore: the hydrate-gas interface (α), and the hydrate-liquid interface (β). The hydrate phase (H) was

assumed to adopt the form of a concave-convex lens as depicted in Figure 5, in agreement with the experimental observations by Bahman Tohidi et al.[82] and Li et al.[83,84]

From geometry, the volume of gas hydrate formed in the cylindrical pore was calculated using the two hemispheres formed by the interfaces, as follows:

$$V^H = |\frac{1}{6}\pi r_p^3\left[\Gamma_\tau(3+\Gamma_\tau^2) - \Gamma_\theta\left(3+\Gamma_\theta^2\right)\right]| \quad (17)$$

Where r_p is the pore radius, the function Γ_θ is defined as $\Gamma_\theta = (1-\sin\theta)/\cos\theta$, and the angle θ can take values between 0° and 90°, depending on the angle of the gas-hydrate interface on a given surface. In a similar way, the function Γ_τ is defined as $\Gamma_\tau = (1-\sin\tau)/\cos\tau$, where τ can take values between 0° and 90°, depending on the angle of the hydrate-liquid interface on a given surface.

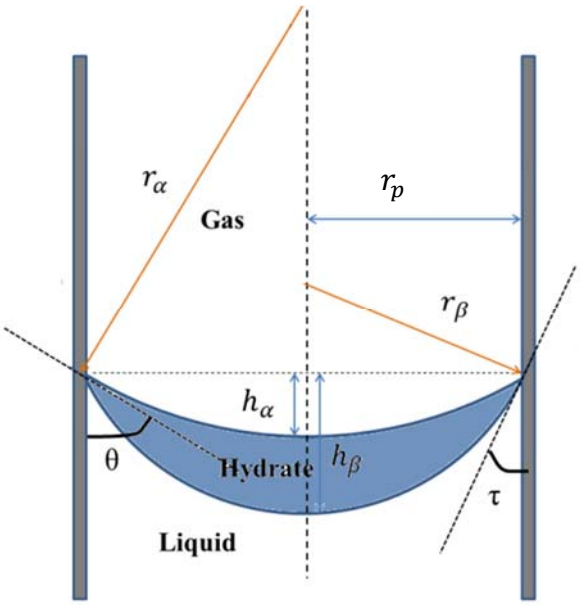

Fig.5. Schematic of the concave-convex gas-hydrate lens formed in the idealized cylindrical pore.

The same geometrical analysis was performed to determine the area of the hemispherical caps as follows:

$$a_\alpha = \pi\left(h_\alpha^2 + r_p^2\right) = \pi r_p^2(1 + \Gamma_\theta^2) \tag{18}$$

$$a_\beta = \pi\left(h_\beta^2 + r_p^2\right) = \pi r_p^2(1 + \Gamma_\tau^2) \tag{19}$$

By differentiating eqs (18) to (19) and then combining with eq (16), the final expression for the mechanical equilibrium conditions is as follows:

$$P^H - P = \frac{\sigma_\alpha 2\pi r_p\left(1 + \Gamma_\theta^2\right) + \sigma_\beta 2\pi r_p(1 + \Gamma_\tau^2)}{0.92 \cdot \left|\frac{1}{2}\pi r_p^2\left[\Gamma_\tau(3 + \Gamma_\tau^2) - \Gamma_\theta\left(3 + \Gamma_\theta^2\right)\right]\right|} \tag{20}$$

The parameters needed to apply the mechanical equilibrium condition are the hydrate-water interfacial tension (σ_β), the hydrate-gas interfacial tension (σ_α), the pore size (r_p) and the wetting angles (θ and τ), which can be obtained from available independent experimental measurements.

3.4.1 Mechanical Equilibrium

The mechanical equilibrium, given by eq (20), requires values of surface interfacial tension and wetting angles since it is based on the premise that the shape of the hydrate phase is determined by the surface interactions and wetting angles of liquid-water and gas-hydrate on the porous wall. Additionally, it was assumed that formation of gas hydrate would initially take place at the gas-water interface. Therefore, the hydrate phase would adopt the shape of a lens, i.e., the thickness of hydrate formed in the center of the pore is expected to be larger than that around the edges. The angle of the gas-hydrate interface on the porous wall is expected to be larger than that of hydrate-liquid interface. In order to keep the model predictive, values for interfacial tensions and wetting angles were procured from independent studies in the open literature.

A. Water-hydrate and gas-hydrate Interfacial tensions

Experimental measurements of interfacial tension between hydrates and liquid water at phase equilibrium conditions in porous media have not been reported in the literature. Therefore, theoretically-estimated values for hydrate-water interfacial tension proposed in the literature[71,81,86,88–90] were used to select the value of interfacial tension (as shown in Table 2). These values were tested against hydrate-ice-equilibrium conditions for 70-Å pores[91]. In 2001, Klauda and Sandler[72,74] proposed that water-hydrate interfacial tension should be the effective interfacial tension during gas hydrate formation in porous media. Klauda and other researchers applied the value of ice-liquid water interfacial tension ($\sigma_{IL} = 26.7\mathrm{mJ}/m^2$) in their models due to the similarities between hydrate and ice. In the following years, other theoretical values for water-hydrate interfacial tension were proposed by applying the Gibbs-Thomson equation to the reduction in hydrate-formation temperature in porous media with respect to this value in bulk phase[81,86,89].

Table 2. Theoretical hydrate-water interfacial tension used to predict methane-hydrate-formation pressures in 70Å-radius silica gel (based on Pesaran and Shariati [92])

hydrate-liquid interfacial tesion (mJ/m^2)	AAD%	References
72	18.89	Clarke *et al*., 1999
39	13.6	Uchida *et al*., 1999
32	12.83	Anderson *et al*.,2003
26.7	12.19	Henry *et al*., 1999; Smith *et a*l., 2002
17	10.98	Uchida *et al*., 2002

Due to the lack of direct experimental data for the interfacial tension between hydrate and liquid water phase, the theoretical value used in this work is the one with the highest accuracy in the prediction of hydrate-formation-pressure inside 70Å-radius silica gel as measured by Handa and Stupin.[85] The value of $17\ \mathrm{mJ}/m^2$ estimated by Uchida et al. in 2002 produced the highest accuracy for predicting hydrate-formation in silica gel with absolute average deviation (AAD%) of 10.98%, as presented in Table 2. As for the interfacial tension of hydrate-gas interface, it is assumed to be similar to the interfacial tension of ice. It has been reported that the interfacial tension of ice is $130\ \mathrm{mJ}/m^2$ [80].

B. Wetting angles

Most previous models [71–74,78,88], assumed that one interface, either between gas and liquid-water or between liquid-water and solid phases, was determinant of equilibrium. Therefore, the other interfaces were neglected. In addition, shape factors were applied in these models. Klauda et al. [72,74] proposed that hydrate initially formed in the shape of a spherical cap (a shape factor of 2) and eventually completely filled the cylindrical pores (a shape factor of 1). Other models assumed that the hydrate-liquid water always maintained a spherical cap (shape factor of 2) [71–74]. However, if the contributions of both interfaces (water-hydrate and gas-hydrate) are comparably significant, shape factors may not capture the hydrate phase accurately. This effect should be more marked at equilibrium conditions above 270K, where liquid water, solid hydrate and gas phase coexist inside the porous medium. An indication of this issue is apparent on the fact that predictions of the wan der Waals-Platteeuw (vdWP) model significantly overestimated the equilibrium pressures at temperatures higher than 269 K and fugacity model showed significant deviation above 274 K [74].

The wetting angle of liquid water on solid surface varies significantly depending on the solid surface. The experimental data for hydrate equilibrium in porous media used to compare the predictive capabilities of the proposed model used silica glass and silica gel as porous material. From the published literature, it was surmised that the measured average contact angles of water on silica glass is 24° [93] and 15.2° on silica gel [94]. There is no experimental measurement of the curvature of hydrate structures in porous media. In addition, there are also no theoretical estimates of the angle between the gas-hydrate-pore-wall phases since the models proposed thus far have not taken into consideration the contribution of the gas-hydrate-solid interactions.

3.4.2 Chemical Equilibrium

The chemical equilibrium, eq (12), was implemented in terms of fugacities rather than chemical potential, i.e., the fugacities of each component in all phases must be equal. Fugacities for each component in the gas phase were calculated from the Peng-Robinson equation of state. The fugacity of methane in liquid was calculated via the application of Henry's Law [2,72]. The fugacity of methane in the hydrate phase was calculated using the Peng-Robinson equation of state.

In the case of water in liquid and hydrate phase, chemical equilibrium requires that:

$$f_w^H(T, P^{H,G}) = f_w^L(T, P) \tag{21}$$

Where the fugacity of water in the hydrate phase can be calculated with the following equation [72]

$$f_w^H(T, P^{H,G}) = \exp\left(\frac{\mu_w^H - \mu_w^{IG}}{RT}\right) = \exp\left(\frac{(\mu_w^H - \mu_w^{e\beta} + \mu_w^{e\beta} - \mu_w^{IG})}{RT}\right)$$

$$= f_w^{e\beta}(T, P^{H,G})\exp(\frac{-\Delta\mu_w^H(T, P)}{RT}) \tag{22}$$

Where $f_w^{e\beta}(T, P^{H,G})$ is the fugacity of the hypothetical empty hydrate lattice. The Van der Waals and Plateeuw (vdWP) model was used to calculate the difference in chemical potential due to occupation of the empty hydrate lattice by gas molecules, as shown in the following equation [2]:

$$\Delta\mu_w^H = \mu_w^{e\beta} - \mu_w^H = \mu_w^{e\beta} - \mu_w^\pi = \Delta\mu_w^\pi \tag{23}$$

In eq (23), $\mu_w^{e\beta}$ is the chemical potential of water in the empty hydrate μ_w^π represents the chemical potential of water in other equilibrium phases (i.e. liquid water, ice, or both). $\Delta\mu_w^H(T, P)$ is the difference between the chemical potential of water in empty hydrate and filled hydrate phase, which can be calculated from the following equation [2,72].

$$\Delta\mu_w^H(T, P) = -RT\sum_m \nu_m \ln(1 - \sum_j \Theta_{mj}) \tag{24}$$

In eq (24), ν_m is the number of cage m per water molecule in the hydrate lattice Θ_{mj} represents the occupancy fraction of cage m by a guest j. The phenomena of cage occupation can be considered to be similar to Langmuir adsorption [2,3,72].

$$\Theta_{mI}(T, P) = \frac{C_{mI}(T) f_I(T, P)}{1 + \sum_j C_{mj}(T) f_j(T, P)} \tag{25}$$

Where $f_I(T, P)$ is the fugacity of guest I in gas phase $C_{mI}(T)$ is the Langmuir constant of component j in the cavity m that is defined as [2,3,72]

$$C_{mI}(T) = \frac{4\pi}{kT}\int_0^{R(cell)-a} \exp(-W(r)/kT) r^2 dr \tag{26}$$

In eq (26), $W(r)$ is the spherically symmetric cell potential, which shows the interaction between a guest and the cavity according to the distance r between the guest molecule and water molecules. This cell potential contains all guest-host interactions in the cage. According to Kihara model [73,95], cell potential can be expressed as

$$W(r) = 2z\varepsilon[\frac{\sigma^{12}}{R(cell)^{11}r}\left(\delta^{10} + \frac{a}{R(cell)}\delta^{11}\right) - \frac{\sigma^{6}}{R(cell)^{5}r}\left(\delta^{4} + \frac{a}{R(cell)}\delta^{5}\right)] \quad (27)$$

Where

$$\delta^N = [(1 - r/R(cell) - a/R(cell))^{-N} - (1 + r/R(cell) - a/R(cell))^{-N}]/N \quad (28)$$

In eq (27) and (28), z is the coordination number, $R(cell)$ is the radius of shell or the cavity. ε is the depth of the energy well, a is the core radius of gas molecule and σ is the core distance at zero potential. The gas parameters ε, a and σ are called Kihara parameters.

According to the vdWP model, the guest-host interactions are assumed to only exist between the first shell of water molecules and guest molecule. However, some other studies [96–99] have proven that the second and third shells of water molecules can also significantly interact with the guest molecule. That is, the cell potential $W(r)$ includes contributions from the first, second, and third shells as follows [72]:

$$W(r) = W(r)^{[1]} + W(r)^{[2]} + W(r)^{[3]} \quad (29)$$

The corresponding coordination numbers and cell radii for each shell used in this work are listed in Table 3 [72].

Table 3. Shell Radii

Struture	Cage	Shell Radius (Å)			Shell Coordination Number		
		1st	2nd	3rd	1st	2nd	3rd
I	5^{12}	3.906	6.593	8.086	20	20	50
	$5^{12}6^2$	4.326	7.078	8.285	24	24	50
II	5^{12}	3.902	6.667	8.079	20	20	50
	$5^{12}6^4$	4.682	7.464	8.782	28	28	50

The fugacity of water in the hypothetical empty hydrate lattice and liquid are calculated from eqs 30 – 31, respectively [72]:

$$f_w^{e\beta}(T, P^{H,G}) = P_w^{sat,e\beta}(T)\phi_w^{sat,e\beta}(T)\exp(V_w^{e\beta}(T, P^{H,G})(P^{H,G} - P_w^{sat,e\beta}(T))/RT) \quad (30)$$

$$f_w^{L}(T, P) = x_w(T, P)\gamma_w(x_w, T)P_w^{sat,L}(T)\phi_w^{sat,L}(T)\exp(V_w^{L}(T, P)(P - P_w^{sat,L}(T)/RT) \quad (31)$$

Where $P_w^{sat,i}(T)$ represents the vapor pressure of water in phase *i*. $\phi_w^{sat,i}(T)$ is the fugacity coefficient which was assumed to be equal to 1 because the vapor pressures of the water phase at the temperatures studied in this work is very low.

The solubility of methane gas in water in equilibrium with gas hydrates was estimated following the work by Klauda *et al*., [72] even though we realize that the confinement from porous medium will somewhat affect the methane gas solubility. In addition, the molar volumes for liquid water and empty hydrate lattice were also estimated by using the equations proposed by Klauda *et al*., [72] eqs (32 – 34). The molar volumes of liquid water phases used in Klauda's model were fitted to experimental data from NIST [100] with the average absolute deviation (%AAD) of 0.57%..

$$V_w^L(T[K], P[MPa])$$
$$= \exp(-10.9241 + 2.5 \times 10^{-4}(T - 273.15) - 3.532 \times 10^{-4}(P - 0.101325)$$
$$+ 1.559 \times 10^{-7}(P - 0.101325)^2)$$

(32)

$$V_w^{e\beta,I}(T[K], P[MPa])$$

$$= (11.835 + 2.217 \times 10^{-5}T + 2.242 \times 10^{-6}T^2)^3 \frac{10^{-30}N_A}{N_w^{\beta}} - 8.006 \times 10^{-9}P$$

$$+ 5.448 \times 10^{-12}P^2$$

(33)

$$V_w^{e\beta,II}(T[K], P[MPa])$$

$$= (17.13 + 2.249 \times 10^{-4}T + 2.013 \times 10^{-6}T^2 + 1.009 \times 10^{-9}T^3)^3 \frac{10^{-30}N_A}{N_w^{\beta}}$$

$$- 8.006 \times 10^{-9}P + 5.448 \times 10^{-12}P^2$$

(34)

The vapor pressures of water in ice and liquid water phase can be calculated with eq (35)[72], which was deduced by fitting the experimental data from the CRC Handbook[101] to quasi-polynomial, QL1 form[102]. This equation can also be applied beyond the range of fitting due to its good predictive capabilities[102]. This equation was proved by Klauda and Sandler [72] to be used to calculate the vapor pressure of water in the empty hydrate lattice, which is dependent on the guest and the structure of hydrate.

$$\ln(P_w^{sat}[Pa]) = A\ln(T) + \frac{B}{T} + C + DT$$

(35)

The values for the constants presented in eq (35) for ice liquid water and empty hydrate lattice were provided by Klauda and Sandler [72] (as shown is Table 4).

Table 4. Vapor Pressure Constants in eq (35) [72]

phase	A	B	C	$D\times10^3$
ice	4.6056	-5501.1243	2.9446	-8.1431
water	4,1539	-5500.9332	7.6537	-16.1277
guest	A	B	C	$D\times10^3$
CH_4 (sI)	4.6477	-5242.979	2.7789	-8.7156

3.5 Results and Discussion

The workflow depicted in Figure 6 was implemented in Matlab in order to solve the model numerically and thus predict the equilibrium pressures of gas hydrates in porous media. Eq (22) and (31) for fugacities are numerically solved with the Matlab variable-step solver with respect to the pressure. First, at a given temperature value, a pressure value was proposed to calculate the pressure in the hydrate phase using the eq (20). Afterwards, the chemical potential and fugacity of water in different phases was calculated from eqs (22, 24 and 31). The objective function to be minimized was the absolute value squared difference of water fugacities in different phases (i.e. chemical equilibrium). The pressure was corrected using a numerical Newton-Raphson technique until the objective function was within a given tolerance (10^{-9}).

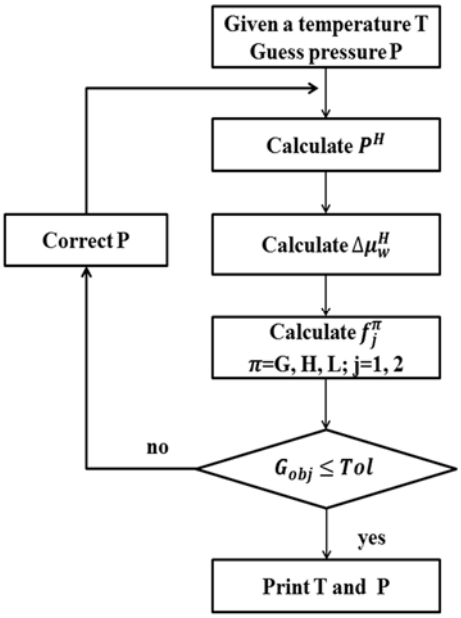

Fig.6. Schematic of the workflow for solving the equilibrium pressure at various temperatures.

3.5.1 Comparison of Model Predictions and Experimental Data

Figure 7, Figure 8, Table 5 and Table 6 depict the model predictions compared to experimental data and other models reported in the literature, respectively. As seen from Table 5 and 6, the proposed model predicts the experimental data with higher accuracy when compared to those of three other models for methane-hydrate-formation in porous media: vdWP model, Clark's model and Klauda's model.

Table 5. Percent AAD from Experiments of the Proposed Model Predictions of Porous Methane Hydrate

Porous media	water contact angle (τ)	hydrate contact angle (θ)	pore size	model %AAD
silica gel	15.2°	75°	34 Å	1.54
			70 Å	0.46
			152.5 Å	0.98
silica glass	24°	85°	59.5 Å	2.47
			154.4 Å	2.38
			247.5 Å	2.11

Table 6. Percent AAD from Experiments of Different Model Predictions of Porous Methane Hydrate

Model	%AAD		
	silica gel (Handa & Stupin 1992)	silica glass (Uchida 1999)	silica gel (Seo 2002)
VdWP model	6.342	7.609-18.243	——
Clark model	0.95-15	——	——
Klauda model	5.688	3.332-6.105	——
This work	0.38-0.56	2.11-2.47	0.55-1.54

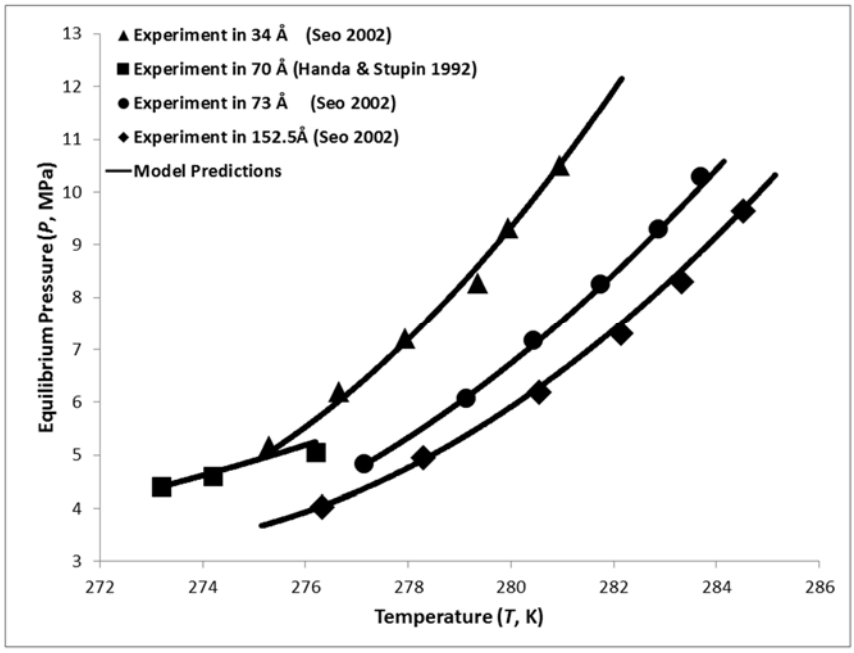

Fig.7. Equilibrium conditions of methane hydrate in silica gel pores.

Handa and Stupin[85] and Seo et al[103] measured equilibrium pressures of methane hydrate in silica-gel-porous-media. As seen in Figure 7 and Table 5, equilibrium pressures predicted with our model for the pore size of 70 Å show good agreement with experimental data provided by Handa and Stupin with percent absolute average deviation (%AAD) of 0.4862%. The model of Clark et.al.[71] overpredicts the equilibrium pressures with a deviation of 15%. The vdWP model performs with an average of 6.342%. Model of Klauda and Sandler also overestimates the equilibrium

pressures of methane hydrate by 5.688% compared with experimental data. Seo et al.[103] measured the equilibrium conditions of methane hydrates in silica gel samples of different pore sizes using a similar experimental procedure to that of Handa and Stupin.[85] As shown in Table 5, our model predictions for the given average-pore-size samples of 34 Å, 70 Å and 152.5 Å by Seo et al.[103] slightly overestimate the equilibrium pressures of methane-hydrate with %AAD of 0.9113%, 0.7951% and 0.1276%, respectively. As explained in the Model Description section, the gas-hydrate-pore wall angle had to be optimized for each material in order to better describe the experimental data. The angle of the gas-hydrate interface on the silica gel surface was determined to be 75° for pore sizes between 34 and 152.5 Å in this work.

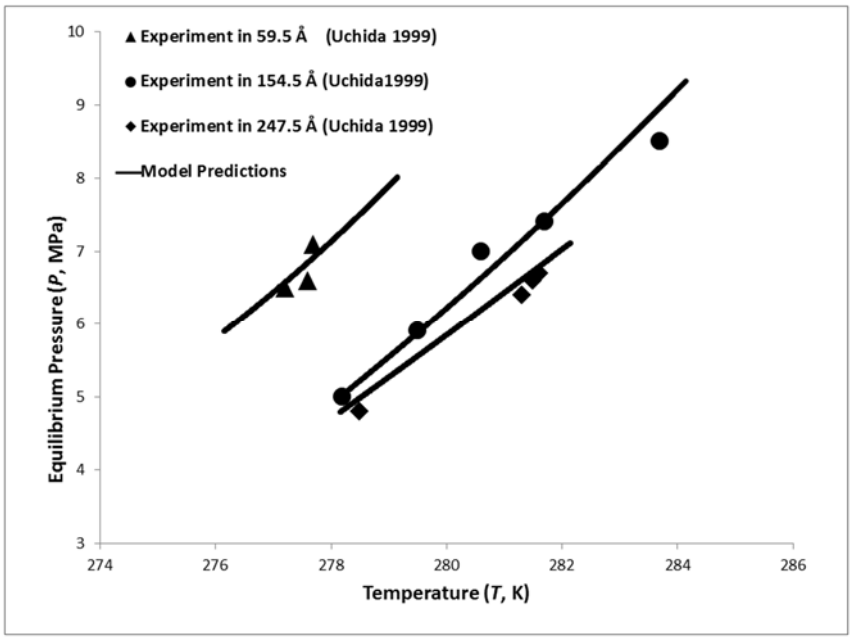

Fig.8. Equilibrium conditions of methane hydrate in silica glass pores.

For silica glass porous media, Uchida et al.[86] investigated the equilibrium pressures of methane hydrate in pore sizes of 59.5 Å, 154.5 Å and 247.5 Å at higher temperatures than 277 K. As shown in Table 6 and Figure 8, predictions of equilibrium pressures using the model proposed

in this work for the experimental samples of Uchida et al.[86] agree with the presented experimental data with %AAD of 2.0675%, 1.2598% and 0.0393%, respectively. The vdWP model over-predicted the equilibrium pressures with average deviations of 18.243%, 9.291% and 7.609%, respectively. The model of Klauda and Sandler also overestimated the equilibrium pressures of methane hydrate by 3.332%, 6.105% and 3.484%, respectively, compared with experimental data.[74] In the case of silica glass, the gas-hydrate interface on the silica glass surface was determined to be 85°.

3.5.2 Effect of Interfaces in Model Accuracy

Clark et al.[71] and Klauda et al.[74] employed shape factors to describe the structure geometries of methane hydrates in porous medium. The morphology of the gas-solid-liquid interfaces might be much more complicated than the assumed spherical cap or cylindrical cap. Interactions between the sediments and all phases present (free gas, liquid water and hydrate phases) probably play a significant role in shaping the geometries of methane hydrates formed in gas-hydrate reservoirs, as stated in Chong's work[75]. In order to investigate the effects of sediment properties on the equilibrium conditions of methane hydrates in porous media, contact angles, which relate to the wettability of porous surface, were incorporated in the new model as described in the Model Description section. This approach may explain why the proposed model depicted higher accuracy for describing experimental data when compared to previous models.

It has been proposed that the wettability of the sediments' surface can significantly influence the equilibrium pressures of gas hydrate in gas-hydrate reservoirs[75]. Surfaces can be classified into two types: hydrophilic (water attracting), and hydrophobic (water repellent) surface according to the surface properties. The hydrophilicity of the surface is captured by the contact

angle and the interfacial energy of water on the surface in the proposed model. In the hydrophilic surfaces, a larger amount of energy might be required to incorporate tightly-bound water to the surface into the hydrate phase, thus resulting in higher equilibrium pressures. The contact angle of water on silica glass and silica gel are similar. Thus, as depicted in Figure 9, the experimental equilibrium pressures of methane hydrate at similar pore sizes are also indistinguishable in these two porous materials. It is necessary to conduct a series of experiments with materials of dissimilar surface properties in order to determine the effects of wettability of the sediment on the equilibrium conditions of gas hydrate in porous media, which is described by the proposed model.

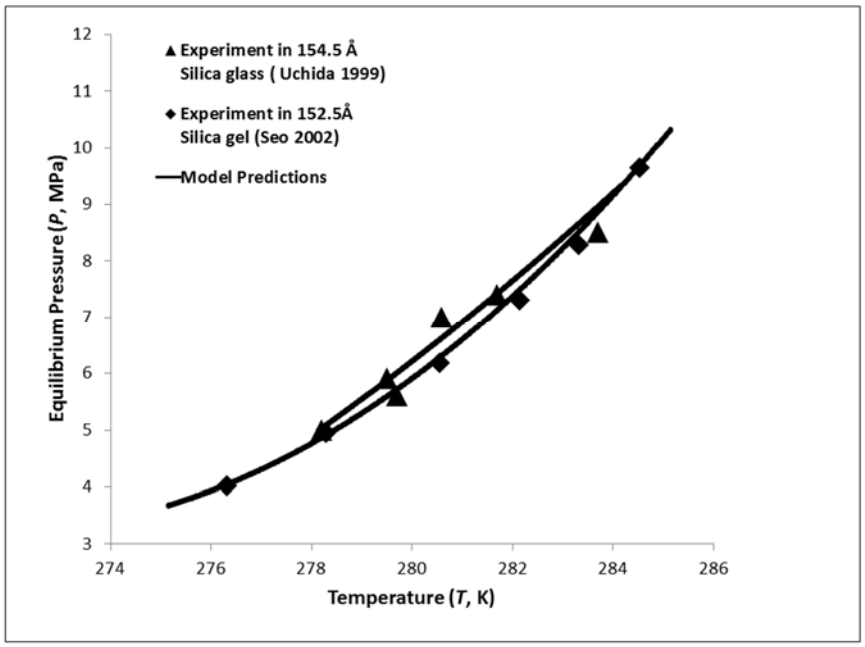

Fig.9. Equilibrium conditions of methane hydrate in 152-154 Å-radii porous media for different materials.

3.5.3 Effect of Kihara Potential Parameters on Model Accuracy

Investigations on previous models point towards the fact that model predictions are very sensitive to the values of Kihara parameters used, which can significantly influence the cavity occupations of gas hydrates[72]. Kihara parameters can be calculated from results of viscosity

measurements[104] or be derived from the second virial coefficient[105]. The values of Kihara potential parameters for methane guest used in gas hydrates reported in literature are listed in Table 7. In fact, the parameters for the Kihara potential were "tuned" to improve the performance of models in order to better predict experimental data in some cases.

In this work, we adopted parameters of the Kihara potential that were obtained via experiments aimed at characterizing the crystalline structure of hydrates. The parameter *a* (Å) represents the core radius of the guest gas molecule, which is considered a spherical core. In general, parameter a is believed to be a reliable parameter of general validity that should not be fitted, and it was fixed at 0.3834 Å (value provided by Sloan [3]). The parameter ε corresponds to the maximum attractive potential which is a measure of how strongly the guest molecule and the water molecules attract each other. This parameter is assumed to be constant in this paper for any given hydrate structure and it was fixed at the value provided by Sloan [3]. Finally, parameter σ, which stands for the core distance between guest molecule and water molecule at zero intermolecular potential, was allowed to float between the range of values listed in Table 7.

Table 7. Kihara potential parameters of CH4 from literature.

Reference	ε/k(K)	a (Å)	σ (Å)	Methods
JM Herri 2012	166.36	0.3834	3.05	Kihara parameters were calculated from experimental data
JM Herri 2011	157.85	0.3834	3.1439	Experimental study Kihara parameters were regressed from experimental results of this study
	154.47	0.3834	3.111	
	158.71	0.3834	3.1503	
Sloan 1998	154.54	0.3834	3.165	Experimentally fitted hydrate guest Kihara parameters
Sloan 2007	155.593	0.3834	3.1439	
A. L. Ballard 2000	154.1815	0.3834	3.1695	
L.S.Tee 1966	232.2	0.3834	2.7382	Kihara parameters were determined from experimental viscosities and/or second virial coefficients
Klauda & Sandler 2000	232.2	0.28	3.505	Kihara parameters were derived from viscosity or second virial coefficient data
Mohammadi 2005	153.69	0.295	3.2512	Experimental and model
Y. S. Kim 2003	141.52	0.3834	2.9488	Experimental and modeling work Kihara parameters were fitted to available data.
J. P. Schroeter 1983	153.22	0.30017	3.2363	Experimental study
D. Avlonitis 1993	227.13	0.393	2.779	Kihara potential parameters of gases from second virial coefficient data
M. A. Clarke 2003	151.7117	0.3834	2.2699	Kihara parameters were regressed by minimizing the differences between experimental data and predicted value.

In order to get a representative core-distance value, we simultaneously validated the model with the available experimental data points for each of the experimental systems used in this work. The goal was to maximize the probability of representing as many experimental data points as possible, within the constraint that the core distance correlated linearly with the temperature at the same rate (i.e., equal slope). It was found that the core distance slightly decreases with increasing pore size in the proposed model, as depicted in Figure 10. The reason for this phenomenon may be that the proposed model captures the effect of confinement on gas-hydrate-equilibrium conditions in porous media via slight variations of the core distance value. The value of core distance for different pore sizes ranged from 2.73 Å to 3.06 Å. When the pore radius becomes larger, the core distance value σ decreases towards the value for bulk hydrate phase. [104]

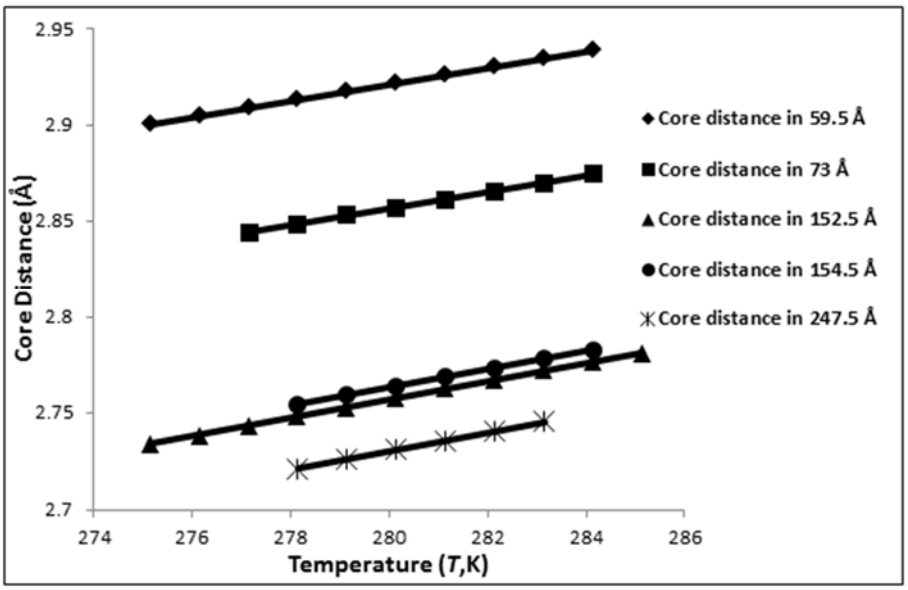

Fig.10. Schematic of relation between core distance and temperatures.

3.5.4 Prediction of Gas-hydrate Equilibrium in Large Sediment Pores

Gas hydrates naturally occur in the form of small hydrate crystals in sedimentary porous media. According to visual observations of gas hydrates within natural sediments, there are mainly

three types of gas-hydrates reservoirs: (1) poorly consolidated coarser-grained sediments containing massive blocks or sheets of gas hydrates; (2) unconsolidated, fine-grained and low permeability sediments containing cemented hydrates; and (3) consolidated rock such as clay and mud containing hydrate nodules, layers, and fracture- and vein-infillings[106–108]. The pore sizes of these common sediment samples are usually measured by mercury porosimetry and proton nuclear magnetic resonance (NMR)[107,109,110]. It has been found that pore diameters in these scenarios range from a macroscopic to microscopic scale[107]. For instance, sandstone usually has about 50% of its pores with size smaller than 54 microns. While shale has about 50% of its pores with size smaller than 20 nm[109,110]. Permafrost sediments are usually composed of unconsolidated gravels which can form larger pore sizes in millimeter scale[111]. Little experimental work has been conducted on predicting the equilibrium conditions of gas hydrates in large pores with diameter ranges from a few micrometers to few millimeters, as to provide suitable experimental data for validation of the proposed model.

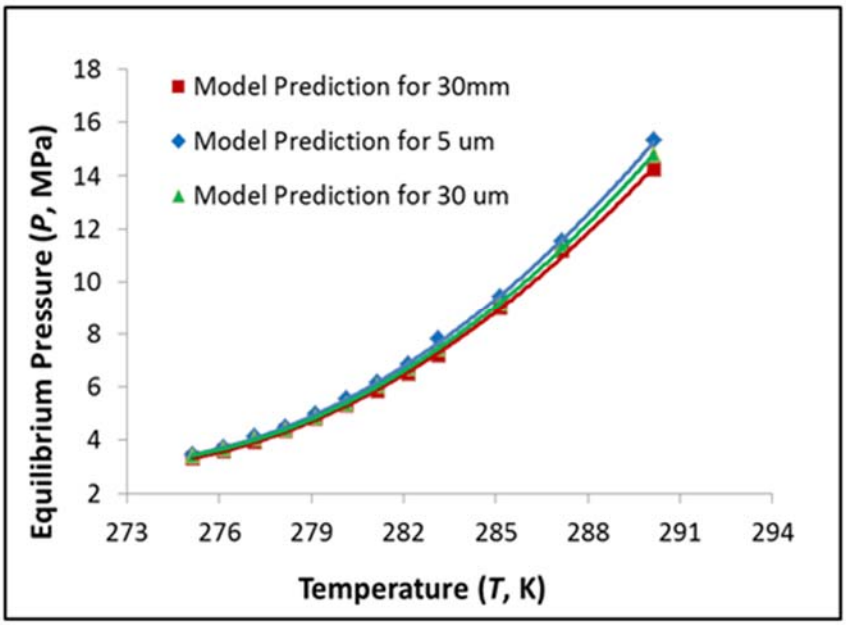

Fig.11. Model predictions for gas hydrate equilibrium in sample natural sediments. Note that no fittings were used in order to improve the smoothness of the predicted data.

In order to better understand the equilibrium conditions of gas hydrates in natural sediments, the equilibrium conditions of gas hydrates in porous media with mean pore radii of 5 μm, 30 μm and 30 mm are predicted with the proposed model. As shown in Figure 11, the equilibrium pressure of gas hydrates in these types of porous media range from 3.4 MPa to 15.3 MPa when the temperature increase from 275.15 K to 290.15 K. In porous media with smaller pore size, slightly larger pressures are required to help gas hydrates reach at the equilibrium states.

3.6 Conclusions

A model for gas-hydrate equilibrium in pores developed from basic thermodynamic analysis is proposed and validated against available experimental data in this work. The proposed model presents high predictive accuracy when compared to experimental data with the average AAD of less than 1%. The mechanical equilibrium condition of the model takes the effects of sediment properties (wettability, interfacial tension) into account to describe the conditions of stability of gas hydrate in porous media, in a very straight-forward manner. The wettability of the pore surface affects the equilibrium pressures of gas hydrate formed in porous media, and the shape of the hydrate phase. However, experimental data are available only for surfaces of similar surface properties. The effects of sediment properties captured in the proposed model should be further tested experimentally.

CHAPTER 4 INTERFACIAL EFFECTS ON THE ENERGY BARRIER FOR GAS-HYDRATE CAGE AND ICE HETEROGENEOUS NUCLEATION

4.1 Motivation

Naturally, hydrate-bearing sediments usually exhibit low porosity and permeability with microscale pore sizes[74,75,112]. In synthetic porous media for gas-hydrates formation, nanoscale pore sizes are commonly encountered[81,85,86]. Thus, heterogeneous nucleation takes place more frequently than homogeneous nucleation because of the extremely slow nucleation rate of homogeneous nucleation[113]. With the presence of foreign surfaces, including gas-liquid interfaces, solid-liquid interfaces and gas-liquid-solid triple boundary lines, the energy barrier for nucleation can be effectively reduced, and nucleation can be facilitated. Therefore, it is critical to understand how foreign surfaces modulate the energy barrier enabling heterogeneous nucleation.

The phenomenon of ice formation and growth in porous media (e.g. sediments) has attracted considerable research effort in recent years due to the fact that large parts of the earth's surface are covered by cold or seasonally-frozen regions. In these regions, sediment pores are filled with ice and expanded by the growth of ice crystals due to water transfer and accumulation from unfrozen areas to frozen areas. When temperature is above the freezing point, the melting of solid ice weakens the pore structure because the damaged pores lose the support of solid ice[114–117]. As a result, the cycle of liquid freezing in the winter and thawing in the spring results in severe damage to external facilities, such as road pavement, natural gas or water pipelines, buildings and other civil structure foundations. From the freshwater resource perspective, about 75% of the freshwater on earth is stored as ice in sediments. Preventing the phenomenon of frost heave, i.e. ice formation, may benefit the biota in those sediments[118]. Therefore, it is crucial to understand the nucleation and growth processes of ice in porous media in order to predict and further prevent the phenomenon of frost heave.

Most of the experimental and theoretical work on frost heave has focused on the growth of existing ice crystals inside porous media[114–116,118,119]. According to the work of K. A. Jackson and Bruce Chalmers, the types of soil, contact angles for the ice-soil interface, grain size and permeability of the soil may significantly influence the rate of growth of heave[120]. However, there is a dearth of work on the nucleation process itself, i.e., the birth of ice crystals in the first place. As we all know, nucleation is the first step in the kinetic formation of a new thermodynamic phase. It will be extremely helpful to slow down the heave rate by reducing the nucleation rate or inhibiting nuclei formation.

With respect to the formation of gas hydrates, understanding the nucleation process of gas hydrates is of great importance to understand the formation mechanisms of gas hydrates. Gas hydrates form in natural gas pipelines and laboratory environments under proper temperature and pressure conditions. In addition, gas hydrates naturally exist in mesoporous sediments containing pores with diameters in the micro-size or nano-size region[121,122]. In bulk liquid or large pores, some experimental work on gas hydrates formation suggests that gas hydrates preferentially form a hydrate film at the gas/liquid interface[123,124]. In micro-size or nano-size pores, gas hydrates are likely to form at the triple boundary lines along the gas/liquid/solid three phases[125]. Therefore, the gas/liquid interfaces and the triple boundary lines play an important role in the heterogeneous nucleation process of gas hydrates formation.

Studying the nucleation process with experimental methods is extremely challenging due to the experimental-resolution limitations on time and space scale. Recently, some researchers studied the nucleation of ice in the presence of solid surfaces with Molecular Dynamics (MD) Simulations, which is an effective method to study the mechanism of heterogeneous nucleation process[67,126–128]. However, the nucleation rate of ice in porous media can’t be quantitatively

analyzed with MD simulations due to limitations of time and length scale. Experimental methods can provide macroscopic rates of crystal growth, but not initial nucleation rates[129–132]. Therefore, a macroscopic mathematic model that captures nucleation rate and incorporates this phenomenon in the rate of crystal growth to allow comparison with experimental data, would be the most effective approach to study the problem. In recent years, some theoretical investigations have been conducted to study the heterogeneous nucleation of ice on the surface of insoluble particles using the theoretical framework of Classical Nucleation Theory (CNT)[133–135]. However, there are few theoretical studies aiming to quantitatively describe how sediment surfaces modulate the nucleation process. In addition, to the best of our knowledge, few theoretical work has been conducted to describe the effects of gas/liquid interfaces on gas hydrates nucleation and no work reported on gas hydrates nucleation at the triple boundary lines.

In this chapter, a mathematical model was developed with incorporation of careful thermodynamic analyses in order to understand the effects of confinement surfaces properties, including contact angle, substrate size and surface geometry, on the nucleation energy barrier of ice/gas-hydrates in porous media. Taking this study one step further, future work will be conducted to predict the nucleation rate of ice and gas-hydrates in porous media and understand how various interfaces properties modulate the nucleation process of ice/gas-hydrates in porous media.

4.2 Types of Interfaces

Foreign interfaces are very commonly encountered during the heterogeneous nucleation process in sedimentary porous media. For example, confinement walls within sediments, dust particles or inhibitors in porous media, liquid-solid interfaces (planar, concave and convex surfaces) are frequently encountered during the nucleation process[136]. With the assumption of the presence

of continued gas and liquid phases in porous media, gas-liquid interface should be considered during the nucleation process in bulk solution or in large pores. With the formation of ice/gas-hydrates in small pores, three-phase boundary lines might exist in porous media. The properties of these interfaces (contact angle, interfacial energy, and substrate curvature) no doubt play an important role in modulating the nucleation process of gas hydrates.

4.3 Model Description on Correction Factors

According to classical nucleation theory (CNT), the nucleation of ice/gas hydrates is a process of statistical fluctuation of building molecules in supersaturated liquid due to thermal vibration, which can result in the occurrence of some unstable ordered solid molecular clusters. These clusters will shrink or expand as the fluctuation of monomers in the liquid allows for incorporation of water molecules into the clusters. In this case, the flux of building molecules into the critical nucleus is thermodynamically favored. Then, a stable solid phase can be formed from the liquid phase after the nucleation and growth processes taking place[133]. The nucleation process can be described by the nucleation rate, which is characterized as the number of critical nuclei formed over a time unit. In order to quantitatively analyze the nucleation process, a thermodynamic component (the change of Gibbs free energy during the formation of the critical ice nucleus from the liquid phase) and a kinetic component (diffusive flux of water molecules) should be incorporated into the formulation of nucleation rate[133,134].

Heterogeneous nucleation is more common in nature due to the presence of interfaces, including gas/liquid interface, liquid/solid interface, and gas/liquid/solid triple boundary lines. In the case of ice, the nature of the interaction between water molecules and the surface may also play a role in nucleation, i.e., hydrophobic or hydrophilic interactions. These effects will be

relevant when studying ice nucleation in soils and porous materials. Three types of surfaces, including flat, concave and convex surfaces, are the most common surfaces in porous materials and sediments. From the thermodynamic perspective, a flat surface is the simplest geometry which can significantly lower the energy barrier for heterogeneous nucleation[136–138]. From the perspective of practical situations, concave surfaces such as pore walls and convex surfaces such as dust particles are more commonly encountered in mesoporous sediments[136,137,139]. In the case of gas hydrates, the nucleation of gas hydrates likely happens at the interface of gas/liquid in the bulk of aqueous solution or in large pores and fractures as suggested in open literature[123,124]. In micro-size or nano-size pores, the triple boundary line plays an important role in the nucleation process of gas hydrates.

4.3.1 Correction factors for heterogeneous nucleation at the gas/liquid interface

In the bulk of an aqueous solution or in large pores, the interface of gas/liquid is flat. A lens-shaped critical nucleus forms at the gas/liquid interface (Figure. 12). As shown in Figure. 12, θ_1 and θ_2 represent the angles of the crystal/gas and the crystal/liquid interfaces, respectively. The values of θ_1 and θ_2 depend on the interfacial energies between the phases present (σ_{12}, σ_{13} and σ_{23}). The radius of the two hemispherical caps are described with r_1 and r_2, respectively. The change of Gibbs free energy during nucleation process can be mathematically expressed as follows, including a volume term and a surface term:

$$\Delta G = \Delta g_v V_i + \sigma_{12} A_{12} + \sigma_{23} A_{23} - \sigma_{13} A_{13} \tag{36}$$

Where numbers 1, 2 and 3 denote the gas phase, critical nucleus and liquid surface, respectively. The parameter σ_{ij} is the interfacial energy between phase i and phase j. The quantity A_{ij} is the

interfacial area between phase i and phase j. Parameter V_i is the geometrical volume of the critical nucleus.

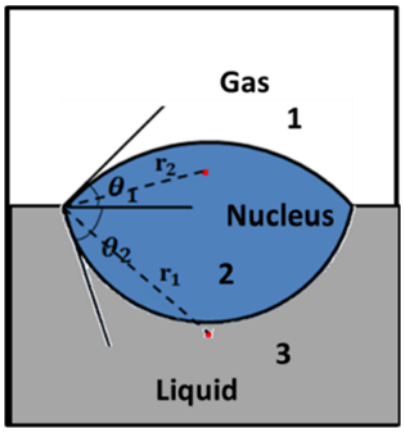

Fig. 12. Schematic of the formation of a lens-shape nucleus at the gas/liquid interface.

Through careful geometrical and mathematical analysis, we can get a suite of correlations between nucleus volume and interfacial areas. The correlations are as follows,

$$V_i = \frac{1}{3}\pi[r_1^3(2 - 3m_1 + {m_1}^3) + r_2^3(2 - 3m_2 + {m_2}^3)] \tag{37}$$

$$A_{12} = 2\pi r_1^2(1 - m_1) \tag{38}$$

$$A_{23} = 2\pi r_2^2(1 - m_2) \tag{39}$$

$$A_{13} = \pi r_1^2(1 - {m_1}^2) \tag{40}$$

Where $m_1 = cos\theta_1, m_2 = cos\theta_2$. The relationship between interfacial energies and geometrical angles is given by eq (41) according to the Law of Sines.

$$\frac{\sigma_{12}}{sin\theta_2} = \frac{\sigma_{23}}{sin\theta_1}$$

(41)

and

$$r_1 sin\theta_1 = r_2 sin\theta_2$$

(42)

Combining all these equations, we can derive the free energy ΔG for the nucleation of critical nucleus at the gas/liquid interface by substituting Equation (37) – (40) into eq (36). In so doing, we are naturally incorporating the effects of the gas/liquid interface into the expression of the energy barrier for nucleation, as follows:

$$\Delta G = \frac{1}{3}\pi[(\Delta g_v r_1^3 + 3\sigma_{12} r_1^2)(2 - 3m_1 + {m_1}^3) + (\Delta g_v r_2^3 + 3\sigma_{23} r_2^2)(2 - 3m_2 + {m_2}^3)]$$

(43)

Where r_1 is represents the radius of the critical nucleus required for a given energy barrier for the nucleation of a critical nucleus. By taking the first derivative of this free energy with respect to r_1, we obtain eq (44).

$$\frac{\partial \Delta G}{\partial r_1} = \pi r_1 (r_1 \Delta g_v + 2\sigma_{12})(2 - 3m_1 + {m_1}^3)$$

(44)

When we set the first derivative to zero, we can get the critical radius of nucleus leading to crystal growth and its associated energy barrier, which includes a correction factor for modifying the homogeneous nucleation energy barrier to be used in heterogeneous nucleation at the gas/liquid

interface. The corresponding equations for the critical radius, the energy barrier and the correction factor are given below:

$$r_1 = -\frac{2\sigma_{12}}{\Delta g_v} \tag{45}$$

$$\Delta G^* = \frac{16\pi\sigma_{12}^3}{3\Delta g_v^2} f(\theta) \tag{46}$$

$$f(\theta) = \frac{1}{4}[(2 - 3m_1 + {m_1}^3) + \left(\frac{1 - {m_1}^2}{1 - {m_2}^2}\right)^{3/2} (2 - 3m_2 + {m_2}^3)] \tag{47}$$

Where $f(\theta)$ represents the correction factor to describe the effects of the gas/liquid interface on the energy barrier for heterogeneous nucleation.

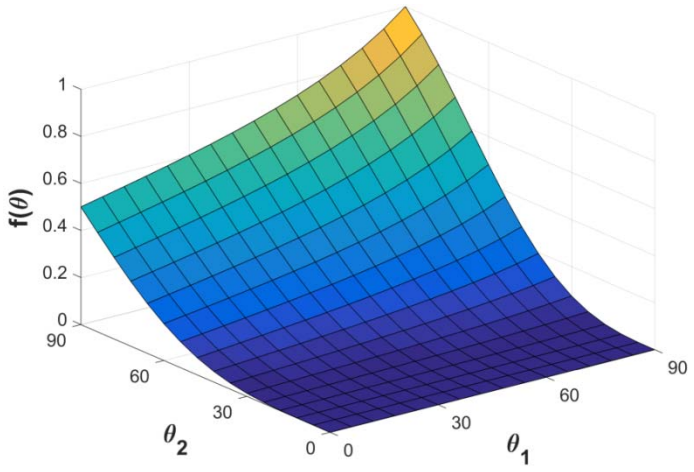

Fig. 13. Correction factor for nucleation at gas/liquid interface as a function of angle θ_1 and angle θ_2.

Figure 13 depicts the dependence of the correction factor $f(\theta)$ on the geometrical angles of the crystal nucleus. As shown in Figure 13, the correction factor increases with incresing value of θ_1 and θ_2, and varies in the range of $0 \sim 1$. When both of θ_1 and θ_2 take the value of $90°$, the correction factor is 1, and the critical nucleus will form the shape of sphere. This scenario corresponds to homogeneous nucleation, which is highly unlikely. Conversely, when the values of θ_1 and θ_2 are equal to zero, the correction factor is zero. In this case, there is no energy barrier for the nucleation process. The nucleation process happens spontaneously at the interface of gas/liquid in the shape of a flat film. This scenario takes place at very beginning of the nucleation process. However, as the nucleus grows, it adopts a lens shape with the hemispherical caps determined by interfical energies. Lenses of ice or gas hydrates have been observed in nature.

4.3.2 Correction factors for heterogeneous nucleation on a solid substrate

A good starting point for the analysis of heterogeneous nucleation on a solid surface is to study the nucleation process on a planar surface. Furthermore, the nucleation process on a planar surface can be used as a control system to examine the physical meaning of models for concave surfaces (i.e., pore wall and porous materials) and convex surfaces (i.e., dust particles). In fact, a pore can be modeled via imposing curvature on a flat surface to form a cylinder. A particle surface can be assumed as a curved flat surface with spherical shape.

The flat surface is assumed to be smooth in order to better formulate the model for the nucleation process from the thermodynamic perspective. Figure 14 depicts a schematic of a spherical-cap nucleus forming on a flat surface. Numbers 1, 2 and 3 are used to represent the liquid phase, critical nucleus and solid flat surface, respectively. The parameter σ_{ij} is the interfacial energy between phase i and phase j.

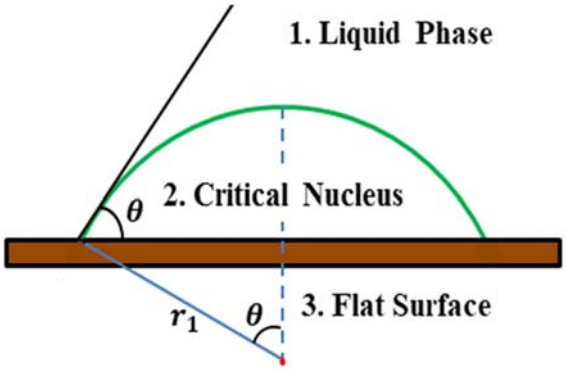

Fig. 14. Schematic of the formation of a spherical-cap ice nucleus on a planer surface.

Applying the same procedure used for nucleation at a gas/liquid interface, one formulates an expression for the Gibbs free energy required to form the critical nucleus and calculates its first derivative to obtain the critical radius [136]:

The only difference is the application of Young's Equation in order to correlate contact angle to interfacial energies for the system depicted in Figure 14:

$$\sigma_{13} - \sigma_{23} = \sigma_{12} cos\theta \tag{48}$$

We can obtain the following equation for the Gibbs free energy required to form the critical nucleus; as described above:

$$\Delta G = (\frac{1}{3}\pi r_1^3 \Delta g_v + \pi r_1^2 \sigma_{12})(2 - 3cos\theta + cos^3\theta) \tag{49}$$

The critical size of the nucleus and the energy barrier for forming the nucleus are derived by differentiating eq (49) with respect to nucleus radius (r_1). The first-order derivative must be zero, which allows to obtain the critical size r_1, as shown below.

$$\frac{\partial \Delta G}{\partial r_1} = \frac{(4\pi r_1^2 \Delta g_v + 8\pi r_1 \sigma_{12})(2 - 3cos\theta + cos^3\theta)}{4}$$

(50)

There is only one solution for $\frac{\partial \Delta G}{\partial r_1} = 0$ in this case:

$$r_1 = -\frac{2\sigma_{12}}{\Delta g_v}$$

(51)

Then we can obtain the critical energy ΔG^* for the critical nucleus on the smooth flat surface by substituting Equation (51) into Equation (49), which allows for the identification of a correction factor for Gibbs energy that takes into consideration the presence of the flat surface.

$$\Delta G^* = \frac{16\pi\sigma_{12}^3}{3\Delta g_v^2} f(\theta)$$

(52)

$$f(\theta) = (2 - 3cos\theta + cos^3\theta)/4$$

(53)

Where $f(\theta)$ is the correction factor for heterogeneous nucleation in the presence of a smooth flat surface, value of this correlation varies with the contact angle with the flat surface. One should note that the shape of the nucleus as a hemispherical cap on the flat surface is reflected in the correction factor. A similar analysis procedure is employed in order to derive the correction factors for nucleation on concave and convex surfaces in the following sections.

Pores of mesoporous sediments are idealized as cylindrical pores (concave surfaces) and dust particles are assumed to take the shape of spheres (convex surfaces). Figure 15 shows a schematic of the expected geometries for nucleation on curved surfaces: a semi-spherical-cap nucleus inside the pore wall (concave surface), and a semi-spherical-cap nucleus on the outer surface of the spherical particle (convex surface), respectively. Similar to the case of a flat surface, 1, 2 and 3 represent the liquid phase, critical nucleus and solid substrate, respectively. The

parameter V_i represents the volume of the formed critical nucleus. The quantity σ_{ij} is the interfacial energy between phase i and phase j. The parameter A_{ij} is the interfacial area between phase i and phase j. The angle θ is the contact angle between the critical nucleus and the substrate, while angles θ_1 and θ_2 are the geometric angles. The following radii are defined as follows: r_1 is the critical size of the nucleus and r_2 is the radius of the substrate. In the case of concave surface, $\theta = \theta_1 + \theta_2$. However, in the case of convex surface, $\theta = \theta_1 - \theta_2$.

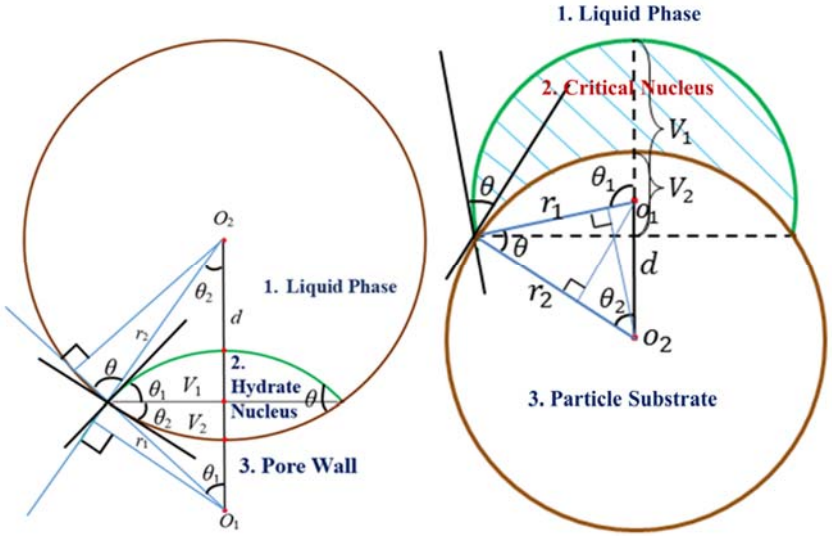

Fig. 15. Schematic of the formation of a spherical-cap ice nucleus on the pore wall (left) and dust particle (right).

From geometric analysis, the volume of the critical nucleus with critical size on the solid substrate can be calculated from the following equations:

$$V_i = \frac{1}{3}\pi r_i^3\left(2 - 3cos\theta_i + cos\theta_i{}^3\right) \quad (i = 1, 2) \tag{54}$$

Here, if the nucleation process occurs on concave surface, $V_i = V_1 + V_2$. Otherwise, if nucleation process happens on convex surface, $V_i = V_1 - V_2$. In addition, from the same geometrical analyses, the interface areas of the spherical-cap nucleus are derived as follows:

$$A_{12} = 2\pi r_1^2(1 - cos\theta_1)$$

(55)

$$A_{23} = 2\pi r_2^2(1 - cos\theta_2)$$

(56)

Substituting equations (54) through (56) into equation (36), the final expression for the change in free energy is as follows:

$$\Delta G = \frac{1}{3}\pi\Delta g_v[r_1^3\left(2 - 3cos\theta_1 + cos{\theta_1}^3\right) + r_2^3\left(2 - 3cos\theta_2 + cos{\theta_2}^3\right)] + 2\pi\sigma_{12}[r_1^2(1 - cos\theta_1) - r_2^2(1 - cos\theta_2)cos\theta]$$

(57)

$$\Delta G = \frac{1}{3}\pi\Delta g_v[r_1^3\left(2 - 3cos\theta_1 + cos{\theta_1}^3\right) - r_2^3\left(2 - 3cos\theta_2 + cos{\theta_2}^3\right)] + 2\pi\sigma_{12}[r_1^2(1 - cos\theta_1) - r_2^2(1 - cos\theta_2)cos\theta]$$

(58)

Equations (57) and (58) correspond to the free energy change for nucleation on a concave pore wall and a convex particle, respectively. The critical size of the nucleus and the energy barrier for forming the nucleus can be obtained via differentiating the equations (57) and (58) with respect to radius and equating the results to zero, in a similar way as it was done for the flat surface case. The first-order derivative of ΔG corresponds to the following equation:

$$\frac{\partial\Delta G}{\partial r_1} = \pi r_1(\Delta g_v r_1 + 2\sigma_{12})\left(2 - 3cos\theta_1 + cos{\theta_1}^3\right)$$

(59)

When equating the previous expression to zero, the critical size r_1 is obtained:

$$r_1 = -\frac{2\sigma_{12}}{\Delta g_v}$$

(60)

Substituting equation (60) into equations (57) and (58) and rearranging terms, the equations used to calculate the free energy required to form the critical nucleus of critical size of r_1 can be obtained for both cases as follows:

$$\Delta G^* = \frac{16\pi\sigma_{12}^3}{3\Delta g_v^2} f(x,\theta)$$

(61)

$$f(\theta) = [1 - X^3 - 3x^2 cos\theta(1 - Y) - x^3(2 - 3Y + Y^3)]/2$$

(62)

$$f(\theta) = \left[1 - X'^3 - 3x^2 cos\theta(1 - Y') + x^3\left(2 - 3Y' + Y'^3\right)\right]/2$$

(63)

Where $x = r_2/r_1$; $X = \frac{1+xcos\theta}{\sqrt{1+x^2+2xcos\theta}}$; $Y = \frac{x+cos\theta}{\sqrt{1+x^2+2xcos\theta}}$; $X' = \frac{xcos\theta-1}{\sqrt{1+x^2-2xcos\theta}}$; $Y' = \frac{x-cos\theta}{\sqrt{1+x^2-2xcos\theta}}$

Where x is the aspect ratio, i.e., the ratio of substrate radius to critical radius of nucleus. Again, the parameter f coresponds to the correction factor or geometric factor to describe the effects of surfaces on the energy barrier for heterogeneous nucleation. Eqs (62) and (63) present the geometric factor for concave surface and convex surface, respectively. These two equations, are similar to the ones derived by Fletcher [139] and Qian [136,137] for the case of convex surfaces, and can be used in order to incorporate the effects of concave and convex surfaces on the energy barrier of nucleation. These two equations show that the correction factor f depends on contact angle θ and aspect ratio x.

The difference between the correction factors for the three types of surfaces (flat, convex or particle, and concave or pore) and the correction factor for the flat surface, , $\Delta f(\theta)$ is plotted as

a function of contact angle for different values of aspect ratio in Figure 16. Blue lines represent the difference between the correction factor for pore surfaces (concave) and flat surface as a function of contact angle at vaying values of aspect ratio (aspect ratio captures the relationship between pore size and critical nucleus radius). Green lines present the values of the difference in correction factor between convex surfaces (particles) and flat surfaces as a function of contact angle for different values of aspect ratio. The red line represents the reference, i.e., flat surface. The blue lines and green ones mostly overlapped with the red line when $x > 100$, which indicates that the substrate surface can be taken as a flat surface when the radius of the substrate is about 100 times larger than that of the critical ice nucleus ($r_2 = 100r_1$). When the contact angle is 180° (highly hydrophobic surface) the corresponding value of the correction factor is 1. In this case, the critical energy for forming critical nucleus is the same as that for homogeneous nucleation, i.e., the surface has no effect or benefit towards nucleation. When the contact angle is 0° (the surface is highly hydrophilic), there is no energy barrier for the nucleation process because the value of correction factor is 0, which suggests the formation of a solid film on the surface. Finally, when the aspect ratio, x, is infinite, the correction-factor equations for concave and convex surfaces simplify to the case of a flat surface (as shown in Figure 16), which implies that the effect of the curvature is lost.

One should also notice that nucleation on a concave pit (i.e., concave surface) is more favorable that nucleation on a particle (i.e., convex surface) from a correction factor perspective.

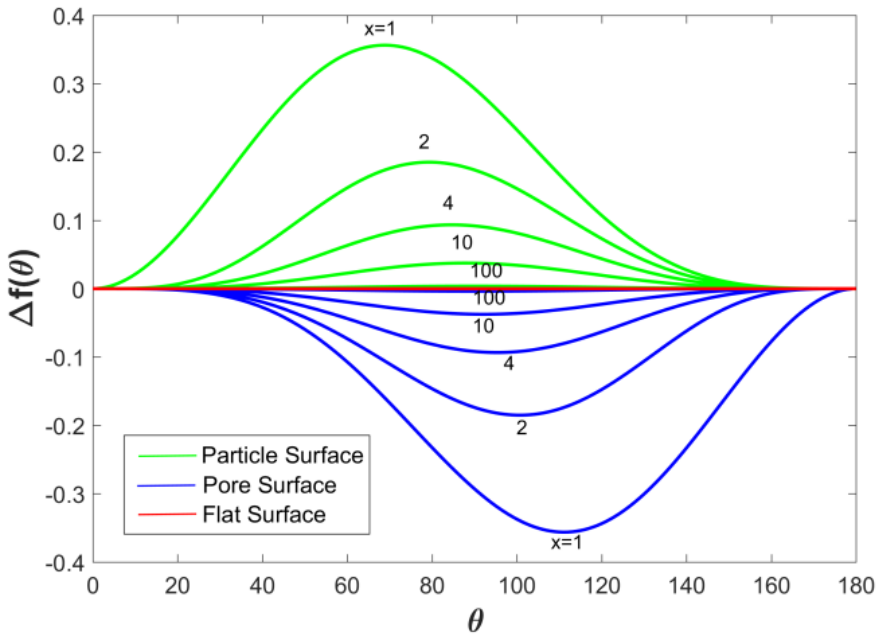

Fig. 16. Difference between the correction factor on a curved surface and a flat surface ($\Delta f = f_{substrate} - f_{flat}$) as a function of contact angle θ at different values of aspect ratio x.

4.3.3 Correction factors for heterogeneous nucleation at the gas/liquid/solid triple boundary line

In porous media, when gas, liquid and solid (three phases) are present in the system, the interfaces between the three phases can play an important role in the nucleation process. In the case of gas hydrates nucleation, experimental work has shown that the nucleation process of gas hydrates prefers to take place at the triple boundary line in porous media containing free gas and liquid phase [125]. In order to understand how the gas/liquid/solid triple boundary line affects the nucleation process inside pores, a similar thermodynamic analysis as the one used in the previous sections is applied to formulate the correction factor for lens-shaped crystal clusters formed along the gas/liquid/solid boundary lines (as shown in Figure 17). The parameters of θ_1 and θ_2 describe the contact angles of liquid and critical nucleus inside the confinement surface, respectively. The

values of angles θ_1 and θ_2 depend on the wettability properties of the confinement surface (i.e., the pore walls).

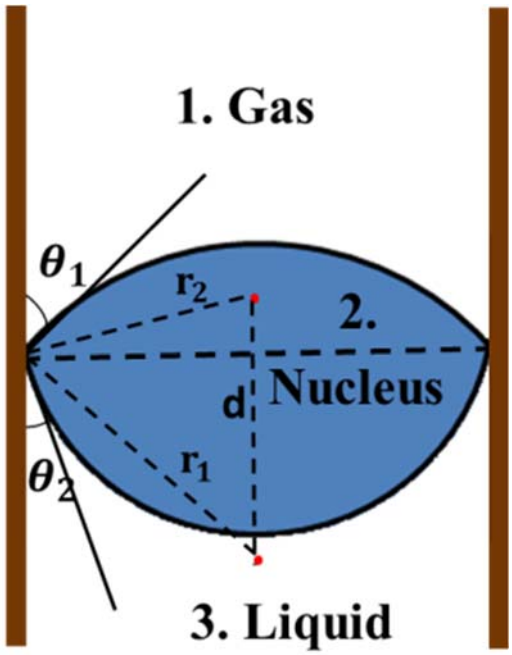

Fig. 17. Lens-shaped nucleus of hydrates at the gas/liquid interface in nanoscale pores.

The Gibbs free energy required to form the shape of nucleus along the triple boundary line depicted in Figure 17 is given by eq (64).

$$\Delta G = \Delta g_v V_i + \sigma_{12} A_{12} + \sigma_{23} A_{23} - \sigma_{13} A_{23} \tag{64}$$

Numbers 1, 2 and 3 are used to represent the gas phase, critical nucleus and liquid phase, respectively. The parameter σ_{ij} is the interfacial energy between phase i and phase j. The quantity A_{ij} is the interfacial area between phase i and phase j. Parameter V_i is the geometrical volume of the critical nucleus.

After careful geometrical and mathematical analysis, we can get the correlations for the volume of critical nucleus and interfacial areas. The correlations are as follows:

$$V_i = \frac{1}{3}\pi[r_1^3(2 - 3m_1 + {m_1}^3) + r_2^3(2 - 3m_2 + {m_2}^3)]$$

(65)

$$A_{12} = 2\pi r_1^2(1 - m_1)$$

(66)

$$A_{23} = 2\pi r_2^2(1 - m_2)$$

(67)

Where $m_1 = sin\theta_1, m_2 = sin\theta_2$. The relationship between interfacial energies and geometrical angles should follow eq (68) according to Young's Equation.

$$\sigma_{13} = \sigma_{23} + \sigma_{12}\cos[\pi - (\theta_1 + \theta_2)]$$

(68)

Then we can derive the free energy ΔG required to form the critical nucleus at the gas/liquid/solid triple boundary line by substituting equation (65) – (68) into eq (64), which allows for taking the incorporation of the effects of the triple boundary line into the expression for Gibbs free energy change.

$$\Delta G = \frac{1}{3}\pi\Delta g_v[r_1^3(2 - 3m_1 + {m_1}^3) + r_2^3(2 - 3m_2 + {m_2}^3)] + 2\pi\sigma_{12}[r_1^2(1 - m_1) + r_2^2(1 - m_2)\cos(\theta_1 + \theta_2)]$$

(69)

Where r_1 is assumed to represent the radius of the critical nucleus in order to obtain the energy barrier for the nucleation of critical nucleus. By taking the first derivative of free energy with respect to r_1, we can get eq (70).

$$\frac{\partial \Delta G}{\partial r_1} = \pi r_1 (r_1 \Delta g_v + 2\sigma_{12})(2 - 3m_1 + {m_1}^3)$$

(70)

Then set the first derivative to be equal to zero in order to obtain the critical radius of nucleus and energy barrier, which includes a correction factor for adjusting the term for homogeneous nucleation for application to heterogeneous nucleation at the gas/liquid/solid triple boundary line.

$$r_1 = -\frac{2\sigma_{12}}{\Delta g_v}$$

(71)

$$\Delta G^* = \frac{16\pi\sigma_{12}^3}{3\Delta g_v^2} f(\theta)$$

(72)

Through careful thermodynamic and mathematical analyses, the expression for the correction factor $f(\theta)$ of the lens-shaped hydrate nucleus inside pores is given by (73).

$$f(\theta) = \frac{1}{2}\left\{1 - {m_1}^3 + 3\frac{1 - {m_1}^2}{1 + m_2}\left(\sqrt{(1 - {m_1}^2)(1 - {m_2}^2)} - m_1 m_2\right)\right.$$

$$\left. - \left(\frac{1 - {m_1}^2}{1 - {m_2}^2}\right)^{3/2} [2 - 3m_2 + {m_2}^3]\right\}$$

Similar to the situation of nucleation at gas/liquid interface, the value of correction factor for nucleation at the triple boundary line depends on the values of θ_1 and θ_2. Where $m_1 = sin\theta_1$, $m_2 = sin\theta_2$, and the value of angle θ_1 varies from 0° to 180°, depending on the angle of the gas hydrates interface on a given solid surface. The angle θ_2 can take values between 0° and 180°, depending on the angle of the hydrate-liquid interface on a given surface. The values of these two

angles depend on the specific surface energies of gas/liquid, gas/hydrate and hydrate/liquid interfaces. The shape of the critical hydrate nucleus is determined by the values of these two contact angles. When these two angles vary in the range of 0° ~ 90°, it means that the confinement surface is water wetting (hydrophilic). Otherwise, when the confinement surface is hydrophobic, both of the angles will locate in the range of 90° ~ 180°.

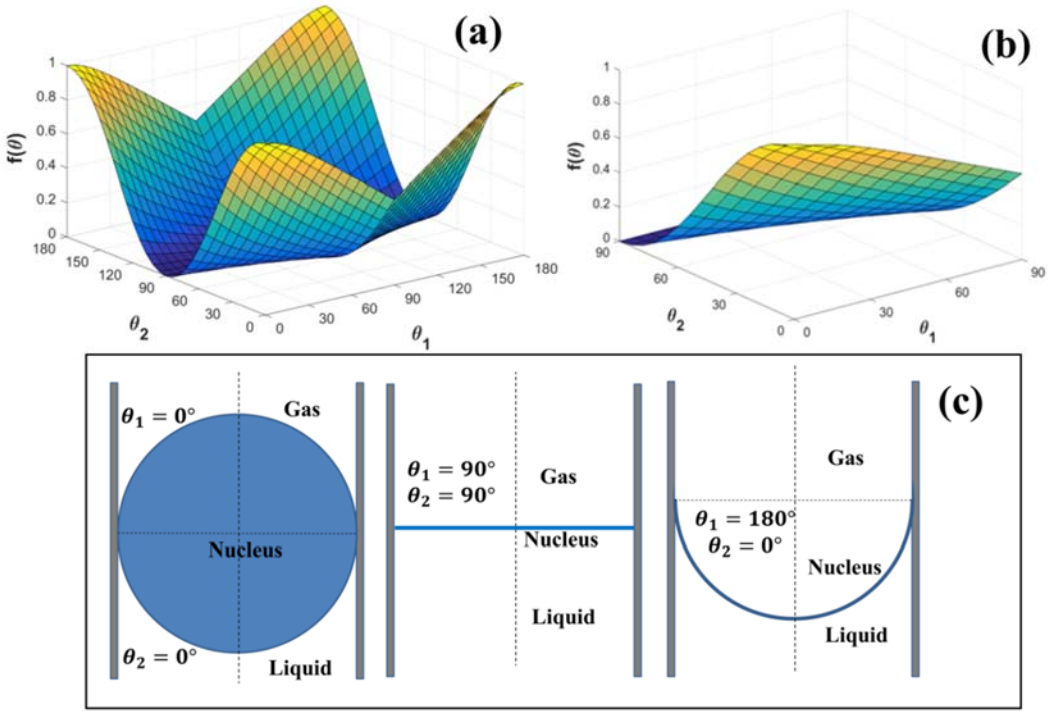

Fig. 18. Correction factor for nucleation at gas/liquid/solid triple boundary line as a function of contact angle θ_1 and θ_2 (a), (b) zooms in the region of 0° ~ 90° and (c) shows the schematics of nucleus formed under special conditions.

The correction factor for heterogeneous nucleation at the triple boundary line is plotted as a function of contact angle θ_1 and θ_2 (Figure 18(a) and 18(b)). As shown in Figure 18(c), at the special condition of $\theta_1 = 0°, \theta_2 = 180°$ or $\theta_1 = 180°, \theta_2 = 0°$, the correction factor takes the value of 1. This situation corresponds to the formation of a thin, spherical lens on a fully hydrophobic surface, which has not been observed. When θ_2 takes the value of 90° and for any

value of θ_1, the correction factor is equal to zero. Under this condition, the triple boundary line is flat and the nucleation process spontaneously occurs at the triple boundary line in the form of a flat film. This case has not been observed inside pores, but on gas/liquid interfaces. With respect to the conditions of $\theta_1 = 0°$, $\theta_2 = 0°$ or $\theta_1 = 180°$, $\theta_2 = 180°$, the critical nucleus takes a spherical shape that is the same as homogeneous nucleation. Thus, the values of correction factor are equal to 1. When $\theta_1 = 90°$, $\theta_2 = 0°$ or $\theta_1 = 90°$, $\theta_2 = 180°$, semi-spherical nuclei form at the gas/liquid/solid interface in the solution. In this case, the energy barrier for heterogeneous nucleation at the triple boundary line is half of that for homogeneous nucleation.

When the values of the contact angles zoom in the region of $0° \sim 90°$, as shown in Figure 18(b), we can observe that the value of correction factor for nucleation at the triple boundary line decreases with increasing the values of the contact angles θ_1 and θ_2. When $\theta_1 = 0°$, $\theta_2 = 0°$, the value of correction factor is equal to unity and the critical nucleus will take the shape of a sphere. In this case, water molecules in the liquid prefer to immobilize on the solid surface, and the triple boundary line doesn't support the nucleation process. The energy barrier for this condition is the same as that for homogeneous nucleation. That is, highly hydrophilic sediment surfaces do not support the nucleation process in the center of the pore. Nucleation preferentially occurs in porous media with slightly hydrophobic surface properties. Finally, the interaction of the liquid phase with the surface (captured in θ_2) more strongly determines the nucleation process.

4.4 Effects of Interfaces on Energy Barrier for Nucleation

4.4.1 Gas/liquid interface – bulk

The effects of gas/liquid interface on the energy barrier for nucleation are analyzed based on the previous thermodynamic work on correction factors. The model is applied to ice nucleation in order to explore its capabilities. Therefore, the parameter of interfacial energy σ_{12} for gas/ice is

applied to obtain the energy barrier for heterogeneous nucleation at the gas/liquid interface. The shape of the formed nucleus depends on the values of the geometrical angles θ_1 and θ_2.

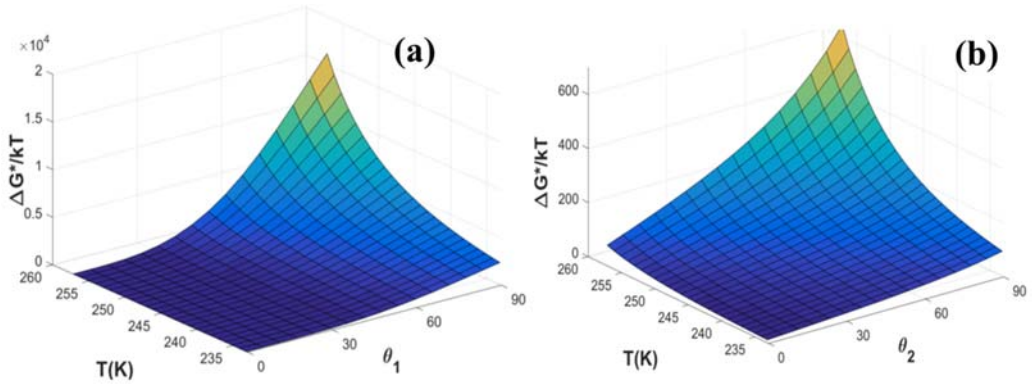

Fig. 19. (a) Energy barrier for nucleation at the gas/liquid interface as a function of θ_1; (b) Energy barrier for nucleation at the gas/liquid interface as a function of θ_2.

As shown in Figure 19, with increasing the temperature of the system, the energy barrier for nucleation will increase when either θ_1 or θ_2 is determined by the properties of water and gas phase. In order to understand the effects of geometrical angles on the kinetic nucleation, the effects of θ_1 and θ_2 on energy barrier for nucleation were studied separately. When the value of θ_2 is set as 30° (Figure 19(a)), the value of energy barrier increases with the value of θ_1 at any temperature plane. In a similar way, Figure 19(b) shows that the energy barrier also increases with θ_2 at any temperature plane when θ_1 is set at a certain value, for example 30° in this case. However, it must be noted that a much larger energy barrier must be overcome when θ_1 reaches a value of 90° in Figure 19(a) compared to that in Figure 19(b). Therefore, it's relatively easier for kinetic nucleation to occur on the liquid side of the interface rather than on the gas side.

4.4.2 Convex surface – particles and particulates

When the nucleation process occurs on grain particles, the properties of the particle surface can also modulate the nucleation process of ice in porous media. Figure 20(a) clearly shows that the energy barrier for ice nucleation on particle surfaces is smaller than that for homogeneous nucleation. When the contact angle is close to the value of 180°, particle surfaces do not support the nucleation process of ice. In this case, the value of the energy barrier for heterogeneous nucleation on particle surface (convex surfaces) is the same as that for homogeneous nucleation. As for the effects of contact angles, the nucleation process is favored by smaller contact angles, i.e., hydrophilic surfaces. In addition, the energy barrier for nucleation is increased with increasing temperature and the hydrophobicity of the system when the value of contact angle varies from 20° to 100°. The advantage of the presence of particles as nucleation sites is increasingly lost for contact angles greater than 100°.

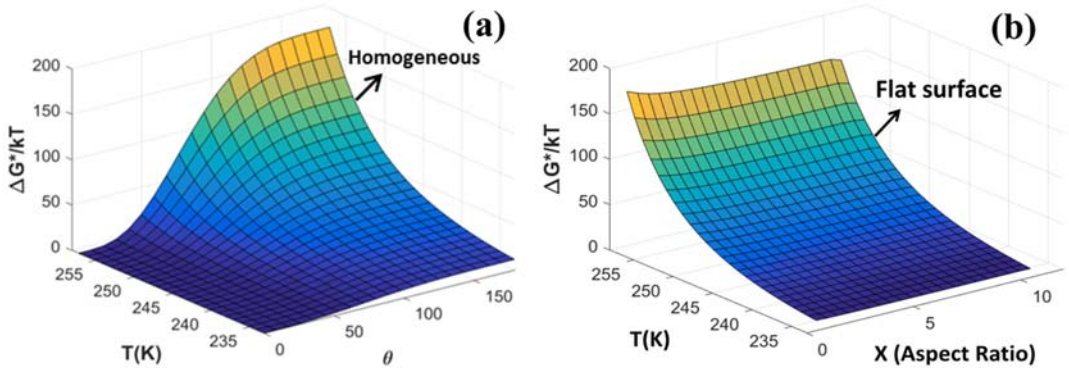

Fig. 20. (a) Energy barrier for nucleation on convex surfaces as a function of temperature and contact angle; (b) Energy barrier for nucleation on convex surfaces as a function of temperature and particle size.

As opposed to the beneficial effects of confinement on nucleation, one can see that the effects of particle size are marginal on nucleation. Figure 20(b) presents the dependence of energy barrier for nucleation on aspect ratio (x) (i.e., ratio of particle size over critical nucleus). It is clear

that the energy barrier for ice nucleation decreases with increasing the value of aspect ratio (x) for a given contact angle. That is, it is easier to nucleate on larger particles due to the smaller energy barrier for the nucleation process. In fact, the energy barrier for nucleation on convex surfaces is slightly larger than that on flat surfaces. As for the effects of particle size, the value of energy barrier decreases slightly when the aspect ratio increases from 0.5 to 10 at very low temperatures. Furthermore, the energy barrier on a convex particle surface is almost the same as that on a flat surface when the aspect ratio reaches at the value of 10. Interestingly, temperature, and not the presence of the surface, is the main factor influencing the energy barrier for nucleation on convex (i.e., particle) surfaces.

4.4.3 Concave surfaces – porous media

4.4.3.1 Effects of contact angles

In this section, effects of concave surfaces (pore wall) on the nucleation process are studied. In order to study the effects of contact angles on the energy barrier in porous media, the pore sizes were maintained at preselected values. Figure 21(a) depicts the effects of contact angle and temperature on the number of building units (i.e., water molecules) required to form a critical nucleus at an aspect ratio of 2, which translates into a pore radius twice as large as the critical nucleus radius. In the case of highly hydrophilic surfaces (contact angles close to zero) the pore surface resulted in smaller critical nuclei at all temperatures, i.e., less number of building-block molecules (n) were required to be incorporated into the critical nucleus. For contact angles between $30°$ and $150°$, lower temperatures significantly enhance the nucleation process by decreasing the number of building units needed to form a critical nucleus. In the case of highly hydrophobic surfaces, contact angles between $160°$ and $180°$, the positive effects of the pore walls

towards nucleation are increasingly lost at higher temperatures, leading to a region (represented by bright yellow in the figure), where nucleation happens as if in a homogenous phase. In addition, as we can see from Figure 21(a), larger super cooling (the difference between experimental temperature and water freezing point) consistently improves the kinetic nucleation of ice by reducing the size of the critical nucleus.

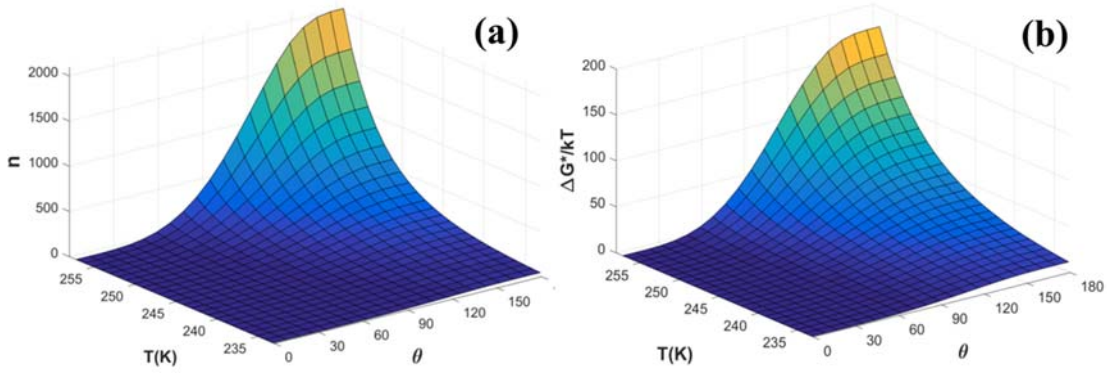

Fig. 21. (a) Size of critical ice nucleus changes with temperatures and contact angles in porous media; (b) Energy barrier for ice nucleation changes with respect to temperatures and contact angles in porous media.

Similarly, the energy barrier for ice nucleation is also modulated by the surface wettability of the porous media for any given pore size (Figure 21(b)). As shown in Figure 21(a), when the surface is highly hydrophilic (contact angle greater than zero and less than 40°), the energy barrier for nucleation is very close to zero. As the contact angle increases at any given temperature plane, one can notice a steep increase of the energy barrier at contact angles greater than 40°. In fact, when the contact angle is larger than 160°, the energy barrier for ice nucleation is almost the same as that for homogeneous nucleation. When the contact angle between ice nucleus and the pore surface is equal to 180°, the energy barrier becomes larger and equivalent to that for homogeneous nucleation of ice, i.e., the advantage gained by the presence of the surface is lost. This phenomenon

can be visualized on Figure 21(a), where it is clear that the smaller the contact angle, the lower the energy barrier for nucleation. It is clear that increasing contact angle drives the system towards homogeneous nucleation of ice. When temperature changes in the range of 233-260 K, the value of energy barrier increases dramatically with the temperature. That is, the energy barrier for ice nucleation is lowered under increased sub-cooling. Furthermore, the effect of contact angle is diminished by lowering temperature. Interestingly, the nature of the surface is not as crucial when the energy driving force is high.

4.4.3.2 Effect of pore size

In order to visualize how pore size of sediment affects the nucleation process of ice on confinement surface in porous media at a given wettability property of the system, the wettability of the confinement surfaces was maintained at a certain value. Figure 22 depicts the dependence of the number of water molecules required to form a critical nucleus as a function of temperature and aspect ratio (i.e., the ratio of pore radius to size of critical nucleus) at a contact angle of $120°$. As shown in Figure 22, it was found that larger pores require larger amount of water molecules involved in the formation of the ice nucleus. That means, larger pores will generate larger ice germs. Therefore, smaller pores favor ice nucleation, i.e., fewer water molecules need to be immobilized in the solid phase to form a nucleus. When aspect ratio x changes from 0.5 to 2, the critical size of ice nucleus increases sharply. In fact, when the pore size is ten times larger than that of the critical nucleus, the critical size of ice germ is very close to that formed on a flat surface.

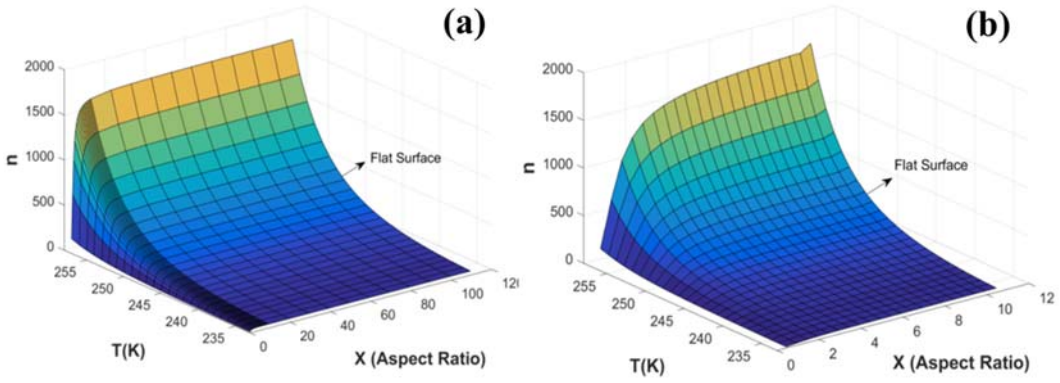

Fig. 22. Water molecules required for critical nucleus as a function of temperature and pore size for (a) aspect ratios up to 100, and (b) zoom in on aspect ratios up to 10. The right boundary of the surfaces represents the behavior of flat surfaces. The contact angle was maintained at 120°.

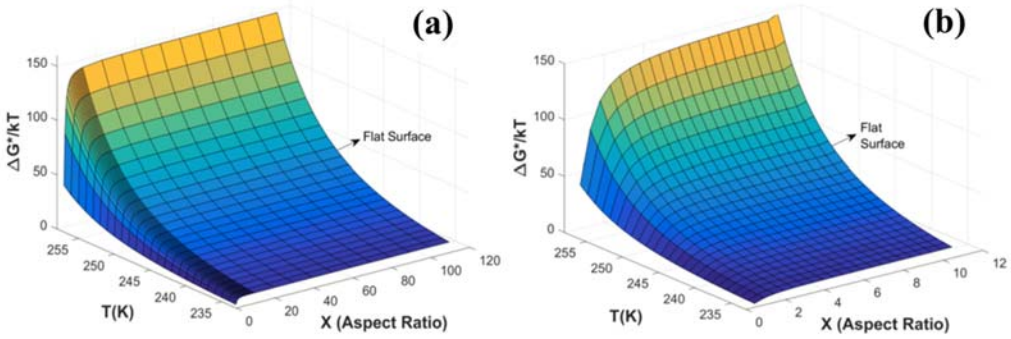

Fig. 23. Energy barrier as a function of temperature and pore size for (a) aspect ratios up to 100, and (b) zoom in on aspect ratios up to 10. The right boundary of the surfaces represents the behavior of flat surfaces. The contact angle was maintained at 120°.

As for the effects of pore size on energy barrier for nucleation in porous media, it was found that nucleation energy barrier increases with increasing temperature and aspect ratio. Figure 23 depicts similar behavior for energy barrier to that of the number of water molecules required to form a nucleus: energy barrier for ice nucleation is lowered by lower temperatures. In addition, the nucleation energy barrier is enhanced when the aspect ratio x gets larger. The energy barrier increases sharply with aspect ratio x, when x is less than 2, at which point it increases at a slow rate. When the aspect ratio x is larger than 100, the energy barrier for nucleation in porous media

is almost the same as that for nucleation on the planar surface. In this case, the pore surface acts as a planar surface. This confirms that nucleation is more favorable in smaller, more confined spaces, when nucleation happens on the pore walls (i.e., nuclei growth on the solid surface).

4.4.4 Gas/liquid/solid triple boundary

As for the effects of triple boundary line on the energy barrier for nucleation in porous media with three phases, it was found that the energy barrier increases with the temperature (as shown in Figure 24). The disadvantages of high temperatures during nucleation process can be counterbalanced by changing the highly hydrophilic surface into hydrophobic surface (increasing the value of contact angle θ_1 or θ_2). In addition, when contact angle θ_1 or θ_2 takes the value of 90°, the energy barrier for nucleation at the triple boundary line is close to zero. In this case, the triple boundary line is flat, which is the same as that for nucleation at gas/liquid interface. Additionally, the maximum energy barrier is much higher than that for other cases. Therefore, it is possible that nucleation at the three-phase boundary line is the most challenging one among all the cases discussed in this work.

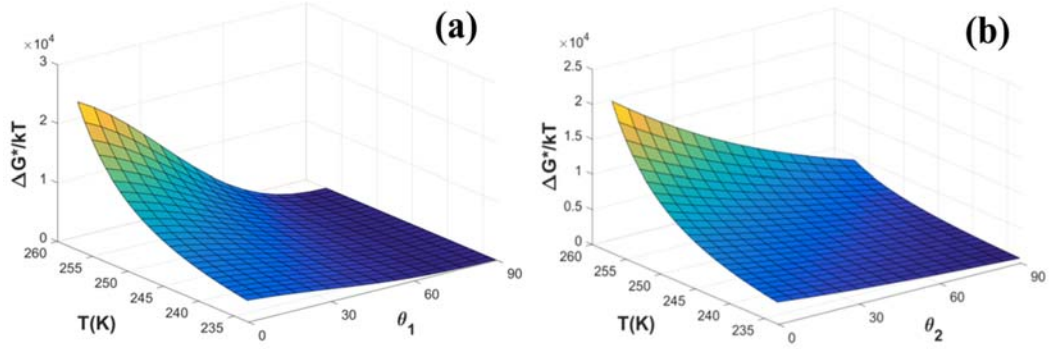

Fig. 24. (a) Energy barrier for nucleation at the gas/liquid/solid triple boundary line as a function of θ_1; (b) Energy barrier for nucleation at the gas/liquid/solid triple boundary line as a function of θ_2.

It must be noted that nucleation at the triple boundary line inside pores is favored by larger pores of hydrophobic surfaces. This outcome contradicts the findings of nucleation on the concave surfaces, where nucleation on hydrophilic pores of smaller diameters is favorable. These are not contradictory findings, but reflections of two different scenarios. In the case of the triple-boundary line in larger pores, the nucleus sits at the center of the pore. On the other hand, on the concave surface of very small pores, the nucleus rests on the pore wall.

It is well known that the energy change (ΔG) determines the energy barrier for nucleation when the size of the nucleus reaches the critical size. In this case, thermodynamic analysis for the homogeneous nucleation leads to the expression: $\Delta G^*_{hom} = \Delta g_v \cdot \frac{4}{3}\pi r_1^3 + \sigma_{12} \cdot 4\pi r_1^2$. According to the discussion in previous sections, an appropriate correction factor is applied to extend the expression of energy barrier for homogeneous nucleation to the case of heterogeneous nucleation in different types of situations. Therefore, the thermodynamic analysis for energy barrier for heterogeneous nucleation leads to interesting conclusions regarding the shape of crystalline phases at different interfaces. It can be easily noticed from equation (74) that the spherical nucleus expected in homogeneous nucleation is "modified" by correction factor according to different scenarios. That is, the effects of foreign surfaces on the nucleation process lead to different shapes of nuclei which deviate from spherical shapes. Accordingly, the correction factor can be understood as a shape factor that characterizes the relationship between the shapes of nuclei formed at foreign interfaces and that expected during homogeneous nucleation.

$$\Delta G^*_{het} = \Delta G^*_{hom} \cdot f(\theta) \; = \Delta g_v \cdot \frac{4}{3}\pi r_1^3 \cdot f(\theta) \; + \sigma_{12} \cdot 4\pi r_1^2 \cdot f(\theta) \tag{74}$$

It is clear that viable nucleation aided by interfaces results in the formation of crystal lenses, rather than spherical particles. These predictions agree with observations of ice and natural gas hydrates in porous media [114,115,123,124].

4.5 Conclusions

In this work, three types of surfaces, including gas/liquid interface, solid surfaces (planar, concave and convex surfaces) and three-phase boundary lines, are modeled with the aim to understand their effects on heterogeneous nucleation in porous media. Careful thermodynamic analyses are conducted on the correction factor that characterizes the effects of foreign interfaces on nucleation activation energy. The correction factor for energy barrier for heterogeneous nucleation can also be understood as the shape factor that adjusts the spherical shape for homogeneous nucleation into that of lense-shaped nuclei formed at foreign interfaces.

As for the interface of gas/liquid, the value of correction factor determines the shape of the formed nucleus. Nucleation process preferentially occurs along the interface and inside the liquid phase. When the critical nucleus is in the shape of sphere, correction factor is 1. In this case, energy barrier for nucleation at gas/liquid interface is exactly the same as that for homogeneous nucleation.

As for the effects of solid surfaces, our results suggest that the correction factor for convex surface is always larger than that for flat surface, as opposed to the trend for concave surfaces where the correction factor is lower than the flat-surface one. In other words, there exists a higher energy barrier for nucleation on convex surfaces (particles) than that on flat surfaces, and the lowest energy barrier occurs on concave surfaces (inside small pores).

Additionally, by considering that the wettability of the solid surfaces can vary from highly hydrophilic to highly hydrophobic (contact angle from 0° to 180°), it was found that the nucleation of ice is more energetically favorable on surfaces with smaller contact angles. Contact angles

ranging from 0° to 160° can significantly enhance the nucleation process of ice in porous media. As for the effects of substrate size, it was found that larger pores result in larger ice germs in the case of concave pore surfaces, and smaller pores can enhance the nucleation process. However, as the pore size increases, nucleation rate within the pore wall approximates that on a flat surface, resulting in the loss of the advantage induced by confinement. In the case of convex surfaces, the particle size has only marginal effect on the energy barrier, and approximates the flat surface as particle size increases. In fact, ice nucleation is more energetically favorable on concave surfaces (on small pore walls) and less so on convex surfaces (on particles) with nucleation on flat surfaces as the boundary between these two regions.

As for the triple boundary lines, the value of correction factor is determined by the wettability of solid surface and the radius of the pore. Interestingly, it was also found that the correction factor is smaller in porous media with larger contact angle value, suggesting that the nucleation process is favored by hydrophobic confinement surfaces. Compared to other cases, nucleation at the triple boundary line needs to overcome higher energy barriers. In addition, the nucleation process mostly prefers to occur at solid surfaces with lower energy barrier, form a thermodynamic perspective.

CHAPTER 5 INTERFACIAL EFFECTS ON KINETIC NUCLEATION OF GAS-HYDRATE

5.1 Motivation and Background

The formation of gas hydrates is a stochastic process which mainly consists of three stages before reaching equilibrium conditions: saturation, induction, and growth[140]. The first stage is the dissociation of gas molecules in the liquid until the liquid is completely saturated with gas. It takes a certain amount of equilibration time to reach the saturation point. The second stage is the induction stage, in which small hydrate nuclei form or randomly dissociate until a critical cluster radius is reached[140]. This stage is also known as nucleation stage. Once the time necessary to form nuclei of critical radius has been reached, the growth stage begins. During this last stage, gas hydrate particles grow rapidly, and gas consumption increases linearly with time when measured experimentally[141]. Understanding the nucleation process of gas hydrates could be the key point to understand other applications including the extraction of gas containing especially methane from gas-hydrate accumulations, the storage and transportation of natural gas and the flow assurance of natural gas and oil pipelines.

Gas hydrates naturally form in sedimentary porous media, where foreign interfaces (i.e., gas/liquid interface, liquid/solid interface, and three-phase boundary line) are very commonly encountered during the formation of gas hydrates. The properties of these interfaces (contact angle, interfacial energy, and substrate curvature) no doubt play an important role in modulating the nucleation process of gas-hydrates. Li and his coworkers[142] studied the growth kinetics of hydrate film in synthetic systems by injecting a single gas bubble to liquid phase into a gas chamber and found that a hydrate layer formed at the gas/liquid interface. According to the work of Dimo Kashchiev[143], Eric F, May and his coworkers[144], heterogeneous nucleation on solid substrate is more energetically favorable than nucleation either in the bulk solution or on the gas/liquid interface. Additionally, Molecular Dynamics (MD) simulations conducted by Defever et al. have

shown that the wettability of solid surfaces influences the nucleation of gas hydrates by adjusting the concentration of gas molecules[145].

Unfortunately, there is no clear understanding on the effects of the various interface properties on the nucleation process of gas hydrates in porous media. Very little work has been conducted to quantitatively describe how these interfaces and their properties (i.e., surface wettability, interface curvature and interfacial energies) modulate the nucleation rate of gas hydrates and which interface is most energetically favorable for gas-hydrate nucleation at the beginning. Furthermore, it is very difficult to study this problem with experimental methods. On the one hand, nucleation is perhaps the most challenging part to understand due to difficulties in obtaining direct experimental measurements of the nucleation process or statistically collecting significant dataset to obtain the whole range of formation probability distribution[146]. On the other hand, the application of experimental approaches is limited to certain conditions (low driving force) with a narrow range of research variables[146].

Molecular Dynamics (MD) simulations are considered a powerful tool to understand the nucleation mechanisms of gas hydrates microscopically when the driving force is high enough. Molecular Dynamics simulations are limited in terms of quantitatively analyzing the effects of various interfaces present in porous media due to limitations of time, length scale and computation capacities of molecular approaches[146]. Thus, a macroscopic mathematic model, incorporating the interface properties, can be a promising and efficient way to capture the effects of various interfaces on the hydrate nucleation quantitatively and to make comparisons in a wide range. Incorporating this phenomenon into expressions for the rate of hydrate growth would enable validation with experimental data on hydrate formation. Such an approach would then effectively

provide a fundamental understanding on how to control the formation and dissociation of gas hydrates by modulating the properties of presented foreign interfaces.

5.2 Model for Kinetic Nucleation Rate of Gas-hydrate

The kinetic-nucleation of gas-hydrates involves the fluctuation of hydrate-building units in supersaturated liquid due to temperature or pressure vibrations of the system. The nucleation rate of gas hydrates can be characterized as the number of hydrate clusters with critical size formed over time. According to classical nucleation theory (CNT), two components, including a thermodynamic component (the change of Gibbs free energy during the formation of the critical hydrate nucleus from the liquid phase) and a kinetic component (diffusive flux of hydrate building units in the liquid to incorporate into the clusters), are involved to describe the nucleation rate of gas hydrates[133,134,143]. Once the clusters achieve the critical size, the incorporation of hydrate building units into the nuclei is thermodynamically favored, which will further facilitate the growth of the water clusters. Nucleation rate of gas hydrates indicates the rate at which critical hydrate nuclei will form in a volume of liquid phase per second.

Kashchiev and Firoozabadi[143] analyzed the nucleation rate of gas hydrates both in isothermal and isobaric regimes based on the nucleation theory. The stationary nucleation rate of one-component gas hydrates J ($m^{-3}s^{-1}$ or $m^{-2}s^{-1}$) can be calculated with the following formulation (eq (75))[143].

$$J = Z \cdot f_e^* \cdot C_0 \exp\left(\frac{\Delta\mu}{k_B T}\right) \cdot \exp\left(-\frac{\Delta G^*}{k_B T}\right) \tag{75}$$

In that equation, f_e^* can be applied to represent the frequency with which the hydrate building units would attach to the hydrate nucleus at equilibrium conditions; C_0 (m^{-3} or m^{-2}) is the concentration of nucleation sites in the system, which is determined by the type of nucleation; and k_B is the Boltzmann constant. The term of ΔG^* represents the energy barrier required to overcome to form a hydrate cluster with n hydrate building units. The term of $\Delta\mu$ is the driving force for the incorporation of hydrate building units into hydrate nucleus. In the isobaric regime with constant pressure, the driving force is estimated from $\Delta\mu \approx \Delta s_e(T_e - T) - (\Delta c_{p,e}/2T_e)(T_e - T)^2$, where Δs_e is the difference between the entropies of the old and the new phase at $T = T_e$. The value of Δs_e can be estimated from the correlation $\Delta s_e = \Delta h_e/T_e$ where Δh_e (J) is the enthalpy of latent heat (per hydrate building unit) of dissociation of the hydrate crystal into gaseous phase and liquid phase at $T = T_e$. At 0.1 MPa and 273.2 K, $\Delta h_e = 9.0 \times 10^{-20} J$ and $\Delta c_{p,e} = 4.63 \times 10^{-22} J/K$ is measured for methane hydrate[147]. The values of Δh_e produce $\Delta s_e = 22.2 k_B$ at $T_e = 293.2$ K and $\Delta s_e = 23.2 k_B$ at $T_e = 281.2$ K for methane hydrate[143,147].

The kinetic parameter of Zeldovich factor (Z) represents the non-equilibrium feature of the nucleation process, which describes the probability of the subcritical nuclei to grow into a stable crystal due to Brownian motion of the subcritical nuclei. The parameter Z usually has a value between 0.01 and 1. The value of 1 can be achieved when the system reaches equilibrium state. In other cases, the value of Z can be estimated with the correlation[143]:

$$Z = \sqrt{\frac{\Delta G^*}{3\pi k_B T n^2}} \qquad (76)$$

Where n is the number of hydrate building units incorporated into a hydrate nucleus. Based on the classical nucleation theory, the terms of n and ΔG^* for one-component gas hydrate nucleation can be estimated with the following expressions[143]:

$$n = 8c^3 v_h^2 \sigma^3 f/27\Delta\mu^3 \quad (77)$$

$$\Delta G^* = 4c^3 v_h^2 \sigma^3 f / 27 \Delta\mu^2 \quad (78)$$

In those expressions, the parameter c is a numerical shape factor (e.g., $c = (36\pi)^{1/3}$ for spherical, cap, or lens-shaped nucleus), v_h is the volume of a hydrate building unit composed of one gas molecule, and n_w water molecules. One can use $v_h = 0.216\, nm^3$ for methane hydrate. The parameter σ represents the surface free energy of hydrate/liquid interface, which is estimated to be 17 mJ/m^2 based on the public literature (as found in Chapter 3). With the presence of foreign interfaces, the term f incorporates the correction factors with which the critical size and energy barrier for homogeneous nucleation is adjusted for heterogeneous nucleation. The schematics of the foreign interfaces commonly encountered in porous media are shown in Figure 25, including three types of liquid/solid interfaces, gas/liquid interface and gas/liquid/solid triple boundary lines.

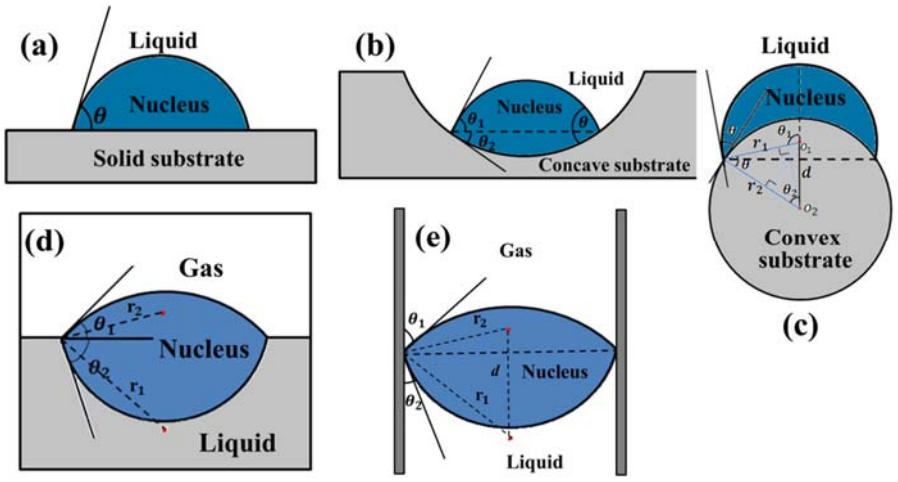

Fig. 25. (a) Schematic of planar liquid/solid interface; (b) Schematic of concave liquid/solid interface; (c) Schematic of convex liquid/solid interface; (d) Schematic of gas/liquid interface; (e) Schematic of gas/liquid/solid triple boundary line.

From chapter 4, the correlations for correction factors f for various interfaces (gas/liquid interface, planar liquid/solid interface, concave liquid/solid interface, convex liquid/solid interface and the three-phase boundary line) are as follows:

$$f(\theta) = \frac{1}{4}\left[(2 - 3m_1 + {m_1}^3) + \left(\frac{1 - {m_1}^2}{1 - {m_2}^2}\right)^{3/2}(2 - 3m_2 + {m_2}^3)\right]$$

$$m_1 = cos\theta_1, m_2 = cos\theta_2$$

(79)

$$f(\theta) = \frac{1}{4}(2 - 3cos\theta + cos^3\theta)$$

(80)

$$f(\theta) = \frac{1}{2}[1 - X^3 - 3x^2cos\theta(1 - Y) - x^3(2 - 3Y + Y^3)]$$

$$x = r_2/r_1;\ X = \frac{1+xcos\theta}{\sqrt{1+x^2+2xcos\theta}};\ Y = \frac{x+cos\theta}{\sqrt{1+x^2+2xcos\theta}}$$

(81)

$$f(\theta) = \frac{1}{2}\left[1 - X'^3 - 3x^2cos\theta(1 - Y') + x^3\left(2 - 3Y' + Y'^3\right)\right]$$

$$x = r_2/r_1;\ X' = \frac{xcos\theta-1}{\sqrt{1+x^2-2xcos\theta}};\ Y' = \frac{x-cos\theta}{\sqrt{1+x^2-2xcos\theta}}$$

(82)

$$f(\theta) = \frac{1}{2}\left\{1 - {m_1}^3 + 3\frac{1 - {m_1}^2}{1 + m_2}\left(\sqrt{\left(1 - {m_1}^2\right)(1 - {m_2}^2)} - m_1m_2\right)\right.$$

$$\left. - \left(\frac{1 - {m_1}^2}{1 - {m_2}^2}\right)^{3/2}[2 - 3m_2 + {m_2}^3]\right\}$$

$$m_1 = sin\theta_1, m_2 = sin\theta_2$$

(83)

Where θ_1, θ_2 and θ are geometrical angles which depend on surface energy of foreign interface.

With the nucleation rate predicted with Classical Nucleation Theory (CNT), the probability of hydrate formation can be expressed as a function of time when a constant driving force is applied on the system (as shown in eq (84))[144,146]. The fluctuation of induction time and formation probability of hydrate formation can also be examined in terms of the effects of foreign interfaces on the nucleation process of gas hydrates, using the following expression:

$$P(t) = 1 - exp(-J \cdot t) \tag{84}$$

Where $P(t)$ represents the cumulative formation probability of gas hydrates. J is the stationary nucleation rate of gas hydrates estimated by equation (75). $t(s)$ is the induction time[144,146].

5.3 Effects of Foreign Interfaces on Nucleation Process of Gas-hydrate

5.3.1 Concave liquid/solid interface

5.3.1.1 Effects of concave surface wettability

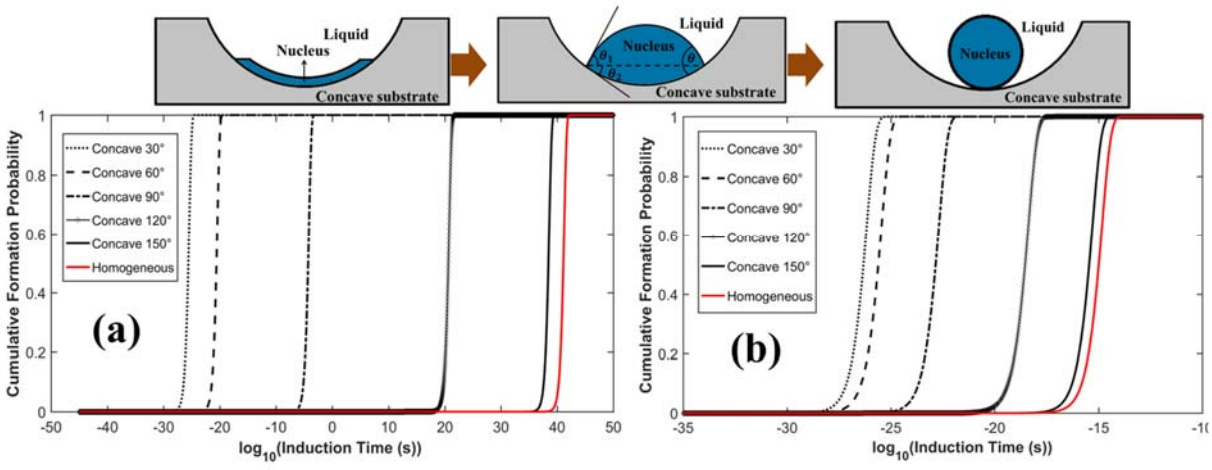

Fig. 26. (a) Cumulative probability of methane hydrates formation on concave surface versus time and contact angle at subcooling of 8 K; (b) Cumulative probability of methane hydrates formation on concave surface versus time and contact angle at subcooling of 20 K.

Figure 26 depicts the effects of contact angle of decreasing hydrophilicity on the cumulative formation probability to form a critical hydrate nucleus at an aspect ratio of 2 (i.e., the radius of the concave surface is twice as large as the critical nucleus radius) and a constant driving force. Figure 26 (a) and (b) are correspond to constant driving forces of 8 K (sub-cooling $\Delta T = 8K$) and 20 K ($\Delta T = 20K$), respectively. It was found that the sensitivity of formation probability to concave surface wettability can be significantly reduced by increasing the driving force (the degree of sub-cooling). As shown in Figure 26, the induction time for methane hydrate formation increases when the wettability of the concave surface is changed from hydrophilic to hydrophobic. This trend is more obvious when contact angle is larger than $90°$. When contact angle is larger than the value of $150°$, the advantage of the presence of substrate surface as nucleation sites is increasingly lost. In this case, the induction time required for methane-hydrates formation on concave liquid/solid interface is very close to that for homogeneous nucleation.

5.3.1.2 Effects of concave surface curvature

Surface curvature is inversely proportional to the aspect ratio x (i.e., the ratio of the radius of the pore to the critical nucleus). In order to visualize how the curvature of the concave surface influences the nucleation rate and induction time of methane hydrates, the wettability of the concave surfaces and driving force for the system was maintained at a certain value. Figure 27 depicts the dependence of the cumulative probability of methane hydrates formation on time and aspect ratio (i.e., the ratio of concave surface radius to the radius of critical hydrate nucleus) when the contact angle is fixed at $120°$. Figure 27(a) and Figure 27(b) is for the system with sub-cooling values corresponding to 8 K and 20 K, respectively. As in the previous case, increase in the degree of sub-cooling (driving force) can significantly reduce the sensitivity of nucleation process of methane hydrates to the curvature (aspect ratio) of concave surface.

As shown in Figure 27, it was found that nucleation of methane hydrates is always favorable on concave liquid/solid interface rather than flat liquid/solid interface. With the fluctuation of the surface curvature, it was shown that induction time for methane hydrates formation increases with the aspect ratio of concave surface. Therefore, nucleation of methane hydrates is favored by concave surfaces with larger curvature (smaller aspect ratio). When the aspect ratio is larger than 10 ($x \geq 10$), the induction time for nucleation on concave liquid/solid interface is close to that on flat liquid/solid interface. The advantages of concave surfaces as the nucleation sites over flat surface is completely lost when aspect ratio is large than 100 ($x \geq 100$).

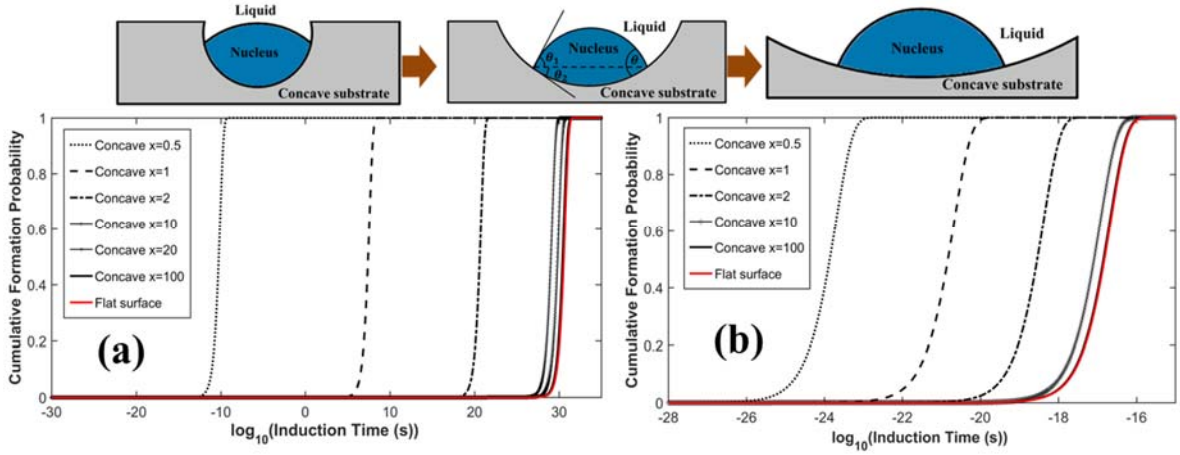

Fig. 27. (a) Cumulative probability of methane hydrates formation on concave surface versus time and aspect ratio at subcooling of 8 K; (b) Cumulative probability of methane hydrates formation on concave surface versus time and aspect ratio at subcooling of 20 K.

5.3.2 Convex liquid/solid interface

5.3.1.1 Effects of convex surface wettability

When the nucleation of methane hydrates occurs on grain particles, the properties of convex liquid/solid interface (wettability, particle size or curvature) play an important role during the nucleation process of methane hydrates in porous media. Figure 28 shows the effects of wettability of convex surface on the cumulative probability of methane hydrates formation when a constant driving force is given (sub-cooling $\Delta T = 8K$).

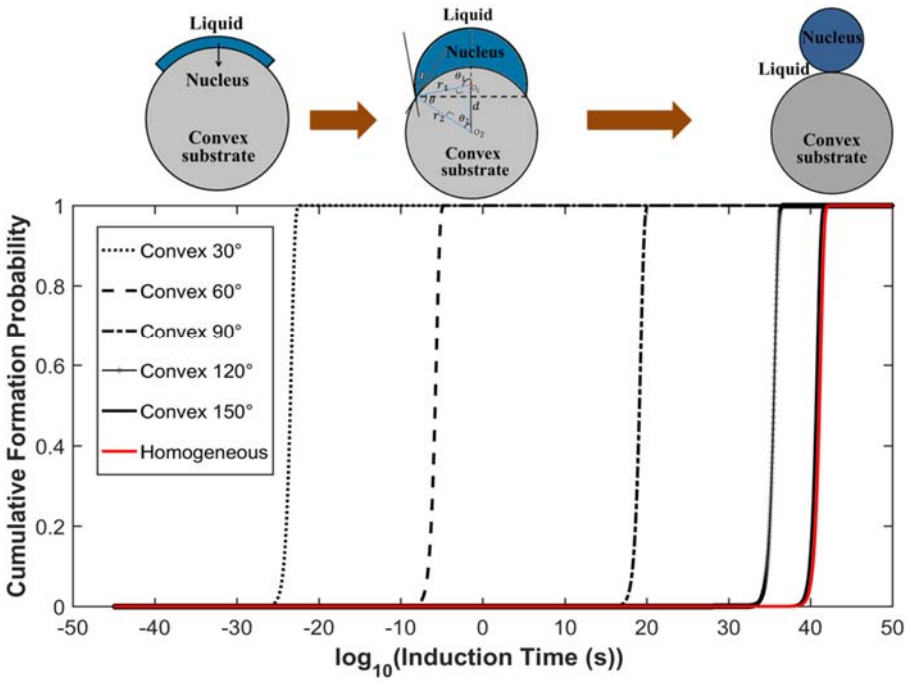

Fig. 28. Cumulative probability of methane hydrates formation on convex surface versus time and contact angle at subcooling of 8 K.

It was found that the induction time for hydrate formation increases as the wettability of the convex surface goes from slightly hydrophilic to highly hydrophobic. In this case, the nucleation process of methane hydrate preferentially takes place on the convex surface with smaller contact angle (i.e., hydrophilic surface). In addition, the cumulative probability of methane hydrates formation on convex liquid/solid interfaces is always larger than that for homogeneous nucleation in the case of hydrophilic surfaces. As shown in Figure 28, when the contact angle is larger than the value of 150°, the formation probability is almost the same as that for homogeneous nucleation. Hydrophobic particle surfaces do not support the nucleation process. Additionally, the advantage of the presence of particles as nucleation sites is increasingly lost for contact angles greater than 90°. That is, the nucleation process of methane hydrates is more sensitive to contact

angles when the nucleation process occurs on hydrophilic particle surface compared to the case of hydrophobic surface.

5.3.1.2 Effects of convex surface curvature

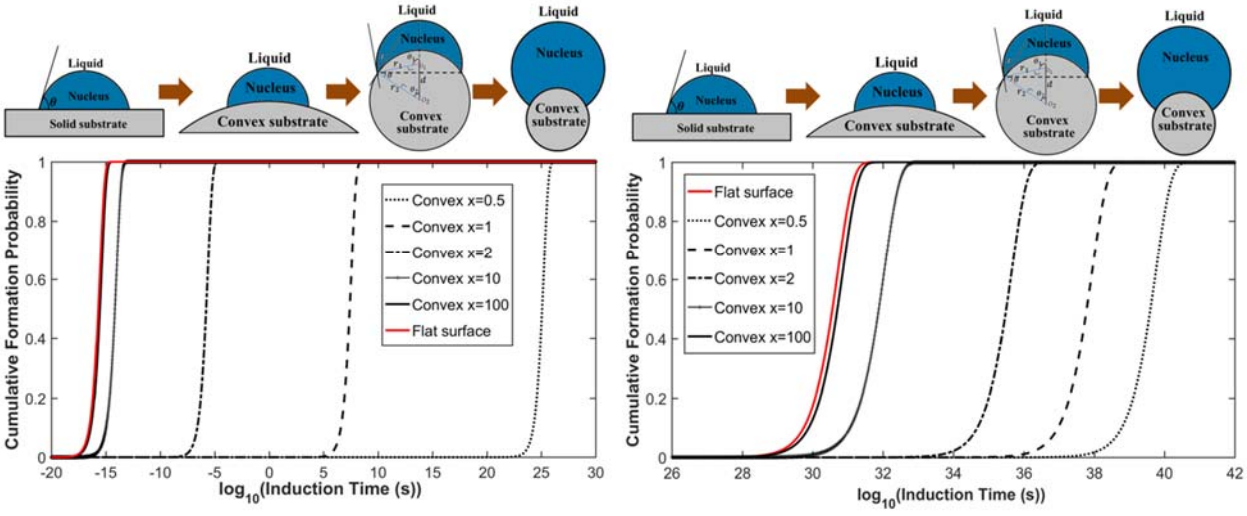

Fig. 29. Cumulative probability of methane hydrates formation on hydrophilic convex surface (left: contact angle is 60°) and hydrophobic convex surface (right: contact angle is 120°) versus time and aspect ratio (surface curvature) at subcooling of 8 K.

As opposed to the beneficial effects of surface wettability on nucleation, one can see that the effects of curvature (particle size) of convex surface are marginal on the probability of methane hydrates formation and detrimental in character compared to flat surfaces (as shown in Figure 29). Figure 29 presents the dependence of the cumulative formation probability of methane hydrates on aspect ratio (i.e., ratio of particle radius over the radius of critical nucleus). It is clear that smaller particles have a detrimental effect on nucleation process for a given contact angle (as shown in figure 29: left $\theta = 60°$ and right $\theta = 120°$) and driving force (sub-cooling $\Delta T = 8K$). In fact, the induction time for hydrates formation is slightly longer than that on flat surface. Regarding to the effects of particle sizes, it shows that the induction time for hydrate formation gradually decreases

when the aspect ratio increases from 0.5 to 10. When the aspect ratio reaches at the value of 100, the induction time required for nucleation on convex particle surface is almost the same as that on flat surface.

5.3.3 Gas/liquid interface

In the bulk of an aqueous solution or large pores, the interface of gas/liquid is flat. A lens-shaped critical nucleus forms at the gas/liquid interface (as shown in Figure 25(d)). As shown in Figure 25(d), θ_1 and θ_2 represent the angles of the crystal/gas and the crystal/liquid interfaces, respectively. The values of θ_1 and θ_2 depend on the interfacial energies between the phases present, including the interfacial energy between gas phase and hydrate phase σ_{gh}, the interfacial energy between gas phase and liquid phase σ_{gl} and the interfacial energy between hydrate phase and liquid phase σ_{hl}.

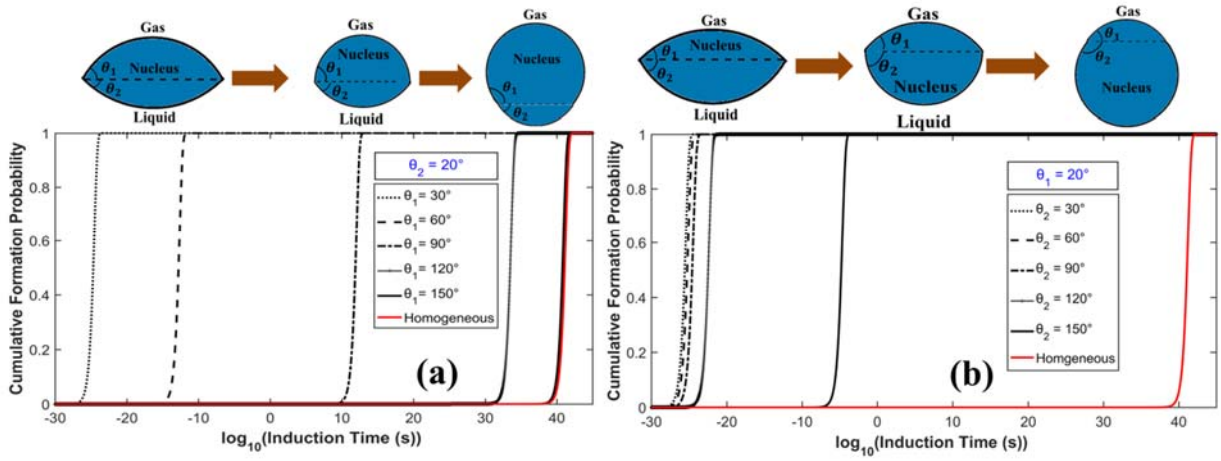

Fig. 30. (a) Cumulative probability of methane hydrates formation on gas/liquid interface versus time and angle θ_1 at subcooling of 8 K; (b) Cumulative probability of methane hydrates formation on gas/liquid interface versus time and angle θ_2 at subcooling of 8 K.

Figure 30(a) shows the cumulative formation probability of methane hydrates as a function of time and crystal/gas angle θ_1 when a constant crystal/liquid angle ($\theta_2 = 20°$) and driving force

(sub-cooling $\Delta T = 8K$) is given. And, Figure 30(b) describes the cumulative formation probability of methane hydrates as a function of time and crystal/liquid angle θ_2 when the crystal/gas angle ($\theta_1 = 20°$) and driving force (subcooling $\Delta T = 8K$) is given. It was found that the time required for the nucleation of hydrate crystals increases with increasing either angle θ_1 or angle θ_2. As shown in Figure 30(a), the induction time for cumulative formation probability of 0.0027 varies from 10^{-27} s to $10^{38.4}$ s when the angle θ_1 increases from 30° to 150°. Figure 30(b) shows that the induction time for cumulative formation probability of 0.0027 increases from 10^{-28} s to $10^{-7.2}$ s when the angle θ_2 increases from 30° to 150°. The induction time for methane-hydrates nucleation is more sensitive to angle θ_1 than angle θ_2. Therefore, nucleation of methane hydrates is more energetically favorable to occur inside the liquid phase rather than in the gas phase.

5.3.4 Gas/liquid/solid triple boundary

In porous media with small pore radius, when gas, liquid and solid (three phases) are present in the system, the interfaces between the three phases can play an important role in the nucleation process. As shown in Figure 25(e), a lens-shaped crystal cluster formed along the gas/liquid/solid boundary lines inside the cylindrical pore. The parameters of θ_1 and θ_2 describe the contact angles of liquid and critical nucleus on the confinement surface, respectively. The values of angles θ_1 and θ_2 depend on the wettability properties of the confinement surface (i.e., the pore walls).

Figure 31 shows that cumulative formation probability of methane hydrates is significantly reduced with decreasing the value of θ_1 or θ_2. That is, the induction time for hydrates nucleation increases when surface (pore wall) wettability changes from hydrophobic to hydrophilic. Highly

hydrophilic pore walls will not support the nucleation of methane hydrates at the triple boundary line. In addition, the induction time for hydrates nucleation is more sensitive to contact angle of θ_1 than θ_2. The nucleation of methane hydrates prefers to take place inside the liquid phase rather than in the gas phase.

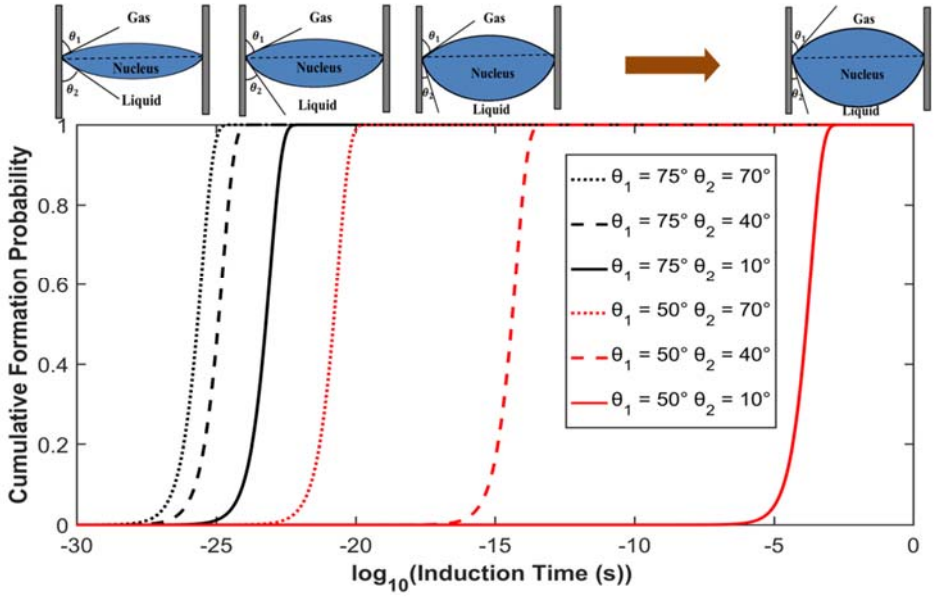

Fig. 31. Cumulative probability of methane hydrates formation on gas/liquid/solid triple boundary line versus time and contact angles θ_1 and θ_2 at subcooling of 8 K.

5.4 Discussion

5.4.1 Effects of liquid/solid interfaces

Regarding the effects of liquid/solid interfaces on the nucleation process of methane hydrates, Table 8 shows the sensitivity of induction time to contact angle at a cumulative probability equal to 0.27 % for the three surfaces discussed above. The value of 0.27% is corresponding to the inflection point of the curve for cumulative formation probability, which is assumed to represent the beginning of nucleation process in this work. It was found that induction

time increases with increasing the contact angle when a constant driving force (sub-cooling $\Delta T = 8K$) and aspect ratio ($x = 2$) is given. Given a certain contact angle, nucleation on concave surface requires shorter induction time while that on convex surface needs longer induction time and that on flat surface falls in between. Highly hydrophilic surfaces can significantly increase the nucleation rate of methane hydrates. In addition, the advantage of the presence of solid surface as nucleation sites is almost lost for contact angles greater than $150°$. In this case, induction time required for nucleation on all the solid substrates is very close to that for homogeneous nucleation.

Table 8. Induction time required for cumulative formation probability of 0.27% for substrate surface at various contact angle.

	$\theta = 60°$	$\theta = 90°$	$\theta = 120°$	$\theta = 150°$
Concave Surface	10^{-24}	$10^{-7.7}$	$10^{17.2}$	10^{35}
Flat Surface	10^{-19}	10^{4}	$10^{27.2}$	$10^{36.8}$
Convex Surface	10^{-9}	$10^{15.7}$	$10^{32.1}$	$10^{37.3}$
Homogeneous	$10^{37.7}$			

Table 9 summarizes the effects of curvature (reciprocal of aspect ratio x) of liquid/solid interfaces for a contact angle for all the substrate surfaces equal to $60°$. It was found that nucleation of methane hydrates is more energetically favorable on concave surfaces and less so on convex surfaces with nucleation on flat surface in between when a constant driving force (sub-cooling $\Delta T = 8K$) is given. The induction time required for cumulative probability of 0.27% on concave surface increases with increasing aspect ratio, as shown in Table 9. That is, nucleation of methane hydrates is favored by concave surfaces with larger curvatures. As for convex surfaces, induction

time for cumulative probability of 0.27% decreases with increasing the aspect ratio. Therefore, nucleation of methane hydrates is more favorable to occur on larger particles (larger aspect ratio). When the aspect ratio of curved surfaces (concave and convex surfaces) exceeds the value of 10, the induction time for nucleation on curved surfaces is very close to that on flat surface. The advantages of curved surfaces over flat surface as the nucleation sites are almost lost.

Table 9. Induction time required for cumulative formation probability of 0.27% for substrate surface with various aspect ratio.

	$x = 0.5$	$x = 1$	$x = 2$	$x = 10$
Concave Surface	$10^{-27.01}$	$10^{-25.26}$	10^{-23}	$10^{-19.42}$
Convex Surface	$10^{22.67}$	10^{5}	$10^{-8.2}$	$10^{-16.58}$
Flat Surface	$10^{-18.1}$			

5.4.2 Effects of gas/solid interfaces

As mentioned in Chapter 3, methane hydrates in smaller pores required higher pressure of lower temperature to guarantee the stability and equilibrium status. Here, comparisons and analysis of methane-hydrates nucleation in large pores (nucleation on gas/liquid interface) and small pores (nucleation on gas/liquid/solid triple boundary line) are carried out. For the same shape and volume of hydrate crystal, induction time increases when nucleation propagates from large pores to small pores (as shown in Figure 32). That is, the formation of methane hydrates preferentially occurs in larger pores rather than in smaller pores. This phenomenon can be understood from a strictly physical perspective. The nucleus critical size is the minimum size required for the newly-formed, gas-hydrate phase to grow. If the nucleus critical size required for the formation and growth of a hydrate phase exceeds the space available within the sediment pore, the probability of developing

a hydrate phase is extremely low. In other words, the induction time required for the formation and growth of a hydrate phase will be extremely large.

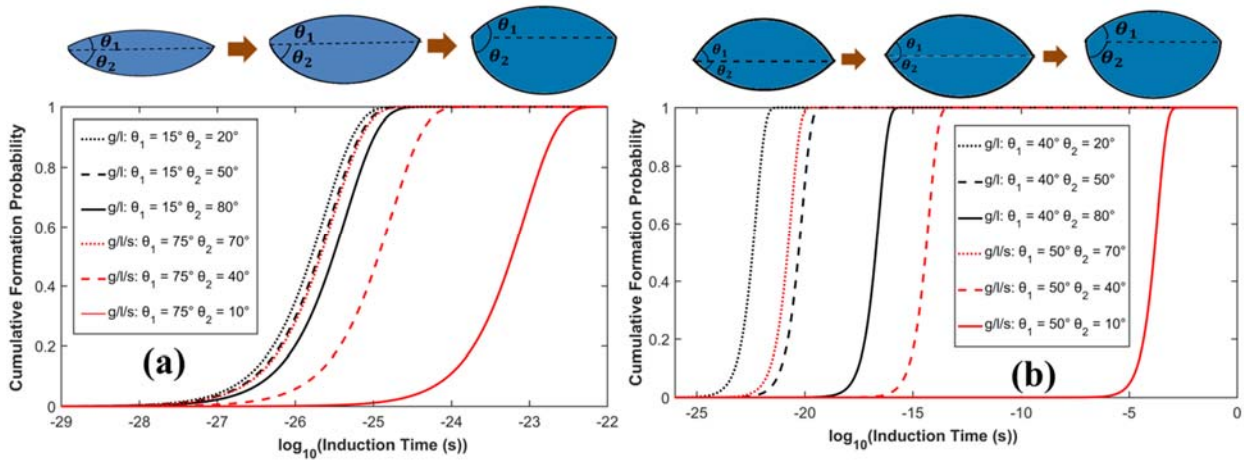

Fig. 32. Cumulative probability of methane hydrates formation on gas/liquid interface and gas/liquid/solid triple boundary line versus time and contact angles θ_1 and θ_2 at subcooling of 8 K.

5.4.3 Effects of various interfaces

In order to better understand the effects of different types of interfaces on the nucleation process, comparisons and analysis between these interfaces under the proposed same conditions are conducted (as shown in Figure 33).

Figure 33 shows that the preference of nucleation on different interfaces depends on not only the interfacial energies (the volume of the formed hydrate crystal) and also the substrate curvature. For example, when the driving force and surface curvature is held constant, nucleation on gas/liquid interface and gas/liquid/solid triple boundary line presents shorter induction time than all the liquid/solid interfaces when the substrate surface is less hydrophilic (contact angle of 75° as shown in Figure 33(a)). Increasing the hydrophilicity of the substrate surface can significantly reduce the induction time (as shown in Figure 33(b) and (c)). In other words, at the beginning of nucleation with thin lens-shaped hydrate crystal formed, methane hydrates

energetically favors to form at gas/liquid interface and gas/liquid/solid boundary line and then moves to from on the liquid/solid interface. In another case, when a constant driving force is given to form a certain lens-shaped hydrate crystal, the preference for nucleation on convex liquid/solid interface is significantly reduced when the aspect ratio for the curved surface changes from 2 to 0.5.

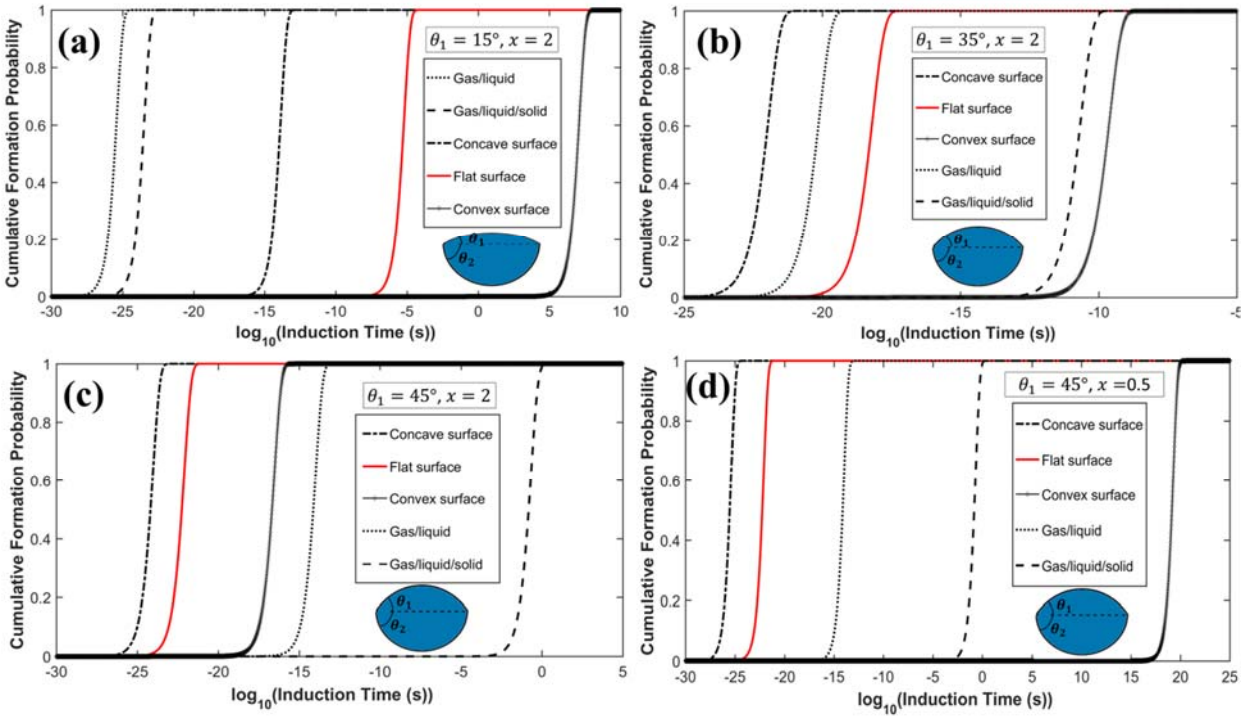

Fig. 33. Cumulative probability of methane hydrates formation at various interfaces versus time at subcooling of 8 K.

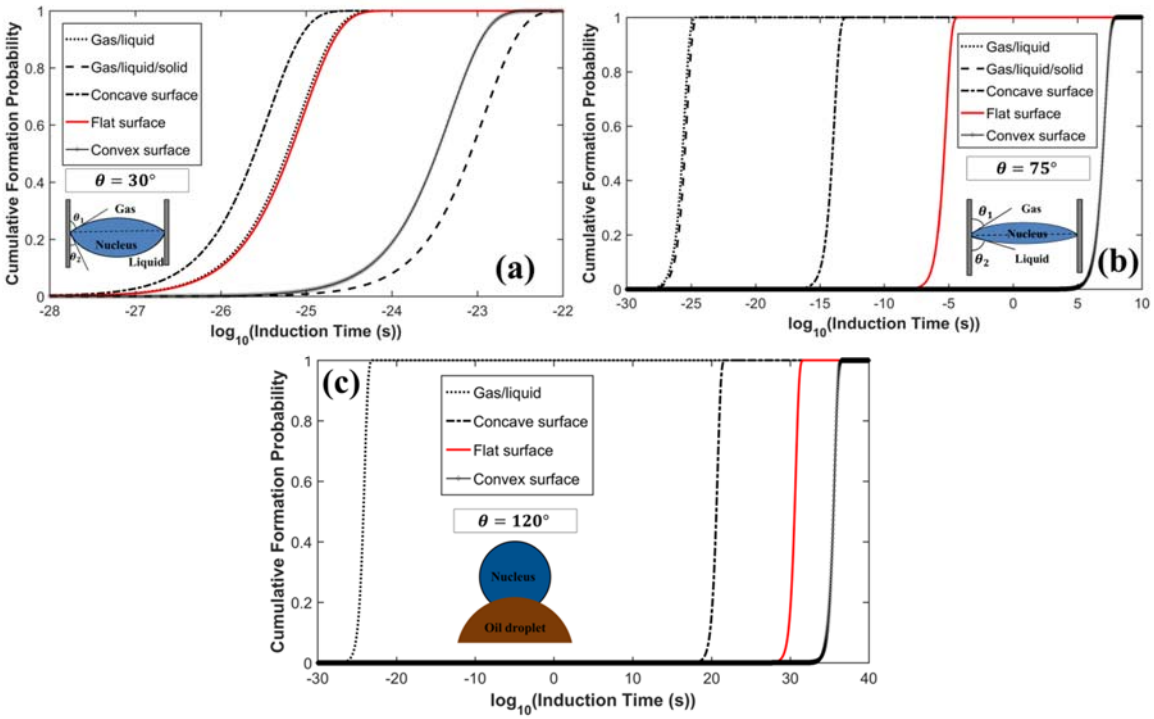

Fig. 34. Cumulative probability of methane hydrates formation in different sediment porous media at sub-cooling of 8K: (a) coarse-grain sandstone porous media; (b) fine-grain clay porous media; (c) pipeline with oil droplets in water.

In order to understand the effects of natural sediments on the formation of gas hydrates, the formation probability of methane hydrates in three types of natural systems are analyzed. Figure 34 (a) shows the formation probability of methane hydrates in a coarse-grain sandstone system, which is highly hydrophilic with contact angle of 30°. It was found that gas-hydrate formation in this system has a very short induction time. In addition, the preference of gas-hydrate formation follows this order: concave surface, gas/liquid interface, flat surface and convex surface, and finally gas/liquid/solid boundary line. In the case of fine-grain clays, which is less hydrophilic than sandstone, as shown in Figure 34 (b), formation of gas hydrates requires shorter induction time at the interface of gas/liquid and three-phase boundary line than that at all of the liquid/solid interfaces. Figure 34 (c) depicts a pipeline system with the presence of gas phase, liquid phase and

oil droplets. The surface of oil droplets is highly hydrophobic with a constant contact angle of 120°. In this pipeline system, formation of gas hydrates is energetically favorable at the gas/liquid interface and less so by the interfaces with oil on them. These model predictions on formation probability of methane hydrates qualitatively agree with the experimental observations on gas hydrates formation.

5.5 Conclusions

Gas hydrates have attracted a lot of research attention due to the wide applications, including natural gas pipeline flow assurance, natural gas storage and transport, energy resource and environmental effects. Understanding the nucleation process of gas hydrates could be the key point to understand these applications. Modeling of the kinetic nucleation of gas-hydrates can be applied to predict and analyze the effects of various interfaces on the nucleation process of gas hydrates in an efficient and more general way as they do not have the limitations of experimental methods in time and scale of measurements.

In this work, a model for the kinetic nucleation of gas hydrates on different interfaces, including gas/liquid interface, liquid/solid interface and gas/liquid/solid triple boundary line, was developed based on classical nucleation theory. The concept of cumulative formation probability of gas hydrates was applied to intuitively compare and analyze the effects of various foreign interfaces on the nucleation process. It was found that the formation probability of gas hydrates can be significantly affected by the driving force and interface properties (i.e., interfacial energies, wettability, and surface curvature). When the driving force is large enough, the sensitivity of nucleation to interfacial properties is significantly diminished.

With respect to the effects of liquid/solid interfaces on nucleation of methane hydrates, it was found that nucleation is always more energetically favorable on concave surfaces and less so on convex surfaces while nucleation on flat surfaces falls in between for the same value of driving force. In addition, nucleation of methane hydrates on solid surfaces is more favored by hydrophilic surfaces, which translates into shorter induction time to achieve a certain formation probability. When the contact angle is greater than $150°$, the advantage of the presence of solid surfaces as nucleation sites is almost lost. Regarding to surface curvatures, nucleation of methane hydrates preferentially occurs on concave surfaces with larger curvatures (smaller aspect ratio x) than on flat surface, and even less on convex surfaces with smaller curvatures (larger x). As for the effects of gas/liquid interface and gas/liquid/solid triple boundary line, longer induction time is required to form the same volume of hydrate crystal on gas/liquid/solid triple boundary line than that on gas/liquid interface. That is, nucleation of methane hydrates preferentially occurs in large pores rather than in small pores. Furthermore, the preference in terms of formation of methane hydrates on different interfaces changes with the size of the formed hydrate crystal and the curvature of the solid surfaces for any given driving force. Modeling predictions show that methane hydrates form first on concave surface and gas/liquid interface then other liquid/solid interfaces and last on gas/liquid/solid triple boundary line in a hydrophilic coarse-grain sandstone system. In a less hydrophilic fine-grain clay system, modeling predictions show that methane hydrates form first on gas/liquid interface and gas/liquid/solid triple boundary line and then on liquid/solid interfaces. In a pipeline system with highly hydrophobic oil droplets, methane hydrates preferentially form on gas/liquid interface and then on liquid/solid interfaces.

CHAPTER 6 SUMMARY AND CONCLUSIONS

Gas-hydrates are ice-like crystalline inclusion-compounds stabilized by gas molecules trapped in a host lattice formed by water molecules, which form a hydrogen-bonded framework under proper conditions, pressure and temperature. Understanding the behavior of gas-hydrates has become increasingly important in the fields of flow assurance, gas storage and transport, energy resource management and climate change. Being able to fully estimate the volume and gas-content of natural gas-hydrate reservoirs in sediments is not just important in terms of potential natural gas exploitation, but also from an environmental perspective, considering that methane gas is a potent greenhouse gas. In addition, it's crucial to understand the kinetic nucleation of gas-hydrates in order to better predict the patterns of formation of gas hydrates in natural sediments or inhibit the formation of gas-hydrates for flow assurance. The key to gaining understanding and predictive capabilities of the formation and stability of gas hydrates in sediments lays in capturing accurately the role that the sediment plays in these processes. Therefore, the hypothesis guiding this work is that the inclusion of appropriate sediment-properties, i.e., pore size, wettability, surface curvature and interfacial energies, can enable more accurate prediction of gas-hydrate stability and mathematically capturing nucleation scenarios and probabilities.

In this work, a model for gas-hydrates equilibrium in pores was developed from basic thermodynamic analysis and validated against available experimental data published in the literature. The model organically incorporates sediment properties like pore size, wettability and interfacial energy. The proposed model presents high predictive accuracy when compared to experimental data with the average AAD of less than 2%. The mechanical equilibrium condition of the model takes the effects of sediment properties (wettability, interfacial tension) into account to describe the conditions of stability of gas hydrate in porous media, in a very straight-forward manner. It was found that equilibrium conditions for gas-hydrates are highly dependent on the pore

size. The wettability of the pore surface affects the equilibrium pressures of gas hydrate formed in porous media, and the shape of the hydrate phase. However, experimental data are available only for surfaces of similar surface properties. The effects of sediment properties captured in the proposed model should be further tested experimentally. The success of the proposed model in predicting experimental data of gas-hydrate equilibrium in porous media can be attributed to the successful incorporation of sediment properties into its constitutive equations. This supports the validity of the hypothesis.

In this work, a mathematical model was developed in order to describe the effects of foreign interfaces (i.e., gas/liquid interface, liquid/solid interface and three-phase boundary line) on kinetic nucleation of gas-hydrates in sediments of varying characteristics. The model incorporates interface properties (interfacial interaction energies, wettability and substrate size), and was applied to quantitatively describe the effects of various foreign interfaces on the cumulative formation probability of methane hydrates. The model included a successful incorporation of sediment properties in the thermodynamic component of hydrate nucleation rates within the framework of the Classical Nucleation Theory (CNT). It was found that the nucleation process of methane hydrates can be significantly affected by the interplay between driving force and interfacial properties. The sensitivity of probability and induction time for nucleation to interfacial properties can be significantly diminished by increasing the driving force (sub-cooling), i.e., interfacial effects on the activation energy required for nucleation can be effectively counterbalanced with larger driving forces for the process. In addition, it was shown that nucleation of methane hydrates is kinetically favored within large sediment pores rather than within small pores. This model prediction agrees with observations of core samples of gas-hydrate-bearing sediments. As for the effects of liquid/solid interfaces, it was found that the formation

probability of methane hydrates can be significantly modulated by surface wettability and surface curvature. Nucleation of methane hydrates is always more energetically favorable on concave surfaces and less so on convex surfaces, with the flat surface case acting as the barrier in between the two behaviors. In addition, nucleation of gas hydrates is favored by highly-hydrophilic surfaces and concave surfaces with smaller curvatures, when considering nucleation of hydrate on solid interfaces. The curvature of convex liquid/solid interface has only marginal effects on the nucleation process of methane hydrates. Finally, the location where gas hydrate will start nucleating on different types of interfaces is a function of the size of the formed hydrate crystal and the curvature and wettability of the solid surface for a given driving force. Modeling predictions show that methane hydrates form first on concave liquid/solid interface and gas/liquid interface then other types of liquid/solid interfaces and last on gas/liquid/solid triple boundary line in a hydrophilic coarse-grain sandstone system. In a less hydrophilic fine-grain clay system, modeling predictions show that methane hydrates form first on gas/liquid interface and gas/liquid/solid triple boundary line and then on liquid/solid interfaces. In a pipeline system with highly hydrophobic oil droplets, methane hydrates preferentially form on gas/liquid interface and then on liquid/solid interfaces. One can picture hydrate lenses growing from the center of the pore towards the perimeter, and then starting to plug the pores by covering the pore walls during continuous growth. This prediction agrees with growth mechanisms proposed based on observations of core samples from hydrate-bearing sediments,[125,142,148] which also supports the validity of the hypothesis guiding the present work.

Summarizing, it can be stated that the hypothesis guiding the present work was proven: incorporation of appropriate sediment-properties (i.e., pore size, surface interaction energies, surface wettability and surface geometry) can better predict and analyze the equilibrium conditions

and provide insight into nucleation occurrence of gas hydrates that qualitatively agrees with gas-hydrate observations. The incorporation of sediment properties into the model for gas hydrates equilibrium conditions predicts the available experimental data with an absolute average deviation (%AAD) less than 2%, a significant improvement upon previous modeling attempts. In addition, the inclusion of sediment properties in the models for kinetic nucleation of gas hydrates result in mathematical models that qualitatively capture the information obtained from examination of gas-hydrate core samples and observations of gas hydrates in synthetic systems.

CHAPTER 7 FUTURE WORK RECOMMENDATION

As final remarks, while much work has been done and much has been achieved, the exploration on gas-hydrate equilibrium, stability and kinetics is far from being completed. We would like to recommend some very attractive future work focusing on the areas briefly described below.

First, natural porous media (e.g., sand and silt) usually exhibits a wide range of pore sizes. The pore size distribution can be narrow in some locations, while in others it can be broad. Additionally, natural porous media has a heterogeneous composition with a distribution of interfacial properties. For this reason, developing approaches to incorporate pore size distributions and distribution of properties of natural sediments into the hydrate-equilibrium model can help improve its accuracy, not only in terms of thermodynamic equilibrium, but in terms of the estimates of gas content in gas-hydrate reservoirs.

Second, from the perspective of energy recovery, it is crucial to understand the dissociation process of methane hydrates and methane gas production behavior. Therefore, a theoretical mathematical model, which incorporates the properties of foreign interfaces (e.g., liquid/solid interface, gas/liquid interface and gas/liquid/solid boundary line) present in porous media, can be developed to understand how the foreign interfaces affect the kinetic dissociation process and further control methane hydrate dissociation. This model will be based on the nucleation model developed in the present work.

Finally, from a practical point of view, the findings of the kinetic nucleation study can be applied in two fields: the design of promoters to enhance hydrate formation rates from natural gas storage and transportation perspective; and the design of kinetic hydrate inhibitors (KHI) to prevent the formation of gas hydrates from a flow assurance perspective. For example, hydrophilic surfaces with small pits will help to enhance the nucleation of gas hydrates. Small particles with

wettability of highly hydrophobic nature are promising to be used to delay or inhibit the formation of gas hydrates.

Nomenclature

Characters

$C(T)$ = Langmuir constant

f = fugacity

$\Theta(T,P)$ = fraction of cage capacity

μ = chemical potential

ν = number of cages per water molecule in the crystal lattice

γ = activity coefficient

ϕ = fugacity coefficient

Δ = change in a property

ε = maximum attractive potential

σ = core distance at zero potential

Γ = function depending on contact angle

U = internal energy

S = entropy

H = enthalpy

k = Boltzmann constant

N_A = Avogadro's number

N_w = number of water molecules

r = radial distance

r_p = pore radius

P = pressure

T = Temperature

R = gas constant

$R(cell)$ = cell radius of each shell

V = molar volume

$W(r)$ = cell potential

$W(r)^{[i]}$ = cell potential for shell i

z = coordination number of the cage

Z = compressibility factor

sI = hydrate structure I

sII = hydrate structure II

G_{obj} = objective function

Tol = tolerance

x = molar composition in the liquid phase

Superscripts and subscripts

H = hydrate phase

L = liquid phase

V= vapor phase

eβ = empty hydrate phase

IG = ideal gas phase

α = gas-hydrate interface

β = hydrate-liquid interface

σ_{α} = interfacial energy of gas-hydrate interface

a_{α} = surface area of gas-hydrate interface

σ_{β} = interfacial energy of hydrate-liquid interface

a_{β} = surface area of hydrate-liquid interface

θ = angle of gas-hydrate interface on the surface of porous wall

τ = angle of hydrate-liquid interface on the surface of porous wall

p = pore

w = water

g = guest

sat = saturated conditions

surr = surroundings of the system, i.e., barostat and thermostat

π = ice or liquid water

m = cage type

Δg_v = the Gibbs free energy change for the formation of crystal nucleus per unit volume

$f(\theta)$ = correction factor to describe the effects of foreign interfaces on nucleation

ΔG = energy barrier for homogeneous nucleation

J = number of ice nuclei in a volume of parent phase per second

f_e^* = attach frequency of hydrate building units to the hydrate nucleus at equilibrium conditions

C_0 = concentration of nucleation sites in the system

$\Delta\mu$ = driving force for the transfer of a building unit across the solid-liquid interface

ΔG^* = energy barrier for heterogeneous nucleation

$P(t)$ = the probability of hydrate formation

REFERENCES

(1) Chong, Z. R.; Yang, S. H. B.; Babu, P.; Linga, P.; Li, X.-S. Review of Natural Gas Hydrates as an Energy Resource: Prospects and Challenges. *Appl. Energy* **2016**, *162*, 1633–1652. https://doi.org/10.1016/j.apenergy.2014.12.061.

(2) Sloan, E. D. *Clathrate Hydrates of Natural Gases, Second Edition, Revised and Expanded*; CRC Press, 1998.

(3) Sloan, E. D.; Koh, C. *Clathrate Hydrates of Natural Gases, Third Edition*; CRC Press, 2007.

(4) Makogon, Y. F.; Holditch, S. A.; Makogon, T. Y. Natural Gas-Hydrates — A Potential Energy Source for the 21st Century. *J. Pet. Sci. Eng.* **2007**, *56* (1), 14–31. https://doi.org/10.1016/j.petrol.2005.10.009.

(5) Park, S.-S.; Lee, S.-B.; Kim, N.-J. Effect of Multi-Walled Carbon Nanotubes on Methane Hydrate Formation. *J. Ind. Eng. Chem.* **2010**, *16* (4), 551–555. https://doi.org/10.1016/j.jiec.2010.03.023.

(6) Koh, C. A.; Sloan, E. D.; Sum, A. K.; Wu, D. T. Fundamentals and Applications of Gas Hydrates. *Annu. Rev. Chem. Biomol. Eng.* **2011**, *2* (1), 237–257. https://doi.org/10.1146/annurev-chembioeng-061010-114152.

(7) Claussen, W. F. A Second Water Structure for Inert Gas Hydrates. *J. Chem. Phys.* **1951**, *19* (11), 1425–1426. https://doi.org/10.1063/1.1748079.

(8) Claussen, W. F. Erratum: Suggested Structures of Water in Inert Gas Hydrates. *J. Chem. Phys.* **1951**, *19* (5), 662–662. https://doi.org/10.1063/1.1748327.

(9) Claussen, W. F.; Polglase, M. F. Solubilities and Structures in Aqueous Aliphatic Hydrocarbon Solutions. *J. Am. Chem. Soc.* **1952**, *74* (19), 4817–4819. https://doi.org/10.1021/ja01139a026.

(10) Ripmeester, J. A.; Tse, J. S.; Ratcliffe, C. I.; Powell, B. M. A New Clathrate Hydrate Structure. *Nature* **1987**, *325* (6100), 135–136. https://doi.org/10.1038/325135a0.

(11) Sloan, E. D. Fundamental Principles and Applications of Natural Gas Hydrates. *Nature* **2003**, *426* (6964), 353–363. https://doi.org/10.1038/nature02135.

(12) Jeffrey, G. A. Hydrate Inclusion Compounds. *J. Incl. Phenom.* **1984**, *1* (3), 211–222. https://doi.org/10.1007/BF00656757.

(13) GEO_ExPro_v12i4.Pdf.

(14) Pellenbarg, R. E.; Max, M. D.; Clifford, S. M. Methane and Carbon Dioxide Hydrates on Mars: Potential Origins, Distribution, Detection, and Implications for Future in Situ Resource Utilization. *J. Geophys. Res. Planets* **2003**, *108* (E4). https://doi.org/10.1029/2002JE001901.

(15) Duxbury, N. S.; Nealson, K. H.; Romanovsky, V. E. On the Possibility of Clathrate Hydrates on the Moon. *J. Geophys. Res. Planets* **2001**, *106* (E11), 27811–27813. https://doi.org/10.1029/2000JE001425.

(16) Wood, D. A. Gas Hydrate Research Advances Steadily on Multiple Fronts: A Collection of Published Research (2009–2015). *J. Nat. Gas Sci. Eng.* **2015**, *24*, A1–A8. https://doi.org/10.1016/j.jngse.2015.04.019.

(17) Turner, D. J. *Clathrate Hydrate Formation in Water-in-Oil Dispersions*; Colorado School of Mines., 2005.

(18) Aman, Z. M.; Sloan, E. D.; Sum, A. K.; Koh, C. A. Lowering of Clathrate Hydrate Cohesive Forces by Surface Active Carboxylic Acids. *Energy Fuels* **2012**, *26* (8), 5102–5108. https://doi.org/10.1021/ef300707u.
(19) Colombel, E.; Gateau, P.; Barré, L.; Gruy, F.; Palermo, T. Discussion of Agglomeration Mechanisms between Hydrate Particles in Water in Oil Emulsions. *Oil Gas Sci. Technol. - Rev. IFP* **2009**, *64* (5), 629–636. https://doi.org/10.2516/ogst/2009042.
(20) Jiménez-Ángeles, F.; Firoozabadi, A. Induced Charge Density and Thin Liquid Film at Hydrate/Methane Gas Interfaces. *J. Phys. Chem. C* **2014**, *118* (45), 26041–26048. https://doi.org/10.1021/jp507160s.
(21) Austvik, T.; Li, X.; Gjertsen, L. H. Hydrate Plug Properties: Formation and Removal of Plugs. *Ann. N. Y. Acad. Sci. 912* (1), 294–303. https://doi.org/10.1111/j.1749-6632.2000.tb06783.x.
(22) Gao, S. Hydrate Risk Management at High Watercuts with Anti-Agglomerant Hydrate Inhibitors. *Energy Fuels* **2009**, *23* (4), 2118–2121. https://doi.org/10.1021/ef8009876.
(23) Mokhatab, S.; Wilkens, R. J.; Leontaritis, K. J. A Review of Strategies for Solving Gas-Hydrate Problems in Subsea Pipelines. *Energy Sources Part Recovery Util. Environ. Eff.* **2007**, *29* (1), 39–45. https://doi.org/10.1080/009083190933988.
(24) Kelland, M. A. History of the Development of Low Dosage Hydrate Inhibitors. *Energy Fuels* **2006**, *20* (3), 825–847. https://doi.org/10.1021/ef050427x.
(25) Zerpa, L. E.; Salager, J.-L.; Koh, C. A.; Sloan, E. D.; Sum, A. K. Surface Chemistry and Gas Hydrates in Flow Assurance. *Ind. Eng. Chem. Res.* **2011**, *50* (1), 188–197. https://doi.org/10.1021/ie100873k.
(26) Veluswamy, H. P.; Kumar, A.; Seo, Y.; Lee, J. D.; Linga, P. A Review of Solidified Natural Gas (SNG) Technology for Gas Storage via Clathrate Hydrates. *Appl. Energy* **2018**, *216*, 262–285. https://doi.org/10.1016/j.apenergy.2018.02.059.
(27) Casco, M. E.; Martínez-Escandell, M.; Gadea-Ramos, E.; Kaneko, K.; Silvestre-Albero, J.; Rodríguez-Reinoso, F. High-Pressure Methane Storage in Porous Materials: Are Carbon Materials in the Pole Position? *Chem. Mater.* **2015**, *27* (3), 959–964. https://doi.org/10.1021/cm5042524.
(28) Di Profio, P.; Arca, S.; Rossi, F.; Filipponi, M. Comparison of Hydrogen Hydrates with Existing Hydrogen Storage Technologies: Energetic and Economic Evaluations. *Int. J. Hydrog. Energy* **2009**, *34* (22), 9173–9180. https://doi.org/10.1016/j.ijhydene.2009.09.056.
(29) Hao, W.; Wang, J.; Fan, S.; Hao, W. Evaluation and Analysis Method for Natural Gas Hydrate Storage and Transportation Processes. *Energy Convers. Manag.* **2008**, *49* (10), 2546–2553. https://doi.org/10.1016/j.enconman.2008.05.016.
(30) 2018-Outlook-for-Energy.Pdf.
(31) Anonymous. Methane Hydrates in Quaternary Climate Change: The Clathrate Gun Hypothesis. *Eos Trans. Am. Geophys. Union 83* (45), 513–516. https://doi.org/10.1029/2002EO000359.
(32) Maslin, M.; Owen, M.; Day, S.; Long, D. Linking Continental-Slope Failures and Climate Change: Testing the Clathrate Gun Hypothesis. *Geology* **2004**, *32* (1), 53–56. https://doi.org/10.1130/G20114.1.
(33) Klebnikov, S. The Clathrate Gun Hypothesis: A Call to Action to the EPA. *Penn Sustain. Rev.* **2016**, *1* (8).
(34) Organization, W. M. *WMO Statement on the State of the Global Climate in 2017*; Climate Change; 2017.

(35) Hatzikiriakos, S. G.; Englezos, P. The Relationship between Global Warming and Methane Gas Hydrates in the Earth. *Chem. Eng. Sci.* **1993**, *48* (23), 3963–3969. https://doi.org/10.1016/0009-2509(93)80375-Z.
(36) Ruppel, C. Tapping Methane Hydrates for Unconventional Natural Gas. *Elements* **2007**, *3* (3), 193199. https://doi.org/10.2113/gselements.3.3.193.
(37) Yvon-Durocher, G.; Allen, A. P.; Bastviken, D.; Conrad, R.; Gudasz, C.; St-Pierre, A.; Thanh-Duc, N.; del Giorgio, P. A. Methane Fluxes Show Consistent Temperature Dependence across Microbial to Ecosystem Scales. *Nature* **2014**, *507* (7493), 488–491. https://doi.org/10.1038/nature13164.
(38) Shakhova, N.; Semiletov, I. Methane Release and Coastal Environment in the East Siberian Arctic Shelf. *J. Mar. Syst.* **2007**, *66* (1), 227–243. https://doi.org/10.1016/j.jmarsys.2006.06.006.
(39) Knott, B. C.; Molinero, V.; Doherty, M. F.; Peters, B. Homogeneous Nucleation of Methane Hydrates: Unrealistic under Realistic Conditions. *J. Am. Chem. Soc.* **2012**, *134* (48), 19544–19547. https://doi.org/10.1021/ja309117d.
(40) Kashchiev, D.; Firoozabadi, A. Nucleation of Gas Hydrates. *J. Cryst. Growth* **2002**, *243* (3), 476–489. https://doi.org/10.1016/S0022-0248(02)01576-2.
(41) Bai, D.; Chen, G.; Zhang, X.; Wang, W. Nucleation of the CO2 Hydrate from Three-Phase Contact Lines. *Langmuir* **2012**, *28* (20), 7730–7736. https://doi.org/10.1021/la300647s.
(42) Bai, D.; Chen, G.; Zhang, X.; Sum, A. K.; Wang, W. How Properties of Solid Surfaces Modulate the Nucleation of Gas Hydrate. *Sci. Rep.* **2015**, *5*, 12747. https://doi.org/10.1038/srep12747.
(43) Bai, D.; Chen, G.; Zhang, X.; Wang, W. Microsecond Molecular Dynamics Simulations of the Kinetic Pathways of Gas Hydrate Formation from Solid Surfaces. *Langmuir* **2011**, *27* (10), 5961–5967. https://doi.org/10.1021/la105088b.
(44) Anderson, R.; Llamedo, M.; Tohidi, B.; Burgass, R. W. Experimental Measurement of Methane and Carbon Dioxide Clathrate Hydrate Equilibria in Mesoporous Silica. *J. Phys. Chem. B* **2003**, *107* (15), 3507–3514. https://doi.org/10.1021/jp0263370.
(45) Clennell, M. B.; Hovland, M.; Booth, J. S.; Henry, P.; Winters, W. J. Formation of Natural Gas Hydrates in Marine Sediments: 1. Conceptual Model of Gas Hydrate Growth Conditioned by Host Sediment Properties. *J. Geophys. Res. Solid Earth 104* (B10), 22985–23003. https://doi.org/10.1029/1999JB900175.
(46) Griffiths, F. J.; Joshi, R. C. CHANGE IN PORE SIZE DISTRIBUTION DUE TO CONSOLIDATION OF CLAYS. TECHNICAL NOTE. *GEOTECHNIQUE* **1989**, *39* (1).
(47) Handa, Y. P.; Stupin, D. Yu. Thermodynamic Properties and Dissociation Characteristics of Methane and Propane Hydrates in 70-.ANG.-Radius Silica Gel Pores. *J. Phys. Chem.* **1992**, *96* (21), 8599–8603. https://doi.org/10.1021/j100200a071.
(48) Uchida, T.; Ebinuma, T.; Ishizaki, T. Dissociation Condition Measurements of Methane Hydrate in Confined Small Pores of Porous Glass. *J. Phys. Chem. B* **1999**, *103* (18), 3659–3662. https://doi.org/10.1021/jp984559l.
(49) Uchida, T.; Ebinuma, T.; Takeya, S.; Nagao, J.; Narita, H. Effects of Pore Sizes on Dissociation Temperatures and Pressures of Methane, Carbon Dioxide, and Propane Hydrates in Porous Media. *J. Phys. Chem. B* **2002**, *106* (4), 820–826. https://doi.org/10.1021/jp012823w.

(50) Ripmeester, J. A.; Alavi, S. Some Current Challenges in Clathrate Hydrate Science: Nucleation, Decomposition and the Memory Effect. *Curr. Opin. Solid State Mater. Sci.* **2016**, *20* (6), 344–351. https://doi.org/10.1016/j.cossms.2016.03.005.
(51) Kim, N.-J.; Park, S.-S.; Kim, H. T.; Chun, W. A Comparative Study on the Enhanced Formation of Methane Hydrate Using CM-95 and CM-100 MWCNTs. *Int. Commun. Heat Mass Transf.* **2011**, *38* (1), 31–36. https://doi.org/10.1016/j.icheatmasstransfer.2010.10.002.
(52) Park, S.-S.; Lee, S.-B.; Kim, N.-J. Effect of Multi-Walled Carbon Nanotubes on Methane Hydrate Formation. *J. Ind. Eng. Chem.* **2010**, *16* (4), 551–555. https://doi.org/10.1016/j.jiec.2010.03.023.
(53) Moraveji, M. K.; Golkaram, M.; Davarnejad, R. Effect of CuO Nanoparticle on Dissolution of Methane in Water. *J. Mol. Liq.* **2013**, *180*, 45–50. https://doi.org/10.1016/j.molliq.2012.12.014.
(54) Ganji, H.; Aalaie, J.; Boroojerdi, S. H.; Rod, A. R. Effect of Polymer Nanocomposites on Methane Hydrate Stability and Storage Capacity. *J. Pet. Sci. Eng.* **2013**, *112*, 32–35. https://doi.org/10.1016/j.petrol.2013.11.026.
(55) Arjang, S.; Manteghian, M.; Mohammadi, A. Effect of Synthesized Silver Nanoparticles in Promoting Methane Hydrate Formation at 4.7 MPa and 5.7 MPa. *Chem. Eng. Res. Des.* **2013**, *91* (6), 1050–1054. https://doi.org/10.1016/j.cherd.2012.12.001.
(56) Takahata, M.; Kashiwaya, Y.; Ishii, K. Kinetics of Methane Hydrate Formation Catalyzed by Iron Oxide and Carbon under Intense Stirring Conditions. *Mater. Trans.* **2010**, *51* (4), 727–734. https://doi.org/10.2320/matertrans.M2009369.
(57) Aliabadi, M.; Rasoolzadeh, A.; Esmaeilzadeh, F.; Alamdari, A. Experimental Study of Using CuO Nanoparticles as a Methane Hydrate Promoter. *J. Nat. Gas Sci. Eng.* **2015**, *27*, 1518–1522. https://doi.org/10.1016/j.jngse.2015.10.017.
(58) Najibi, H.; Shayegan, M. M.; Heidary, H. Experimental Investigation of Methane Hydrate Formation in the Presence of Copper Oxide Nanoparticles and SDS. *J. Nat. Gas Sci. Eng.* **2015**, *23*, 315–323. https://doi.org/10.1016/j.jngse.2015.02.009.
(59) Park, S.-S.; An, E.-J.; Lee, S.-B.; Chun, W.; Kim, N.-J. Characteristics of Methane Hydrate Formation in Carbon Nanofluids. *J. Ind. Eng. Chem.* **2012**, *18* (1), 443–448. https://doi.org/10.1016/j.jiec.2011.11.045.
(60) Pasieka, J.; Coulombe, S.; Servio, P. Investigating the Effects of Hydrophobic and Hydrophilic Multi-Wall Carbon Nanotubes on Methane Hydrate Growth Kinetics. *Chem. Eng. Sci.* **2013**, *104*, 998–1002. https://doi.org/10.1016/j.ces.2013.10.037.
(61) 27, M. G. on M.; Am, 2015 at 10:32. MIT researchers pioneer technique for mass-producing graphene http://www.extremetech.com/extreme/206573-mit-researchers-pioneer-technique-for-mass-producing-graphene (accessed Apr 22, 2016).
(62) Ghozatloo, A.; Hosseini, M.; Shariaty-Niassar, M. Improvement and Enhancement of Natural Gas Hydrate Formation Process by Hummers' Graphene. *J. Nat. Gas Sci. Eng.* **2015**, *27, Part 2*, 1229–1233. https://doi.org/10.1016/j.jngse.2015.09.069.
(63) Cheng, Y.; Li, L.; Yuan, Z.; Wu, L.; Mahmood, S. Finite Element Simulation for Fluid–Solid Coupling Effect on Depressurization-Induced Gas Production from Gas Hydrate Reservoirs. *J. Nat. Gas Sci. Eng.* **2013**, *10*, 1–7. https://doi.org/10.1016/j.jngse.2012.10.001.
(64) Tabatabaie, S. H.; Pooladi-Darvish, M. Analytical Solution for Gas Production from Hydrate Reservoirs Underlain with Free Gas. *J. Nat. Gas Sci. Eng.* **2009**, *1* (1), 46–57. https://doi.org/10.1016/j.jngse.2009.03.006.

(65) Warrier, P.; Khan, M. N.; Srivastava, V.; Maupin, C. M.; Koh, C. A. Overview: Nucleation of Clathrate Hydrates. *J. Chem. Phys.* **2016**, *145* (21), 211705. https://doi.org/10.1063/1.4968590.
(66) Bai, D.; Chen, G.; Zhang, X.; Wang, W. Microsecond Molecular Dynamics Simulations of the Kinetic Pathways of Gas Hydrate Formation from Solid Surfaces. *Langmuir* **2011**, *27* (10), 5961–5967. https://doi.org/10.1021/la105088b.
(67) Bai, D.; Chen, G.; Zhang, X.; Sum, A. K.; Wang, W. How Properties of Solid Surfaces Modulate the Nucleation of Gas Hydrate. *Sci. Rep.* **2015**, *5*, 12747. https://doi.org/10.1038/srep12747.
(68) Bai, D.; Chen, G.; Zhang, X.; Wang, W. Nucleation of the CO2 Hydrate from Three-Phase Contact Lines. *Langmuir* **2012**, *28* (20), 7730–7736. https://doi.org/10.1021/la300647s.
(69) Liang, S.; Kusalik, P. G. The Nucleation of Gas Hydrates near Silica Surfaces. *Can. J. Chem.* **2014**, *93* (8), 791–798. https://doi.org/10.1139/cjc-2014-0443.
(70) Walsh, M. R.; Beckham, G. T.; Koh, C. A.; Sloan, E. D.; Wu, D. T.; Sum, A. K. Methane Hydrate Nucleation Rates from Molecular Dynamics Simulations: Effects of Aqueous Methane Concentration, Interfacial Curvature, and System Size. *J. Phys. Chem. C* **2011**, *115* (43), 21241–21248. https://doi.org/10.1021/jp206483q.
(71) Clarke, M. A.; Pooladi-Darvish, M.; Bishnoi, P. R. A Method To Predict Equilibrium Conditions of Gas Hydrate Formation in Porous Media. *Ind. Eng. Chem. Res.* **1999**, *38* (6), 2485–2490. https://doi.org/10.1021/ie980625u.
(72) Klauda, J. B.; Sandler, S. I. A Fugacity Model for Gas Hydrate Phase Equilibria. *Ind. Eng. Chem. Res.* **2000**, *39* (9), 3377–3386. https://doi.org/10.1021/ie000322b.
(73) Waals, J. H. van der; Platteeuw, J. C. Clathrate Solutions. In *Advances in Chemical Physics*; Prigogine, I., Ed.; John Wiley & Sons, Inc., 1958; pp 1–57. https://doi.org/10.1002/9780470143483.ch1.
(74) Klauda, J. B.; Sandler, S. I. Modeling Gas Hydrate Phase Equilibria in Laboratory and Natural Porous Media. *Ind. Eng. Chem. Res.* **2001**, *40* (20), 4197–4208. https://doi.org/10.1021/ie000961m.
(75) Chong, Z. R.; Yang, S. H. B.; Babu, P.; Linga, P.; Li, X.-S. Review of Natural Gas Hydrates as an Energy Resource: Prospects and Challenges. *Appl. Energy* **2016**, *162*, 1633–1652. https://doi.org/10.1016/j.apenergy.2014.12.061.
(76) Moridis, G.; Collett, T. Strategies for Gas Production from Hydrate Accumulations under Various Geologic Conditions. **2003**.
(77) Koh, C. A.; Sum, A. K.; Sloan, E. D. State of the Art: Natural Gas Hydrates as a Natural Resource. *J. Nat. Gas Sci. Eng.* **2012**, *8*, 132–138. https://doi.org/10.1016/j.jngse.2012.01.005.
(78) Clennell, M. B.; Hovland, M.; Booth, J. S.; Henry, P.; Winters, W. J. Formation of Natural Gas Hydrates in Marine Sediments: 1. Conceptual Model of Gas Hydrate Growth Conditioned by Host Sediment Properties. *J. Geophys. Res. Solid Earth* **1999**, *104* (B10), 22985–23003. https://doi.org/10.1029/1999JB900175.
(79) Turner, D. J.; Cherry, R. S.; Sloan, E. D. Sensitivity of Methane Hydrate Phase Equilibria to Sediment Pore Size. *Fluid Phase Equilibria* **2005**, *228–229*, 505–510. https://doi.org/10.1016/j.fluid.2004.09.025.
(80) Hansen, E. W.; Gran, H. C.; Sellevold, E. J. Heat of Fusion and Surface Tension of Solids Confined in Porous Materials Derived from a Combined Use of NMR and Calorimetry. *J. Phys. Chem. B* **1997**, *101* (35), 7027–7032. https://doi.org/10.1021/jp9710594.

(81) Uchida, T.; Ebinuma, T.; Takeya, S.; Nagao, J.; Narita, H. Effects of Pore Sizes on Dissociation Temperatures and Pressures of Methane, Carbon Dioxide, and Propane Hydrates in Porous Media. *J. Phys. Chem. B* **2002**, *106* (4), 820–826. https://doi.org/10.1021/jp012823w.
(82) Tohidi, B.; Anderson, R.; Clennell, M. B.; Burgass, R. W.; Biderkab, A. B. Visual Observation of Gas-Hydrate Formation and Dissociation in Synthetic Porous Media by Means of Glass Micromodels. *Geology* **2001**, *29* (9), 867–870. https://doi.org/10.1130/0091-7613(2001)029<0867:VOOGHF>2.0.CO;2.
(83) Li, S.-L.; Sun, C.-Y.; Liu, B.; Li, Z.-Y.; Chen, G.-J.; Sum, A. K. New Observations and Insights into the Morphology and Growth Kinetics of Hydrate Films. *Sci. Rep.* **2014**, *4*, 4129. https://doi.org/10.1038/srep04129.
(84) Li, S.-L.; Sun, C.-Y.; Liu, B.; Feng, X.-J.; Li, F.-G.; Chen, L.-T.; Chen, G.-J. Initial Thickness Measurements and Insights into Crystal Growth of Methane Hydrate Film. *AIChE J.* **2013**, *59* (6), 2145–2154. https://doi.org/10.1002/aic.13987.
(85) Handa, Y. P.; Stupin, D. Yu. Thermodynamic Properties and Dissociation Characteristics of Methane and Propane Hydrates in 70-.ANG.-Radius Silica Gel Pores. *J. Phys. Chem.* **1992**, *96* (21), 8599–8603. https://doi.org/10.1021/j100200a071.
(86) Uchida, T.; Ebinuma, T.; Ishizaki, T. Dissociation Condition Measurements of Methane Hydrate in Confined Small Pores of Porous Glass. *J. Phys. Chem. B* **1999**, *103* (18), 3659–3662. https://doi.org/10.1021/jp984559l.
(87) Yousif, M. H.; Sloan, E. D. Experimental Investigation of Hydrate Formation and Dissociation in Consolidated Porous Media. *SPE Reserv. Eng.* **1991**, *6* (04), 452–458. https://doi.org/10.2118/20172-PA.
(88) Henry, P.; Thomas, M.; Clennell, M. B. Formation of Natural Gas Hydrates in Marine Sediments: 2. Thermodynamic Calculations of Stability Conditions in Porous Sediments. *J. Geophys. Res. Solid Earth* **1999**, *104* (B10), 23005–23022. https://doi.org/10.1029/1999JB900167.
(89) Anderson, R.; Llamedo, M.; Tohidi, B.; Burgass, R. W. Experimental Measurement of Methane and Carbon Dioxide Clathrate Hydrate Equilibria in Mesoporous Silica. *J. Phys. Chem. B* **2003**, *107* (15), 3507–3514. https://doi.org/10.1021/jp0263370.
(90) Smith, D. H.; Wilder, J. W.; Seshadri, K. Methane Hydrate Equilibria in Silica Gels with Broad Pore-Size Distributions. *AIChE J.* **2002**, *48* (2), 393–400. https://doi.org/10.1002/aic.690480222.
(91) Wilder, J. W.; Seshadri, K.; Smith, D. H. Modeling Hydrate Formation in Media with Broad Pore Size Distributions. *Langmuir* **2001**, *17* (21), 6729–6735. https://doi.org/10.1021/la010377y.
(92) Pesaran, A.; Shariati, A. Effect of Capillary Term Parameters on the Thermodynamic Modeling of Methane Hydrate Formation in Porous Media. *J. Nat. Gas Sci. Eng.* **2013**, *14*, 192–203. https://doi.org/10.1016/j.jngse.2013.06.003.
(93) Li Tong, W.; K. Tan, M.; Kai Chin, J.; S. Ong, K.; Mun Hung, Y. Coupled Effects of Hydrophobic Layer and Vibration on Thermal Efficiency of Two-Phase Closed Thermosyphons. *RSC Adv.* **2015**, *5* (14), 10332–10340. https://doi.org/10.1039/C4RA14589E.
(94) Ouabbas, Y.; Dodds, J.; Galet, L.; Chamayou, A.; Baron, M. Particle–Particle Coating in a Cyclomix Impact Mixer. *Powder Technol.* **2009**, *189* (2), 245–252. https://doi.org/10.1016/j.powtec.2008.04.031.

(95) Parrish, W. R.; Prausnitz, J. M. Dissociation Pressures of Gas Hydrates Formed by Gas Mixtures. *Ind. Eng. Chem. Process Des. Dev.* **1972**, *11* (1), 26–35. https://doi.org/10.1021/i260041a006.
(96) John, V. T.; Holder, G. D. Contribution of Second and Subsequent Water Shells to the Potential Energy of Guest-Host Interactions in Clathrate Hydrates. *J. Phys. Chem.* **1982**, *86* (4), 455–459. https://doi.org/10.1021/j100393a008.
(97) John, V. T.; Papadopoulos, K. D.; Holder, G. D. A Generalized Model for Predicting Equilibrium Conditions for Gas Hydrates. *AIChE J.* **1985**, *31* (2), 252–259. https://doi.org/10.1002/aic.690310212.
(98) Zele, S. R.; Lee, S.-Y.; Holder, G. D. A Theory of Lattice Distortion in Gas Hydrates. *J. Phys. Chem. B* **1999**, *103* (46), 10250–10257. https://doi.org/10.1021/jp9917704.
(99) Sparks, K. A.; Tester, J. W.; Cao, Z.; Trout, B. L. Configurational Properties of Water Clathrates: Monte Carlo and Multidimensional Integration versus the Lennard-Jones and Devonshire Approximation. *J. Phys. Chem. B* **1999**, *103* (30), 6300–6308. https://doi.org/10.1021/jp9903108.
(100) Chase, M. W.; National Institute of Standards and Technology (U.S.). *NIST-JANAF Thermochemical Tables*; American Chemical Society ; American Institute of Physics for the National Institute of Standards and Technology: Washington, D.C.]; Woodbury, N.Y., 1998.
(101) Lide, D. R. *CRC Handbook of Chemistry and Physics: A Ready-Reference Book of Chemical and Physical Data : 1995-1996.*; CRC Press: Boca Raton, 1995.
(102) Růržička, K.; Majer, V. Simple and Controlled Extrapolation of Vapor Pressures toward the Triple Point. *AIChE J.* **1996**, *42* (6), 1723–1740. https://doi.org/10.1002/aic.690420624.
(103) Seo, Y.; Lee, H.; Uchida, T. Methane and Carbon Dioxide Hydrate Phase Behavior in Small Porous Silica Gels: Three-Phase Equilibrium Determination and Thermodynamic Modeling. *Langmuir* **2002**, *18* (24), 9164–9170. https://doi.org/10.1021/la0257844.
(104) Tee, L. S.; Gotoh, S.; Stewart, W. E. Molecular Parameters for Normal Fluids. Kihara Potential with Spherical Core. *Ind. Eng. Chem. Fundam.* **1966**, *5* (3), 363–367. https://doi.org/10.1021/i160019a012.
(105) Intermolecular Potential Functions and the Second and Third Virial Coefficients. *J. Chem. Phys.* **1964**, *41* (2), 429–437. https://doi.org/10.1063/1.1725884.
(106) Madden, M. E.; Ulrich, S.; Szymcek, P.; McCallum, S.; Phelps, T. Experimental Formation of Massive Hydrate Deposits from Accumulation of CH4 Gas Bubbles within Synthetic and Natural Sediments. *Mar. Pet. Geol.* **2009**, *26* (3), 369–378. https://doi.org/10.1016/j.marpetgeo.2008.04.002.
(107) Clennell, M. B.; Hovland, M.; Booth, J. S.; Henry, P.; Winters, W. J. Formation of Natural Gas Hydrates in Marine Sediments: 1. Conceptual Model of Gas Hydrate Growth Conditioned by Host Sediment Properties. *J. Geophys. Res. Solid Earth* **1999**, *104* (B10), 22985–23003. https://doi.org/10.1029/1999JB900175.
(108) Koh, C. A.; Sum, A. K.; Sloan, E. D. State of the Art: Natural Gas Hydrates as a Natural Resource. *J. Nat. Gas Sci. Eng.* **2012**, *8*, 132–138. https://doi.org/10.1016/j.jngse.2012.01.005.
(109) Minagawa, H.; Nishikawa, Y.; Ikeda, I.; Miyazaki, K.; Takahara, N.; Sakamoto, Y.; Komai, T.; Narita, H. Characterization of Sand Sediment by Pore Size Distribution and Permeability Using Proton Nuclear Magnetic Resonance Measurement. *J. Geophys. Res. Solid Earth* **2008**, *113* (B7). https://doi.org/10.1029/2007JB005403.

(110) Zachara, J.; Brantley, S.; Chorover, J.; Ewing, R.; Kerisit, S.; Liu, C.; Perfect, E.; Rother, G.; Stack, A. G. Internal Domains of Natural Porous Media Revealed: Critical Locations for Transport, Storage, and Chemical Reaction. *Environ. Sci. Technol.* **2016**, *50* (6), 2811–2829. https://doi.org/10.1021/acs.est.5b05015.
(111) Gas Hydrates-Not So Unconventional http://www.geoexpro.com/articles/2009/02/gas-hydrates-not-so-unconventional (accessed Nov 10, 2018).
(112) The Outlook for Energy: A View to 2040 http://corporate.exxonmobil.com/en/energy/energy-outlook/2017-highlights/a-view-to-2040 (accessed Mar 17, 2017).
(113) Knott, B. C.; Molinero, V.; Doherty, M. F.; Peters, B. Homogeneous Nucleation of Methane Hydrates: Unrealistic under Realistic Conditions. *J. Am. Chem. Soc.* **2012**, *134* (48), 19544–19547. https://doi.org/10.1021/ja309117d.
(114) Ming, F.; Zhang, Y.; Li, D. Experimental and Theoretical Investigations into the Formation of Ice Lenses in Deformable Porous Media. *Geosci. J.* **2016**, *20* (5), 667–679. https://doi.org/10.1007/s12303-016-0005-1.
(115) Ming, F.; Li, D. Experimental and Theoretical Investigations on Frost Heave in Porous Media https://www.hindawi.com/journals/mpe/2015/198986/ (accessed Mar 26, 2018). https://doi.org/10.1155/2015/198986.
(116) Everett, D. H. The Thermodynamics of Frost Damage to Porous Solids. *Trans. Faraday Soc.* **1961**, *57* (0), 1541–1551. https://doi.org/10.1039/TF9615701541.
(117) Talamucci, F. Freezing Processes in Porous Media: Formation of Ice Lenses, Swelling of the Soil. *Math. Comput. Model.* **2003**, *37* (5), 595–602. https://doi.org/10.1016/S0895-7177(03)00053-0.
(118) Fowler, A.; Krantz, W. A Generalized Secondary Frost Heave Model. *SIAM J. Appl. Math.* **1994**, *54* (6), 1650–1675. https://doi.org/10.1137/S0036139993252554.
(119) Peppin, S.; Majumdar, A.; Style, R.; Sander, G. Frost Heave in Colloidal Soils. *SIAM J. Appl. Math.* **2011**, *71* (5), 1717–1732. https://doi.org/10.1137/100788197.
(120) Jackson, K. A.; Chalmers, B. Freezing of Liquids in Porous Media with Special Reference to Frost Heave in Soils. *J. Appl. Phys.* **1958**, *29* (8), 1178–1181. https://doi.org/10.1063/1.1723397.
(121) Garcia-Bengochea, I.; Altschaeffl, A. G.; Lovell, C. W. Pore Distribution and Permeability of Silty Clays. *J. Geotech. Eng. Div.* **1979**, *105* (7), 839–856.
(122) Kleinberg, R. L.; Griffin, D. D. NMR Measurements of Permafrost: Unfrozen Water Assay, Pore-Scale Distribution of Ice, and Hydraulic Permeability of Sediments. *Cold Reg. Sci. Technol.* **2005**, *42* (1), 63–77. https://doi.org/10.1016/j.coldregions.2004.12.002.
(123) Madden, M. E.; Ulrich, S.; Szymcek, P.; McCallum, S.; Phelps, T. Experimental Formation of Massive Hydrate Deposits from Accumulation of CH4 Gas Bubbles within Synthetic and Natural Sediments. *Mar. Pet. Geol.* **2009**, *26* (3), 369–378. https://doi.org/10.1016/j.marpetgeo.2008.04.002.
(124) Li, S.-L.; Sun, C.-Y.; Liu, B.; Feng, X.-J.; Li, F.-G.; Chen, L.-T.; Chen, G.-J. Initial Thickness Measurements and Insights into Crystal Growth of Methane Hydrate Film. *AIChE J.* **2013**, *59* (6), 2145–2154. https://doi.org/10.1002/aic.13987.
(125) Tohidi, B.; Anderson, R.; Clennell, M. B.; Burgass, R. W.; Biderkab, A. B. Visual Observation of Gas-Hydrate Formation and Dissociation in Synthetic Porous Media by Means of Glass Micromodels. *Geology* **2001**, *29* (9), 867–870. https://doi.org/10.1130/0091-7613(2001)029<0867:VOOGHF>2.0.CO;2.

(126) Bi, Y.; Cao, B.; Li, T. Enhanced Heterogeneous Ice Nucleation by Special Surface Geometry. *Nat. Commun.* **2017**, *8*, 15372. https://doi.org/10.1038/ncomms15372.
(127) Yan, D.; Zeng, Q.; Xu, S.; Zhang, Q.; Wang, J. Heterogeneous Nucleation on Concave Rough Surfaces: Thermodynamic Analysis and Implications for Nucleation Design. *J. Phys. Chem. C* **2016**, *120* (19), 10368–10380. https://doi.org/10.1021/acs.jpcc.6b01693.
(128) Liang, S.; Kusalik, P. G. Nucleation of Gas Hydrates within Constant Energy Systems. *J. Phys. Chem. B* **2013**, *117* (5), 1403–1410. https://doi.org/10.1021/jp308395x.
(129) Campbell, J. M.; Meldrum, F. C.; Christenson, H. K. Observing the Formation of Ice and Organic Crystals in Active Sites. *Proc. Natl. Acad. Sci.* **2017**, *114* (5), 810–815. https://doi.org/10.1073/pnas.1617717114.
(130) Tobo, Y. An Improved Approach for Measuring Immersion Freezing in Large Droplets over a Wide Temperature Range. *Sci. Rep.* **2016**, *6*, 32930. https://doi.org/10.1038/srep32930.
(131) Fukuta, N. Experimental Studies on the Growth of Small Ice Crystals. *J. Atmospheric Sci.* **1969**, *26* (3), 522–531. https://doi.org/10.1175/1520-0469(1969)026<0522:ESOTGO>2.0.CO;2.
(132) Acker, J. P.; Elliott, J. A. W.; McGann, L. E. Intercellular Ice Propagation: Experimental Evidence for Ice Growth through Membrane Pores. *Biophys. J.* **2001**, *81* (3), 1389–1397. https://doi.org/10.1016/S0006-3495(01)75794-3.
(133) Ickes, L.; Welti, A.; Hoose, C.; Lohmann, U. Classical Nucleation Theory of Homogeneous Freezing of Water: Thermodynamic and Kinetic Parameters. *Phys. Chem. Chem. Phys.* **2015**, *17* (8), 5514–5537. https://doi.org/10.1039/C4CP04184D.
(134) Ickes, L.; Welti, A.; Lohmann, U. Classical Nucleation Theory of Immersion Freezing: Sensitivity of Contact Angle Schemes to Thermodynamic and Kinetic Parameters. *Atmos Chem Phys* **2017**, *17* (3), 1713–1739. https://doi.org/10.5194/acp-17-1713-2017.
(135) Hartmann, S.; Niedermeier, D.; Voigtländer, J.; Clauss, T.; Shaw, R. A.; Wex, H.; Kiselev, A.; Stratmann, F. Homogeneous and Heterogeneous Ice Nucleation at LACIS: Operating Principle and Theoretical Studies. *Atmos Chem Phys* **2011**, *11* (4), 1753–1767. https://doi.org/10.5194/acp-11-1753-2011.
(136) Qian, M.; Ma, J. The Characteristics of Heterogeneous Nucleation on Concave Surfaces and Implications for Directed Nucleation or Surface Activity by Surface Nanopatterning. *J. Cryst. Growth* **2012**, *355* (1), 73–77. https://doi.org/10.1016/j.jcrysgro.2012.06.031.
(137) Qian, M.; Ma, J. Heterogeneous Nucleation on Convex Spherical Substrate Surfaces: A Rigorous Thermodynamic Formulation of Fletcher's Classical Model and the New Perspectives Derived. *J. Chem. Phys.* **2009**, *130* (21), 214709. https://doi.org/10.1063/1.3146810.
(138) Volmer M. Über Keimbildung Und Keimwirkung Als Spezialfälle Der Heterogenen Katalyse. *Z. Für Elektrochem. Angew. Phys. Chem.* **2014**, *35* (9), 555–561. https://doi.org/10.1002/bbpc.192900026.
(139) Fletcher, N. H. Size Effect in Heterogeneous Nucleation. *J. Chem. Phys.* **1958**, *29* (3), 572–576. https://doi.org/10.1063/1.1744540.
(140) Clathrate Hydrates of Natural Gases, Third Edition https://www.crcpress.com/Clathrate-Hydrates-of-Natural-Gases-Third-Edition/Sloan-Jr-Koh/9780849390784 (accessed Apr 17, 2016).
(141) Pasieka, J.; Coulombe, S.; Servio, P. The Effect of Hydrophilic and Hydrophobic Multi-Wall Carbon Nanotubes on Methane Dissolution Rates in Water at Three Phase

Equilibrium (V-L-w-H) Conditions. *Ind. Eng. Chem. Res.* **2014**, *53* (37), 14519–14525. https://doi.org/10.1021/ie502457c.
(142) Li, S.-L.; Sun, C.-Y.; Liu, B.; Li, Z.-Y.; Chen, G.-J.; Sum, A. K. New Observations and Insights into the Morphology and Growth Kinetics of Hydrate Films. *Sci. Rep.* **2014**, *4* (1), 1–6. https://doi.org/10.1038/srep04129.
(143) Kashchiev, D.; Firoozabadi, A. Nucleation of Gas Hydrates. *J. Cryst. Growth* **2002**, *243* (3), 476–489. https://doi.org/10.1016/S0022-0248(02)01576-2.
(144) May, E. F.; Lim, V. W.; Metaxas, P. J.; Du, J.; Stanwix, P. L.; Rowland, D.; Johns, M. L.; Haandrikman, G.; Crosby, D.; Aman, Z. M. Gas Hydrate Formation Probability Distributions: The Effect of Shear and Comparisons with Nucleation Theory. *Langmuir* **2018**, *34* (10), 3186–3196. https://doi.org/10.1021/acs.langmuir.7b03901.
(145) DeFever, R. S.; Sarupria, S. Surface Chemistry Effects on Heterogeneous Clathrate Hydrate Nucleation: A Molecular Dynamics Study. *J. Chem. Thermodyn.* **2018**, *117*, 205–213. https://doi.org/10.1016/j.jct.2017.08.021.
(146) Lim, V. W. S.; Metaxas, P. J.; Zhen, J.; Stanwix, P. L.; Johns, M. L.; Aman, Z. M.; May, E. F. Subcooling and Induction Time Measurements of Probabilistic Hydrate Formation. In *Offshore Technology Conference Asia 2018, OTCA 2018*; Offshore Technology Conference, 2018.
(147) Handa, Y. P. Compositions, Enthalpies of Dissociation, and Heat Capacities in the Range 85 to 270 K for Clathrate Hydrates of Methane, Ethane, and Propane, and Enthalpy of Dissociation of Isobutane Hydrate, as Determined by a Heat-Flow Calorimeter. *J. Chem. Thermodyn.* **1986**, *18* (10), 915–921. https://doi.org/10.1016/0021-9614(86)90149-7.
(148) Chaouachi, M.; Falenty, A.; Sell, K.; Enzmann, F.; Kersten, M.; Haberthür, D.; Kuhs, W. F. Microstructural Evolution of Gas Hydrates in Sedimentary Matrices Observed with Synchrotron X-Ray Computed Tomographic Microscopy. *Geochem. Geophys. Geosystems* **2015**, *16* (6), 1711–1722. https://doi.org/10.1002/2015GC005811.